Peptidoglycan recycling is critical for cell division, cell wall integrity and β-lactam resistance in *Caulobacter crescentus*

Pia Richter[1], Anna Merz[1], Jacob Biboy[2], Nicole Paczia[3], Timo Glatter[4], Jared Ng[5], Waldemar Vollmer[5], Martin Thanbichler[1,6,7,*]

[1] Department of Biology, Marburg University, 35043 Marburg, Germany
[2] Centre for Bacterial Cell Biology, Institute for Cell and Molecular Biosciences, Newcastle University, Newcastle upon Tyne, United Kingdom
[3] Core facility for Metabolomics and Small-Molecule Mass Spectrometry, Max Planck Institute for Terrestrial Microbiology, 35043 Marburg, Germany
[4] Core facility for Mass Spectrometry and Proteomics, Max Planck Institute for Terrestrial Microbiology, 35043 Marburg, Germany
[5] Institute for Molecular Bioscience, University of Queensland, Brisbane, QLD, Australia
[6] Max Planck Fellow Group Bacterial Cell Biology, Max Planck Institute for Terrestrial Microbiology, 35043 Marburg, Germany
[7] Center for Synthetic Microbiology (SYNMIKRO), 35043 Marburg, Germany

[*]Correspondence: thanbichler@uni-marburg.de (M.T.)

Keywords
Peptidoglycan, cell wall recycling, β-lactamase, antibiotic resistance, β-lactam, MurU pathway

Abstract

Most bacteria possess a peptidoglycan (PG) sacculus, which is continuously remodeled during cell growth and division. The turnover products generated in this process are typically imported into the cell and reused for PG biosynthesis. While the underlying pathways have been studied intensively in gammaproteobacteria, knowledge of their presence and physiological roles in other bacterial lineages remains limited. Here, we comprehensively investigate PG recycling in the alphaproteobacterial model organism *Caulobacter crescentus*. Characterizing the activities of key enzymes *in vitro* and *in vivo*, we show that this species contains a functional PG recycling pathway, including the MurU shunt. Our results reveal that PG recycling is critical for *C. crescentus* cell morphology and division, and is dynamically regulated to balance the flux of metabolic intermediates toward PG biosynthesis and central carbon metabolism. Importantly, defects in PG recycling strongly impair the intrinsic ampicillin resistance of *C. crescentus* without changing the activity of its β-lactamase BlaA, likely by limiting PG precursor biosynthesis and thereby decreasing the activity of the cell wall biosynthetic machinery in the presence of residual antibiotic. These findings underscore the central role of PG recycling in bacterial fitness and suggest that inhibiting this process could provide a promising strategy to combat β-lactam-resistant pathogens.

Introduction

15 In most bacteria, the cytoplasmic membrane is surrounded by a layer of peptidoglycan (PG), which pro-
16 tects the cell from osmotic lysis, maintains cell shape and serves as a physical barrier against environ-
17 mental assaults (Egan et al., 2020). PG is composed of a dense meshwork of glycan strands made of alter-
18 nating *N*-acetylglucosamine (Glc*N*Ac) and *N*-acetylmuramic acid (Mur*N*Ac) moieties that are connected by
19 short peptides containing unusual D-amino acids (Vollmer et al., 2008a). The integrity of the PG layer is
20 critical for bacterial fitness and survival, which makes it a major target of medically relevant antibiotics
21 (Bugg et al., 2011).

22 PG biosynthesis initiates in the cytoplasm (Barreteau et al., 2008; Höltje, 1998), starting with the trans-
23 formation of fructose-6-phosphate to UDP-Mur*N*Ac. Next, this key intermediate is modified with a tripep-
24 tide, synthesized stepwise by dedicated amino acid ligases, and then completed by the addition of a
25 preformed D-Ala–D-Ala unit, leading to UDP-Mur*N*Ac-pentapeptide (**Figure 1**). The Mur*N*Ac-pentapeptide
26 moiety is then transferred to the lipid carrier undecaprenol phosphate and linked to Glc*N*Ac. The product,
27 lipid II, is then flipped across the cytoplasmic membrane (Sham et al., 2014), where is it used by glycosyl-
28 transferase (GTases) to polymerize the glycan chains. Transpeptidases (TPases) then crosslink the peptides
29 of neighboring glycan strands, thereby establishing the mesh-like architecture of PG (Egan et al., 2020;
30 Höltje, 1998). The most abundant group of TPases are the DD-TPases, which cleave the C-terminal D-Ala–
31 D-Ala unit of a pentapeptide and then transfer the resulting tetrapeptide to an adjacent acceptor peptide
32 (Sauvage et al., 2008). This group of enzymes is also known as penicillin-binding proteins (PBPs), because
33 they recognize penicillin and other β-lactams as non-cognate substrates, based on the structural similarity
34 of their β-lactam ring to the D-Ala–D-Ala moiety of uncrosslinked peptides. These compounds form a stable
35 adduct with the active-site serine of PBPs and thus irreversibly inhibit their crosslinking activity, thereby
36 weakening the cell wall and inducing cell lysis (Cho et al., 2014; Mora-Ochomogo and Lohans, 2021). The
37 sensitivity of DD-TPases to β-lactams represents a vulnerability that is widely exploited to treat bacterial
38 infections, but resistance to this class of antibiotics is rapidly spreading among pathogens (Lima et al.,
39 2020).

40 Cells usually contain both monofunctional PBPs, which contain only a transpeptidase domain, and bifunc-
41 tional PBPs, which contain an additional GTase domain and thus have polymerization as well as crosslinking
42 activity (Sauvage et al., 2008; Vollmer and Bertsche, 2008). To enable the tight spatiotemporal control of
43 PG biosynthesis, these enzymes are often part of dynamic multi-protein complexes that include regulatory
44 factors and cytoskeletal elements (Egan et al., 2020; Typas et al., 2012). In most rod-shaped bacteria,

45 lateral cell wall elongation is carried out by the elongasome, a complex organized by the actin-like protein
46 MreB (Jones et al., 2001). Multiple elongasomes are distributed along the longitudinal axis of the cell and
47 move around its circumference in helical tracks (Garner et al., 2011; van Teeffelen et al., 2011), incorpor-
48 ating new cell wall material in a dispersed manner. Their PG biosynthetic activity is mediated by the GTase
49 RodA and the monofunctional DD-TPase PBP2 (Cho et al., 2016; Meeske et al., 2016), whose functions are
50 closely coupled (Rohs et al., 2018). Cell division, by contrast, is mediated by the divisome, which is
51 orchestrated by polymers of the tubulin homolog FtsZ (Bi and Lutkenhaus, 1991; Bisson-Filho et al., 2017;
52 Yang et al., 2017), with the GTase FtsW and the monofunctional DD-TPase PBP3 acting as the main PG
53 biosynthetic enzymes (Taguchi et al., 2019). The division process also involves bifunctional PBPs, such as
54 PBP1B in *E. coli* (Bertsche et al., 2006; Navarro et al., 2025), although this class of enzymes also appears to
55 act outside larger complexes in the repair of cell wall (More et al., 2019; Pazos and Vollmer, 2021).

56 To enable the incorporation of new cell wall material into the existing sacculus, the PG meshwork needs
57 to be opened at specific sites – a task that is achieved by a diverse set of autolysins (van Heijenoort, 2011;
58 Vollmer et al., 2008b). DD- and LD-endopeptidases cleave the peptides and the crosslinks between them,
59 while amidases remove the entire peptide stem from the glycan chain. The glycan chains are cleaved by
60 glucosaminidases and muramidases. The latter include lytic transglycosylases (LTs), which break the β-1,4-
61 glycosidic bond between Mur*N*Ac and Glc*N*Ac, leading to the concomitant formation of a 1,6-anhydro
62 bond in the Mur*N*Ac moiety (Dik et al., 2017; Vollmer et al., 2008b). The activity of autolytic enzymes
63 generates small PG fragments, called muropeptides. Only a small fraction of these is released into the
64 environment (Goodell and Schwarz, 1985), whereas the majority is transported into the cytoplasm, where
65 they are metabolized and reused in PG synthesis. This process is known as PG recycling and has so far been
66 studied mainly in gammaproteobacteria such as *Escherichia coli* or *Pseudomonas aeruginosa* (Dik et al.,
67 2018; Gilmore and Cava, 2025; Park and Uehara, 2008).

68 During one division cycle, more than 50% of the PG sacculus is broken down in *E. coli*. Most of the turnover
69 products in this and other Gram-negative species are 1,6-anhydro-muropeptides (Vollmer et al., 2008b).
70 They are transported into the cytoplasm by the proton-driven Major Facilitator Superfamily (MFS)
71 permease AmpG (Cheng and Park, 2002; Jacobs et al., 1994), where the sugars and the peptide are
72 separated from each by the combined action of the LD-carboxypeptidase (LD-CPase) LdcA (Templin et al.,
73 1999), the amidase AmpD (Höltje et al., 1994) and the β-hexosaminidase NagZ (Cheng et al., 2000). The
74 Glc*N*Ac moiety is then recycled by conversion to Glc*N*Ac-6-P and then GlcN-6-P, which can either be trans-
75 formed into the PG precursor UDP-Mur*N*Ac or directed into central carbon metabolism by deamination to
76 fructose-6-P (Gilmore and Cava, 2025; Vollmer et al., 2008b). The fate of the anhMur*N*Ac moiety, on the

77 other hand, varies between species. In *E. coli*, it is converted to Glc*N*Ac-6-P (Uehara et al., 2005), whereas
78 *P. aeruginosa* employs the MurU pathway to convert anhMur*N*Ac into UDP-Mur*N*Ac, thereby channeling
79 it directly back into PG biosynthesis (Borisova et al., 2017; Fumeaux and Bernhardt, 2017; Gisin et al., 2013)
80 (**Figure 1**). As the last component, the peptide is typically broken down to single amino acids that are
81 subsequently reused to synthesize new peptide stems (Gilmore and Cava, 2025). An alternative route has
82 been reported for *E. coli*, which trims the released peptide by removal of the terminal D-Ala residues and
83 then attaches the resulting tripeptide to UDP-Mur*N*Ac using the peptide ligase Mpl (Mengin-Lecreulx et
84 al., 1996).

85 The recycling of PG degradation products is an efficient way to save energy and resources, which may be
86 particularly relevant during growth in nutrient-limiting conditions (Gilmore and Cava, 2025). For human
87 commensals or pathogens, it also represents an important strategy for evading detection by the innate
88 immune system, which senses released muropeptides through the NOD1 and NOD2 receptors (Trindade
89 and Chen, 2020). Apart from that, some gammaproteobacteria such as *Citrobacter freundii* and *P. aeru-*
90 *ginosa* use PG recycling as a sensory mechanism to detect the presence of β-lactam antibiotics and initiate
91 a resistance response (Dik et al., 2018). These species possess the inducible β-lactamase AmpC, whose
92 gene is controlled by the LysR-type transcriptional regulator AmpR. The activity of AmpR is modulated
93 through its interaction with muropeptides (Jacobs et al., 1994; Lindquist et al., 1989). In the absence of β-
94 lactams, it is associated with UDP-Mur*N*Ac-pentapeptide, acting as a repressor that prevents *ampC* expres-
95 sion (Jacobs et al., 1997). When cells are exposed to β-lactam antibiotics, the disruption of PG metabolism
96 leads to an increased accumulation of anhydro-muropeptides, thus raising the levels of PG recycling inter-
97 mediates in the cytoplasm. Some of these intermediates, especially anhMur*N*Ac-pentapeptide (Dietz et
98 al., 1997; Vadlamani et al., 2015), can interact with AmpR and competitively displace its co-repressor UDP-
99 Mur*N*Ac-pentapeptide. As a result, AmpR transforms into a transcriptional activator that stimulates *ampC*
100 expression, thereby establishing β-lactam resistance (Dietz et al., 1997; Dik et al., 2018; Jacobs et al., 1997).
101 While PG recycling and its impact on cell physiology as well as β-lactam resistance have been extensively
102 investigated in gammaproteobacteria, these processes are still poorly investigated in other bacterial line-
103 ages.

104 Here, we studied PG recycling in the alphaproteobacterium *Caulobacter crescentus*, a species intrinsically
105 resistant to β-lactam antibiotics due to production of the β-lactamase BlaA, extending recent work on this
106 topic by Modi et al. (Modi et al., 2025). We found that *C. crescentus* encodes a functional PG recycling
107 pathway and characterized the activities of key enzymes, using a combination of biochemical, cell biologic-
108 al, metabolomics and proteomics analyses. Our results demonstrate that PG recycling is required to sustain

109 proper cell morphology and division in this species, especially upon transition to stationary phase. They
110 further show that *C. crescentus* cells regulate their PG recycling pathway to control the flux of internal and
111 external Glc*N*Ac into PG biosynthesis and central carbon metabolism, while employing the MurU pathway
112 to directly convert anhMur*N*Ac back into the PG precursors. Importantly, PG recycling-deficient cells show
113 severe defects in β-lactam resistance, despite normal BlaA production and activity. For the model β-lactam
114 ampicillin, this phenotype can be explained by increased sensitivity of the septal TPase PBP3 to ampicillin-
115 mediated inhibition, likely resulting from a reduced supply of PG building blocks in the absence of PG
116 recycling. Together, our findings indicate that β-lactam efficacy is modulated by the availability of PBP
117 substrates, uncovering a new aspect of the complex interplay between this major class of antibiotics and
118 their cellular targets.

Results

119 **The genome of *C. crescentus* encodes a full PG recycling pathway**

120 To initiate the analysis of PG recycling in *C. crescentus*, we first mined the genome of this species for hom-
121 ologs of proteins that are central to the well-studied PG recycling pathway of *E. coli*. Reciprocal BLAST
122 analysis revealed clear counterparts for the muropeptide permease AmpG as well as for most enzymes
123 involved in the processing of the imported anhydro-muropeptides and the transformation of their sugar
124 and peptide moieties into new PG building blocks (**Table 1** and **Figure 1**). Notably, no homologs were found
125 for the LD-CPase LdcA and the peptide ligase Mpl, which trim tetrapeptides to tripeptides and attach these
126 to UDP-Mur*N*Ac, respectively. Another key enzyme missing in *C. crescentus* is the etherase MurQ, a critical
127 player in the recycling of anhMur*N*Ac that converts Mur*N*Ac-6-P into Glc*N*Ac-6-P and thus enables its re-
128 utilization through the Glc*N*Ac recycling/degradation pathway (Jaeger et al., 2005; Uehara et al., 2006).
129 Instead, we identified a three-step pathway initially found in *P. aeruginosa* (Borisova et al., 2017; Fumeaux
130 and Bernhardt, 2017; Gisin et al., 2013) that leaves the Mur*N*Ac moiety intact and uses it directly to
131 regenerate UDP-Mur*N*Ac. These findings suggest that the two sugar moieties of anhydro-muropeptides
132 are recycled independently in *C. crescentus*. The protein homologs identified are generally well-conserved
133 at the sequence level (**Table 1**) and show the same domain architectures as their *E. coli* and *P. aeruginosa*
134 counterparts. The only exception is the homolog of AmpD, in which the amidase_2 domain is fused to a C-
135 terminal PG_binding 1 domain that is not present in the *E. coli* protein. Due to this difference, this protein
136 will be referred to as 'AmiR' (*Ami*dase for PG *R*ecycling) throughout the present study.

137 **Predicted key players in the PG recycling pathway are functionally active**

138 To test the prediction that *C. crescentus* can recycle PG degradation products, we aimed to verify the acti-
139 vity of the two first enzymes in the recycling pathway, AmiR and NagZ, which mediate the release of the
140 sugar and peptide moieties, thereby providing the basis for their refunneling into PG biosynthesis (see
141 **Figure 1**). To this end, pentapeptide-rich PG sacculi isolated from a DD-carboxypeptidase-deficient *E. coli*
142 strain were treated with the LT Slt from *E. coli* (Betzner and Keck, 1989) to release anhydro-muropeptides
143 (**Figure 2A**). These were then first incubated with AmiR or a catalytically inactive variant of the protein
144 (AmiR*) in which three conserved amino acid residues coordinating the essential Zn^{2+} cofactor of AmpD-
145 like amidases (Généreux et al., 2004; Liepinsh et al., 2003; Uehara and Park, 2007) were replaced by
146 alanine (**Figure 2–figure supplement 1A**). HPLC analysis of the reaction products revealed that AmiR was
147 able to remove the peptide stems from all detectable anhydro-muropeptides, regardless of the length of
148 the peptide or the number of crosslinked peptides (**Figure 2B**). By contrast, no amidase activity was

149 detected in the control reactions containing the mutant AmiR* protein, confirming the critical role of the
150 metal cofactor in the amidase reaction. To determine whether, despite its broad substrate specificity,
151 AmiR had a preference for certain anhydro-muropeptides, we repeated the enzyme assay with limiting
152 enzyme concentrations. The results showed that AmiR efficiently hydrolyzed tetrapeptide-containing frag-
153 ments, whereas anhydro-muropeptides with tripeptide or pentapeptide stems were cleaved with lower
154 efficiency (**Figure 2–figure supplement 1B**). Notably, unlike *E. coli* AmpD (Höltje et al., 1994), it also
155 showed activity towards muropeptides that were produced with the muramidase cellosyl and thus con-
156 tained reducing Mur*N*Ac instead of anhMur*N*Ac moieties, although the efficiencies were slightly lower
157 under these conditions (**Figure 2–figure supplement 1C**). By contrast, no activity was detectable with
158 undigested peptidogylcan sacculi, consistent with a role of the protein in the recycling of PG fragments
159 (**Figure 2–figure supplement 2**). These results confirm that AmiR functions as a *bona fide* amidase involved
160 in peptidoglycan recycling.

161 Next, we used the same approach to study the biochemical activity of *C. crescentus* NagZ. For this purpose,
162 anhydro-muropeptides or reducing muropeptides were incubated with wild-type NagZ or a catalytically
163 inactive variant (NagZ*) in which an essential aspartic acid residue at the catalytic site (Bacik et al., 2012)
164 was replaced with an alanine (**Figure 2–figure supplement 3A**). NagZ removed the Glc*N*Ac moiety from
165 both types of muropeptides and, in each case, hydrolyzed all detectable muropeptide variants, irrespective
166 of the length of the peptide or the degree of crosslinkage (**Figure 2C and Figure 2–figure supplement 3B**).
167 By contrast, NagZ* did not show any activity. Thus, similar to its *E. coli* homolog (Cheng et al., 2000), NagZ
168 acts as an *N*-acetyl-β-D-glucosaminidase with broad substrate specificity. Together, these findings demon-
169 strate that *C. crescentus* possesses enzymes catalyzing the two initial steps of PG recycling.

170 Previous work has shown that the reactions catalyzed by AmpD and NagZ do not constitute a strictly linear
171 pathway but can occur in either order, with AmpD also acting on anhydro-muropeptides that were pre-
172 treated with NagZ and thus lack a Glc*N*Ac residue (Jacobs et al., 1995). To determine whether this was also
173 the case for *C. crescentus* AmiR, we specifically assessed its *in vitro* activity toward the substrate
174 anhMur*N*Ac-tetrapeptide, generated by preincubating purified Glc*N*Ac–anhMur*N*Ac-tetrapeptide with
175 NagZ. Mass spectrometric analysis revealed that AmiR-containing reactions accumulated substantial
176 amounts of free anhMur*N*Ac and free tetrapeptide, while only background levels of this product were
177 observed in reactions containing AmiR* or lacking added protein (**Figure 2–figure supplement 5**). These
178 results demonstrate that the order of the two initial PG recycling steps are also interchangeable in *C. cres-*
179 *centus*.

180 In *E. coli*, PG turnover products are imported by various transporters with different binding specificities
181 (Gilmore and Cava, 2025), but only AmpG recognizes muropeptides containing a Glc*N*Ac–anhMur*N*Ac unit,
182 as typically produced by LTs (Chang et al., 2025; Cheng and Park, 2002; Jacobs et al., 1994). To clarify
183 whether the AmpG homolog of *C. crescentus* has a similar role, we used a metabolomics approach to
184 detect imported anhydro-muropeptides, using the NagZ cleavage products anhMur*N*Ac-pentapep-
185 tide, -tetrapeptide and -tripeptide as a proxy (**Figure 3A**). In the wild-type strain, the levels of these PG
186 fragments were close to the detection limit, suggesting that they are rapidly processed into smaller units.
187 Consistent with this notion, and in line with previous results (Jacobs et al., 1994; Simpson et al., 2023), a
188 strong accumulation of these species was observed in a Δ*amiR* mutant, which lacks the amidase to remove
189 the peptide stem (**Figure 3B**). Upon the deletion of *ampG* in the Δ*amiR* background, the three anhydro-
190 muropeptides were again barely detectable, confirming that AmpG functions as the primary importer of
191 LT-generated PG degradation products in *C. crescentus*.

192 The analysis of cytoplasmic PG degradation intermediates also provided a means to obtain further insight
193 into the nature and relevance of the reactions catalyzed by AmiR and NagZ. Consistent with the results of
194 the *in vitro* activity assays (compare **Figure 2C**), the accumulation of anhMur*N*Ac-peptide species in the
195 absence of AmiR (**Figure 3B**) shows that NagZ can hydrolyze the glycosidic bond in the Glc*N*Ac–anhMur*N*Ac
196 unit while the peptide stem is still attached. Moreover, it indicates that the reaction catalyzed by AmiR is
197 a bottleneck in the PG recycling pathway, because the removal of the peptide appears to be critical for
198 downstream reactions to occur. To clarify whether cleavage of the Glc*N*Ac–anhMur*N*Ac bond was required
199 to further process the disaccharide unit after peptide removal, we assessed the levels of the free disac-
200 charide in different mutant background. Metabolomics analysis revealed that Glc*N*Ac–anhMur*N*Ac was
201 barely detectable in the wild-type strain, suggesting that the initial decomposition of anhydro-muropep-
202 tides by NagZ and AmiR is highly efficient. The disaccharide was also not enriched in Δ*ampG* and Δ*amiR*
203 cells, but highly accumulated in the Δ*nagZ* mutant (**Figure 3C**). Thus, the two sugars need to be separated
204 before further processing steps can initiate.

205 Together, our analyses verify that *C. crescentus* possesses the machinery required to import anhydro-
206 muropeptides and break them down into their sugar and peptide components. Moreover, they indicate
207 that AmiR and NagZ have a broad binding specificity, so that the initial steps of the recycling process do
208 not occur in a strictly linear fashion.

209 **PG recycling is necessary for proper cell division and β-lactam resistance in *C. crescentus***

210 Although a considerable fraction of the PG sacculus (~50% in *E. coli*) is turned over and recycled during
211 each cell division cycle (Goodell, 1985; Goodell and Schwarz, 1985), the model species *E. coli* and *P. aeru-*
212 *ginosa* typically do not display any obvious morphological phenotype upon disruption of the PG recycling
213 pathway (Park and Uehara, 2008; Gilmore and Cava, 2025). The only exception are *E. coli* cells with a defect
214 in the DD-carboxypeptidase LdcA, which promotes the erroneous ligation of UDP-Mur*N*Ac with unpro-
215 cessed tetrapeptides, blocking the addition of the terminal D-Ala–D-Ala unit and inducing cell lysis in the
216 stationary growth phase (Templin et al., 1999). To determine the relevance of PG recycling in *C. crescentus*,
217 we examined the morphology of Δ*ampG*, Δ*amiR* and Δ*nagZ* cells growing in rich (PYE) medium by light
218 microscopy. In each case, the mutation caused significant cell filamentation and widening, with the defects
219 becoming more pronounced upon transition of the cells from the exponential to the stationary growth
220 phase (**Figure 4A,B**). These phenotypes were reversed by ectopic expression of the deleted genes under
221 the control of a xylose-inducible promoter, even when cells were grown in the absence of inducer (**Figure**
222 **4-figure supplement 1A,B**), suggesting that low levels of these proteins resulting from basal promoter
223 activity are sufficient for proper function. Strains in which *amiR* and *nagZ* genes were replaced with alleles
224 encoding the catalytically inactive AmiR* or NagZ* showed phenotypes similar to those of the respective
225 deletion mutants, verifying that the defects observed were due to the absence of the enzymatic activities
226 (**Figure 4–figure supplement 2**). Together, these results indicate that PG recycling is critical for proper cell
227 division and, to some extent, also lateral growth in *C. crescentus*. Notably, the lack of AmpG or AmiR, which
228 prevents the recycling of the peptide stem (**Figure 3B**), caused a more severe phenotype than the lack of
229 NagZ, which blocks the processing of the free Glc*N*Ac–anhMur*N*Ac-disaccharide (**Figure 3C**). Therefore,
230 the supply of amino acids rather than sugars appears to be the major limiting factor in PG precursor
231 biosynthesis. To further investigate the effect of nutrients on the phenotypes of the different mutant
232 strains, we also analyzed cells grown to stationary phase in minimal (M2G) medium. Interestingly, none of
233 the mutant strains showed obvious morphological defects under these conditions (**Figure 4–figure supple-**
234 **ment 3**), possibly because the high glucose content of M2G medium compensates for the lack of PG
235 recycling by facilitating *de novo* PG synthesis.

236 Apart from promoting growth, PG recycling was found to critically contribute to the regulation of β-lactam
237 resistance in organisms such as *C. freundii* and *P. aeruginosa*, which use the level of anhMur*N*Ac-penta-
238 peptide as a readout to sense the presence of β-lactams and control the production of the β-lactamase
239 AmpC (Dietz et al., 1997; Dik et al., 2018; Jacobs et al., 1997). Previous work has also suggested a link
240 between PG recycling and β-lactam resistance in *C. crescentus* (Modi et al., 2025), a species that produces

241 a metallo-β-lactamase (BlaA) conferring intrinsic high-level resistance to ampicillin and related β-lactam
242 antibiotics (Docquier et al., 2002; West et al., 2002). To further clarify the underlying mechanism, we
243 analyzed the ability of the *C. crescentus* Δ*ampG*, Δ*amiR* and Δ*nagZ* mutants to grow on nutrient-agar (PYE)
244 plates at different ampicillin concentrations (**Figure 4C**). Wild-type cells tolerated high levels (50 µg/mL)
245 of the antibiotic without any apparent fitness defects. In comparison, all three mutant strains showed a
246 significant reduction in ampicillin resistance. The strongest effect was observed for Δ*amiR* cells, whose
247 sensitivity approached that of Δ*blaA* cells (**Figure 4C**). Surprisingly, the Δ*ampG* mutant showed the least
248 pronounced resistance defect, although it exhibited the largest fraction of filamentous cells (compare
249 **Figure 4A,B**), indicating that the defects in β-lactam resistance and cell morphology are not strictly con-
250 nected. The mutant phenotypes were largely reversed by ectopic expression of the deleted genes from an
251 inducible promoter, even when cells were analyzed in the absence of the inducer (**Figure 4–figure supple-**
252 **ment 1C**), thereby verifying the validity of the deletion analysis. Interestingly, while growth in minimal
253 (M2G) medium largely abolished the cell filamentation phenotype of PG recycling-deficient cells (compare
254 **Figure 4–figure supplement 3**), it even aggravated their ampicillin sensitivity (**Figure 4–figure supplement**
255 **3C**). Under these conditions, wild-type cells also became more sensitive to the antibiotic, indicating that
256 ampicillin efficacy is influenced by the metabolic state of the cells or the composition of the culture medi-
257 um. Together, the results obtained demonstrate that PG recycling is important for proper growth and β-
258 lactam resistance in *C. crescentus*.

259 Notably, previous work has shown that inactivation of the divisome-associated soluble LT SdpA also leads
260 to a severe decrease in ampicillin resistance in otherwise wild-type cells (Zielinska et al., 2017). This
261 observation suggested that SdpA could represent the main LT in *C. crescentus*, producing the largest share
262 of the anhydro-muropeptides that are fed into the PG recycling pathway. Consistent with this notion, cells
263 lacking SdpA were highly sensitive to even low concentrations of ampicillin (**Figure 4–figure supplement**
264 **4A**). Surprisingly, however, their resistance defect was more pronounced than that of any of the PG
265 recycling-deficient mutants investigated (compare **Figure 4C**). Moreover, in accordance with previous
266 work, Δ*sdpA* cells did not show any signs of cell filamentation (Zielinska et al., 2017), indicating that their
267 reduced ampicillin resistance may not be primarily due to a decrease in the supply of anhydro-muropep-
268 tides available for PG recycling (**Figure 3–figure supplement 4B,C**). Metabolomics analysis indeed showed
269 that the absence of SdpA barely affected the levels of cytoplasmic anhMur*N*Ac-peptide species accumu-
270 lating in the Δ*amiR* background (**Figure 3–figure supplement 4D**). This finding supports the idea that SdpA
271 is not the main producer of anhydro-muropeptides and likely affects β-lactam resistance through a differ-
272 ent pathway, e.g., by preventing the toxic accumulation of non-crosslinked PG strands that form excessive-

273 ly when the TPase domain of bifunctional PBPs is inactivated by β-lactam binding (Cho et al., 2014; Weaver
274 et al., 2022).

275 **The recycling of Glc*N*Ac involves two partially redundant enzymatic systems**

276 After removal of the peptide and cleavage of the Glc*N*Ac–anhMur*N*Ac moiety, the two sugars are recycled
277 in different ways. In *E. coli*, Glc*N*Ac is transformed to Glc*N*Ac-6-P by NagK, which is then reintroduced into
278 *de novo* PG biosynthesis by conversion into GlcN-6-P, catalyzed by the deacetylase NagA (**Figure 1**). Bioin-
279 formatic analysis revealed that this branch of the PG recycling pathway is conserved in *C. crescentus*. Inter-
280 estingly, however, this species contains two NagA homologs (75% identity), which we have named NagA1
281 and NagA2 (**Table 1**). To determine the physiological relevance of Glc*N*Ac recycling, we generated *C. cres-*
282 *centus* Δ*nagK*, Δ*nagA1* and Δ*nagA2* mutants and analyzed their cell morphologies and resistance to
283 ampicillin. None of the strains showed a significant morphological (**Figure 5A,B**) or resistance (**Figure 5C**)
284 phenotype, again suggesting that the supply of sugars is not a major constraining factor in PG biosynthesis.
285 Since it was conceivable that NagA1 and NagA2 had redundant functions, we also aimed to generate a
286 double mutant lacking both *nagA* homologs to fully interrupt the second reaction of the Glc*N*Ac recycling
287 branch. Surprisingly, this was not possible, even though blocking the first step by deletion of *nagK* did not
288 cause any obvious fitness defect, suggesting that the accumulation of Glc*N*Ac-6-P in the complete absence
289 of NagA activity (Plumbridge, 2009) may be toxic to the cells, possibly by allosterically activating the GlcN-
290 6-P deaminase NagB (Álvarez-Añorve et al., 2016) and thus preventing *de novo* PG biosynthesis.

291 In *E. coli*, the expression of *nagA* is controlled by Glc*N*Ac-6-P, which interacts with the transcription factor
292 NagC, thereby converting it from a repressor to an activator (Plumbridge, 1991). The system can also be
293 activated by periplasmic Glc*N*Ac, because *E. coli* possesses a phosphotransferase system (PTS) permease
294 (NagE) that takes up and concomitantly phosphorylates this sugar, releasing it in the cytoplasm as Glc*N*Ac-
295 6-P (Mukhija and Erni, 1996; Plumbridge, 2009). Since *C. crescentus* possesses two *nagE* homologs (**Table**
296 **1**), we decided to analyze its response to externally added Glc*N*Ac to better understand the regulation of
297 NagA1 and NagA2 in this species. Comparing the total proteomes of wild-type cells grown in minimal
298 (M2G) medium with or without Glc*N*Ac, we found that the presence of sugar strongly stimulated the ex-
299 pression of two distinct but similar gene clusters, containing *nagA1* and *nagA2* respectively (**Figure 5D,E**).
300 One of these clusters (CCNA_00452-CCNA_00458) has previously been implicated in the uptake and meta-
301 bolism of Glc*N*Ac in *C. crescentus*, based on the fact that it includes a gene for an outer-membrane TonB-
302 dependent receptor that transports Glc*N*Ac and is essential for its utilization (Eisenbeis et al., 2008). The
303 other genes in the cluster encode a NagE-like PTS permease, its cognate PTS phosphotransferase, NagA2
304 and a NagB homolog (**Figure 5E**), thus providing the complete set of proteins required to import Glc*N*Ac

305 from the periplasm and then funnel it either into PG biosynthesis or central carbon metabolism (see **Figure**
306 **1).** Finally, the cluster contains genes for a β-*N*-acetylhexoaminidase, catalyzing the release of Glc*N*Ac from
307 chitin oligomers, and a transcriptional regulator of unknown function, which does not have an obvious
308 homolog in *E. coli*. The second cluster (CCNA_00566-CCNA_00574) includes homologs of all the above-
309 mentioned genes and additionally features genes for a predicted mannosidase and a predicted mannonate
310 dehydratase, suggesting that it could be additionally involved in the metabolism of mannose derivatives.
311 Collectively, the results of the mutational and proteomics analyses suggest that NagA1 and NagA2 are
312 functionally redundant enzymes whose synthesis is activated by their substrate Glc*N*Ac-6-P.

313 **anhMur*N*Ac is recycled through the MurU pathway**

314 Bioinformatic analysis suggested that *C. crescentus* contains all enzymes of the *P. aeruginosa* MurU path-
315 way, which recycles anhMur*N*Ac independently of the Glc*N*Ac recycling branch, converting it directly back
316 to UDP-Mur*N*Ac (Borisova et al., 2017; Fumeaux and Bernhardt, 2017; Gisin et al., 2013) (**Figure 1** and
317 **Table 1**). To verify the functionality of this predicted pathway and clarify its impact on cell physiology, we
318 introduced deletions in the *anmK* or *amgK* gene, thereby blocking essential steps in the reaction sequence.
319 Microscopic analysis revealed that resulting single mutants did not have any significant morphological
320 defects (**Figure 6A,B**). Importantly, however, both strains showed a moderate increase in their suscep-
321 tibility to ampicillin (**Figure 6C**). This finding indicates that the MurU pathway is active and relevant for β-
322 lactam resistance in *C. crescentus*, thus playing a more important role than the Glc*N*Ac recycling branch
323 (compare **Figure 5A-C**). To determine whether this pathway was the only means for *C. crescentus* to meta-
324 bolize anhMur*N*Ac, we tested whether its disruption would lead to an accumulation of recycling intermedi-
325 ates. Metabolomics analysis indeed revealed a considerable increase in the cytoplasmic level of Mur*N*Ac
326 in cells lacking the Mur*N*Ac kinase AmgK, suggesting the absence of alternative recycling pathways for the
327 anhMurNAc moiety (**Figure 6D**). Notably, previous work has shown that the formation of UDP-Mur*N*Ac
328 from recycled anhMur*N*Ac by the MurU pathway reduces the sensitivity of *P. aeruginosa* to the antibiotic
329 fosfomycin, which inhibits MurA and thus hinders the *de novo* synthesis of this central PG precursor
330 (Borisova et al., 2014). We reasoned that this effect should also be observable in *C. crescentus* if the MurU
331 pathway was active in this species. Antibiotic resistance assays revealed that the Δ*amgK* mutant indeed
332 showed higher sensitivity to fosfomycin than the wild-type strain or the Δ*nagK* mutant, which is defective
333 in Glc*N*Ac recycling (**Figure 6E**). Taken together, these findings strongly suggest that anhMur*N*Ac is recycled
334 via the MurU pathway in *C. crescentus*, thereby enhancing the supply of precursors for peptidoglycan bio-
335 synthesis. This process may be more significant than Glc*N*Ac recycling (compare **Figure 5A-C**) because a

336 reduced production of GlcN-6-P may be compensated by an increased production of this intermediate
337 from fructose-6-phosphate, supplied by central carbon metabolism.

338 As the recycling of Glc*N*Ac and anhMur*N*Ac is mediated by two distinct metabolic routes, cells blocked in
339 one of these routes can still recycle half of the sugars generated by anhydro-muropeptide processing,
340 potentially explaining the relatively mild phenotypes observed for the different single mutants. To clarify
341 the effect caused by inhibiting both sugar recycling pathways, we generated a Δ*nagK* Δ*amgK* double
342 mutant. Metabolomic analysis confirmed that this strain showed highly elevated Mur*N*Ac levels, compar-
343 able to those in the Δ*amgK* single mutant, while this recycling intermediate was barely detectable in Δ*nagK*
344 or wild-type cells (**Figure 7A**). The double mutant showed a slightly higher tendency to form filaments than
345 the wild type (**Figure 7B,C**). However, its susceptibility to ampicillin was not reduced beyond the level seen
346 for the Δ*amgK* single mutant (**Figure 7D**). This observation may be attributed to the presence of Glc*N*Ac in
347 the rich medium used to grow the cells, which can be taken up and concomitantly phosphorylated by the
348 NagE1 and NagE2 permease systems, thereby compensating for the loss of the Glc*N*Ac kinase activity nor-
349 mally provided by NagK (see **Figure 1**).

350 **Defects in PG recycling do not change the levels or activity of the β-lactamase BlaA**

351 In gammaproteobacteria such as *P. aeruginosa* and *C. freundii*, β-lactam resistance is established by in-
352 creased synthesis of the β-lactamase AmpC in the presence of excess anhydro-muropentapeptide, mediat-
353 ed by the transcriptional regulator AmpR (Dietz et al., 1997; Dik et al., 2018; Jacobs et al., 1997). Previous
354 work has suggested that the *C. crescentus* β-lactamase BlaA is constitutively active (Docquier et al., 2002;
355 Modi et al., 2025), raising the question of how its protective effect could be dependent on PG recycling.
356 To address this conundrum, we aimed to reinvestigate the regulation of BlaA activity at the transcriptional,
357 protein accumulation and activity level.

358 Inspecting the genomic contexts of PG recycling genes (**Table 1**), we found that *amiR* is located in a three-
359 gene operon that also includes genes for a predicted drug/metabolite transporter (named TraX) and a
360 PaiB-family transcriptional regulator (named RegX), suggesting that these proteins could be involved in PG
361 recycling and/or the regulation of β-lactam resistance (**Figure 8–figure supplement 1A**). However, in line
362 with the dominant role of the permease AmpG in anhydro-muropeptide import (see **Figure 3**), the absence
363 of TraX did not markedly affect the accumulation of anhMur*N*Ac-peptides observed in the Δ*amiR* back-
364 ground. Similarly, whole-cell proteome analysis showed that the regulon of RegX did not include *blaA* or
365 any genes related to PG recycling. Apart from this, neither Δ*traX* nor Δ*regX* showed any obvious defects in

366 cell division or ampicillin resistance, indicating that these two genes are not involved in PG-related pro-
367 cesses (**Figure 8–figure supplement 1B-F**).

368 Interestingly, the *blaA* gene is located in a five-gene operon, which additionally encodes a predicted trans-
369 criptional regulator and three proteins involved in methionine biosynthesis (**Figure 8A**). To test whether
370 the expression of this operon changes in response to β-lactam stress or disruption of the PG recycling
371 pathway, we fused its upstream region (400 bp) to a β-galactosidase reporter gene (*lacZ*) and analyzed it
372 for promoter activity in the Δ*ampG*, Δ*amiR* and Δ*nagZ* backgrounds both in the absence or in the presence
373 of ampicillin. The results showed that *lacZ* expression was constant in all conditions tested (**Figure 8B**),
374 indicating that the operon as a whole was not subject to transcriptional regulation. However, it was possi-
375 ble that the transcriptional regulator controlled *blaA* expression by acting on an internal promoter. To test
376 this hypothesis, we compared the whole-cell proteomes of the wild-type strain and a mutant lacking the
377 regulatory gene (CCNA_02225). Surprisingly, in the mutant strain, the methionine biosynthetic proteins
378 encoded by the genes flanking *blaA* were significantly upregulated, whereas the levels of BlaA remained
379 essentially unchanged (**Figure 8–figure supplement 2**). This finding may suggest that *blaA* is expressed
380 from a strong and constitutive internal promoter, so that moderate changes in the transcription of the
381 whole operon do not markedly affect the overall levels of the *blaA* transcripts (Plumbridge, 1996). Finally,
382 we tested whether the activity of BlaA could be regulated post-transcriptionally at the level of enzyme
383 activity. To this end, we incubated cells with the chromogenic β-lactam nitrocefin (O'Callaghan et al., 1972)
384 and used its property of developing red color upon cleavage to measure β-lactamase activity *in vivo*. We
385 found the Δ*ampG*, Δ*amiR* and Δ*nagZ* mutants showed behaviors similar to that of the wild-type strain,
386 while the Δ*blaA* mutant lacked activity, validating the assay (**Figure 8C**). Consistent with this finding, whole-
387 cell proteomic analyses showed that cells impaired in PG recycling accumulated BlaA at levels comparable
388 to those in the wild-type strain (**Figure 8D**). Collectively, these results demonstrate that the severe reduc-
389 tion in β-lactam resistance observed in PG recycling-deficient strains is not due to changes in BlaA accu-
390 mulation or activity. This conclusion is supported by the results of growth assays showing that defects in
391 the PG recycling pathway also reduce the resistance of cells to aztreonam, a β-lactam antibiotic that is not
392 cleaved by metallo-β-lactamases such as BlaA (Bush et al., 1982) (**Figure 8E**). Thus, the ampicillin sensitivity
393 phenotypes observed are likely due to changes in the susceptibility and/or activity of target proteins rather
394 than impaired degradation of this antibiotic in the absence of PG recycling.

395 **PG recycling defects sensitize the PG biosynthetic machinery to the inhibitory effect of ampicillin**

396 To shed more light on the connection between PG recycling and β-lactam resistance, we aimed to investi-
397 gate the growth defects induced by the exposure of cells to ampicillin in more detail. To this end, we

398 cultivated wild-type and Δ*amiR* cells in liquid medium containing different concentrations of the antibiotic
399 and analyzed their morphology by light microscopy. Wild-type cells tolerated substantial concentrations
400 of ampicillin without noticeable changes in cell shape (**Figure 9A,B**). However, at 500 µg/mL, they devel-
401 oped a pronounced filamentous phenotype, while exposure to 5,000 µg/mL led to growth arrest and cell
402 lysis. For the Δ*amiR* mutant, similar phenotypes were observed, but cell filamentation and lysis already
403 occurred at the lowest ampicillin concentration tested and were consistently more pronounced than for
404 the wild type across all conditions (**Figure 9A,B**). To better characterize the development of the observed
405 morphological defects, we monitored the growth behavior of the two strains following a shift from plain
406 rich medium to medium supplemented with a low concentration of ampicillin (20 µg/ml). Whereas the
407 wild-type strain grew normally in both conditions (**Figure 9C** and **Figure 9–video 1**), Δ*amiR* cells started to
408 become filamentous and swollen shortly after exposure to the antibiotic and were unable to divide (**Figure**
409 **9C** and **Figure 9–video 2**). Together, these results indicate that, in *C. crescentus*, ampicillin preferentially
410 targets cell division, although it also affects lateral growth when applied at elevated concentrations. More-
411 over, they suggest that PG recycling defects enhance the efficacy of ampicillin by rendering the PG biosyn-
412 thetic machinery more sensitive to its inhibitory effect.

413 To shed more light on the inhibitory activity of ampicillin, we aimed to identify its target proteins. For this
414 purpose, we adapted an assay enabling the visualization of PBPs in SDS-gels after labeling with the fluor-
415 escent β-lactam bocillin-FL (Zhao et al., 1999). Using Δ*blaA* cells to prevent β-lactam degradation, this
416 approach detected all known functional transpeptidases of *C. crescentus* except for PBP2 (Strobel et al.,
417 2014; Yakhnina and Gitai, 2013) as well as the predicted carboxypeptidase CrbA (**Figure 9D**). However,
418 when these proteins were incubated with ampicillin prior to the addition of bocillin-FL, all but one of them
419 (PbpX) remained unlabeled, indicating that ampicillin had blocked their active-site serine, thereby prevent-
420 ing the subsequent reaction with bocillin-FL. Among the ampicillin targets identified were the essential,
421 cell division-specific monofunctional transpeptidase PBP3 as well as the bifunctional PBPs Pbp1A, PbpY
422 and PbpC. The labeling of PBP3 and some bifunctional PBPs was also abolished by preincubation with
423 cephalexin, a β-lactam that specifically targets PBP3 in *E. coli* (Kocaoglu and Carlson, 2015), whereas the
424 PBP2-specific β-lactam mecillinam had only minor effects on the labeling pattern (**Figure 9D**). Given that
425 Pbp1A, PbpY and PbpC have been shown to be dispensible for cell division in *C. crescentus* (Strobel et al.,
426 2014; Yakhnina and Gitai, 2013), these results indicate that the cell filamentation phenotype induced by
427 ampicillin is primarily due to inhibition of PBP3 activity.

428 **PG recycling defects may increase ampicillin sensitivity by limiting the supply of PG precursors**

429 The results obtained suggest that impaired PG recycling does not affect BlaA activity and may rather en-
430 hance the inhibitory effect of ampicillin on PG biosynthesis. It was conceivable that the accumulation of
431 unrecycled PG degradation products in the periplasm could impair the activity of certain PG biosynthetic
432 enzymes, thereby disrupting PG homeostasis. However, sacculi isolated from wild-type and Δ*amiR* cells
433 did not show any significant differences in their muropeptide composition (**Figure 9–figure supplement**
434 **1**), suggesting that a defect in PG recycling does not perturb the global balance of PG biosynthetic and
435 autolytic processes. Notably, mutants blocked in the PG recycling pathway also exhibit a conditional cell
436 division defect, even when not exposed to ampicillin. It was therefore possible that their higher β-lactam
437 sensitivity was linked to a decrease in the overall efficiency of PG biosynthesis, caused by impaired replen-
438 ishment of PG precursors from recycling products. Metabolomics analysis revealed that the Δ*ampG*, Δ*amiR*
439 and Δ*nagZ* mutants indeed showed significantly lower levels of UDP-sugars than the wild-type strain (**Fig-**
440 **ure 9E**). The absence of AmpG and NagZ led to a more than 50% decrease in the UDP-Glc*N*Ac pool, confirm-
441 ing that *de novo* synthesis alone is not sufficient to satisfy the cellular demand for this central metabolite.
442 By contrast, UDP-Glc*N*Ac levels remained unchanged in Δ*amiR* cells, consistent with the observation that
443 Glc*N*Ac can still be released from imported anhydro-muropeptides in the absence of amidase activity (see
444 **Figures 2C** and **3C**). Even stronger effects were observed on the UDP-Mur*N*Ac pool, which was drastically
445 reduced in all three mutant strains (**Figure 9E**). Its depletion in the absence of PG recycling suggests that
446 the formation of UDP-Mur*N*Ac constitutes a bottleneck in the *de novo* PG biosynthetic pathway, with cells
447 relying heavily on anhMur*N*Ac recycling via the MurU pathway to maintain an adequate supply. Collec-
448 tively, these results demonstrate that PG recycling is critical to provide sufficient activated sugars for PG
449 precursor biosynthesis. However, although the Δ*ampG*, Δ*amiR* and Δ*nagZ* mutants show a very similar
450 decrease in cytoplasmic UDP-Mur*N*Ac levels, their morphological and resistance defects differ significant-
451 ly, indicating that the reduced availability of UDP-sugars may not be the only reason for the phenotypes
452 observed. Consistent with this notion, an increase in cytoplasmic Glc*N*Ac-P levels through supplementa-
453 tion of the growth medium with Glc*N*Ac (see **Figure 5**) was not sufficient to improve ampicillin tolerance
454 in the three mutant strains (**Figure 9–figure supplement 2A**). Likewise, addition of the PG-specific sugar
455 Mur*N*Ac did not markedly enhance growth in the presence of the antibiotic (**Figure 9-figure supplement**
456 **2B)**, although it remains unclear whether *C. crescentus* can take up Mur*N*Ac from the environment.

457 It was conceivable that the limited supply of PG precursors in the absence of proper PG recycling causes
458 cell filamentation and lysis by reducing the level of association between PBPs and their substrates, thereby
459 slowing their catalytic activity. To test this idea, we investigated whether the cell division defect of the

460 Δ*amiR* mutant could be ameliorated by artificially increasing the activity of the septal PG biosynthetic
461 machinery. To this end, employed a hyperactive (A246T) variant of the glycosyltransferase FtsW (FtsW*)
462 that leads to increased activity of the septal FtsW-PBP3 PG biosynthetic complex (Lariviere et al., 2019;
463 Modell et al., 2014), resulting in elevated cell constriction rates and shorter cell lengths, especially in
464 stationary phase (**Figure 10A,B**). Interestingly, introduction of the *ftsW** allele almost completely rescued
465 the cell filamentation phenotype of the Δ*amiR* mutant in stationary phase, although it had only little effect
466 in exponentially growing cells, possibly because PG precursors are more limiting under conditions of rapid
467 growth. Thus, hyperactivation of the FtsW-PBP3 complex can, at least in part, reverse the cell division
468 defect induced by defective PG recycling, suggesting that the cell filamentation phenotype observed in the
469 mutant backgrounds could indeed be due to a reduced activity of this complex. Notably, however, the
470 presence of the *ftsW** allele did not relieve the ampicillin sensitivity of Δ*amiR* cells (**Figure 10C**), indicating
471 that an increased activity of the septal PG biosynthetic complex does not reduce its ampicillin-mediated
472 inactivation.

Discussion

473 Bacterial PG biosynthesis has been studied intensively over the past decades. Importantly, apart from the
474 proper spatiotemporal control of peptidoglycan incorporation and cleavage during cell growth and cell
475 division, the recycling of PG degradation products has emerged to play a major role in cellular fitness and
476 survival. This process not only conserves valuable resources (Gilmore and Cava, 2025) but also plays an
477 important role in infection by enabling bacteria to evade the human innate immune system (Trindade and
478 Chen, 2020). Moreover, it was found to critically contribute to AmpR-mediated regulation of β-lactam
479 resistance in *P. aeruginosa* and various enterobacterial pathogens (Dik et al., 2018). Although substantial
480 advances have been made in elucidating the mechanisms and physiological roles of PG recycling within
481 Gammaproteobacteria, these aspects remain incompletely characterized across other bacterial lineages
482 (Gilmore and Cava, 2025). In this study, we demonstrate that the alphaproteobacterial model organism
483 *C. crescentus* possesses a functional PG recycling pathway that includes components from both the *E. coli*
484 and *P. aeruginosa* systems, extending the results of a recent study on this topic (Modi et al., 2025). We
485 find that its function is required for maintaining an adequate supply of peptidoglycan precursors, com-
486 plementing *de novo* synthesis. *C. crescentus* cells impaired in PG recycling show marked defects in cell
487 division and cell wall integrity. Moreover, they exhibit a pronounced decrease in intrinsic β-lactam resist-
488 ance, although the levels and activity of their major β-lactamase BlaA remain unchanged. These findings
489 are in line with previous work in *A. tumefaciens* showing that a defect in PG recycling caused by blocking
490 anhydro-muropeptide import impairs cell wall integrity and thereby reduces AmpC-mediated β-lactam
491 resistance in a manner that extends beyond its effect on AmpC regulation (Gilmore and Cava, 2022). Block-
492 ing critical steps in the recycling pathway therefore emerges as a promising new strategy to combat β-
493 lactam resistant pathogens and thus mitigate the global antibiotic crisis.

494 Our analyses revealed that *C. crescentus* possesses almost all core PG recycling enzymes identified in gam-
495 maproteobacteria. Notable exceptions are the LD-CPase LdcA (Templin et al., 1999), which trims sugar-
496 linked and free tetrapeptides to tripeptides, as well as the murein peptide ligase Mpl, which re-attaches
497 free peptide stems to UDP-Mur*N*Ac, thereby obviating the need for their *de novo* synthesis (Mengin-
498 Lecreulx et al., 1996). In *E. coli*, the activity of LdcA is critical for cell envelope integrity, because its inactiv-
499 ation leads to the accumulation of free tetrapeptides, which are then erroneously ligated with UDP-
500 Mur*N*Ac, giving rise to non-crosslinkable tetrapeptide-containing PG precursors, whose incorporation into
501 peptidoglycan severely destabilizes the cell wall structure (Templin et al., 1999). In some gammaproteo-
502 bacteria, the function of LdcA is taken over by other, unrelated peptidases (Dai et al., 2021; Hernández et
503 al., 2020; Simpson et al., 2021), opening the possibility that *C. crescentus* possesses a thus-far unknown

504 peptide-processing LD-CPase. However, metabolomic analysis showed that Δ*amiR* cells accumulated high
505 concentrations of anhMur*N*Ac-tetrapeptide in their cytoplasm (**Figure 3B**), making the existence of such
506 an enzyme unlikely. In line with the absence of Mpl, *C. crescentus* may thus not recycle tripeptides but
507 rather degrade peptide stems released by AmiR into individual amino acids, which are subsequently re-
508 used for *de novo* PG biosynthesis. A similar situation may be seen for many other Gram-negative and Gram-
509 positive species that lack both an LdcA and an Mpl homolog (Gilmore and Cava, 2025).

510 Apart from the removal of the peptide stem by AmiR, the cleavage of the Glc*N*Ac–anhMur*N*Ac moiety by
511 NagZ is a critical step in the initial processing of imported anhydro-muropeptide species. The results of our
512 enzyme assays (**Figures 2**) and metabolomic analyses (**Figure 3**) show that these two reactions do not
513 follow a defined order but occur independently of each other. Once released, the two amino sugars follow
514 distinct metabolic routes. Glc*N*Ac is phosphorylated to Glc*N*Ac-6-P and then deacetylated by NagA, yield-
515 ing GlcN-6-P, which is then either used as the starting point of *de novo* PG biosynthesis or, alternatively,
516 fed into central carbon metabolism through deamination to frucose-6-P by NagB (**Figure 1**). This branch
517 point is critical since Glc*N*Ac is not only produced during peptidoglycan degradation but also acquired from
518 the environment as a readily available carbon source, primarily derived from the breakdown of chitin
519 (Beier and Bertilsson, 2013). In the presence of external GlcNAc, two related gene clusters are highly
520 upregulated, each of them including genes for an outer-membrane TonB-dependent receptor, a PTS
521 permease together with its cognate phosphorylation system as well as a homolog of the deacetylase NagA
522 and the deaminase NagB (**Figure 5D,E**). Their regulation is likely mediated by GntR-type transcriptional
523 regulators encoded in the same clusters, which may sense the accumulation of Glc*N*Ac-6-P as the first
524 common cytoplasmic intermediate of the PG recycling and Glc*N*Ac uptake pathways, thereby adapting the
525 flux through the Glc*N*Ac recycling/utilization pathway to substrate availability. While one of the TonB-
526 dependent receptors (CCNA_00455) was shown to be specific for Glc*N*Ac (Eisenbeis et al., 2008), the
527 substrate range of the other transport systems still remains to be determined. Overall, the Glc*N*Ac
528 recycling/utilization system of *C. crescentus* shows parallels to that of *E. coli*, which also involves two
529 different PTS permeases, NagE and ManXYZ, for Glc*N*Ac transport (Plumbridge and Vimr, 1999). However,
530 *E. coli* lacks a Glc*N*Ac-specific TonB-dependent receptor, shows a different organization and regulation of
531 the genes involved and only possesses a single set of NagA and NagB proteins. Even more pronounced
532 differences are observed for the recycling of anhMur*N*Ac, which in both species initiates with the forma-
533 tion of anhMur*N*Ac-6-P. In *E. coli*, this intermediate is converted to Glc*N*Ac-6-P by the etherase MurQ and
534 thus funneled into the Glc*N*Ac recycling pathway (Jaeger et al., 2005; Uehara et al., 2006). *C. cresentus*, by
535 contrast, lacks this enzyme and instead uses the alternative MurU pathway, a short-cut that transforms

536 Mur*N*Ac-6-P to UDP-Mur*N*Ac and thus feeds it back directly into PG biosynthesis (**Figures 6 and 7**). This
537 pathway has so-far only been observed in a few other species such as the gammaproteobacteria *P. aeru-*
538 *ginosa* (Borisova et al., 2017; Fumeaux and Bernhardt, 2017; Gisin et al., 2013) and *Legionella pneumophila*
539 (Ratna et al., 2025) as well as *Tannerella forsythia* (Hottmann et al., 2021), a member of the Bacteroidia.
540 Our results, combined with those of a previous study (Modi et al., 2025), show that it is more widespread
541 than previously anticipated and also conserved in the alphaproteobacterial lineage.

542 In previously studied model species, PG recycling was found to be dispensable under laboratory conditions
543 and defects in this process did not lead to any obvious morphological defects (Gilmore and Cava, 2025;
544 Park and Uehara, 2008), except for the lack of LdcA, which causes cell rounding and lysis in stationary
545 phase in *E. coli* (Templin et al., 1999). In *C. crescentus*, it was also possible to introduce single deletions in
546 all PG recycling-related genes, although it was not possible to create a strain lacking both *nagA* homologs
547 simultaneously, suggesting that the accumulation of Glc*N*Ac-6-P may be toxic to the cells. Notably,
548 however, and contrary to a previous report (Modi et al., 2025), most mutants displayed cell division defects
549 and cell filamentation, especially when transitioning to stationary phase. These phenotypes were
550 particularly pronounced for Δ*ampG* and Δ*amiR* cells, which are impaired in anhydro-muropeptide uptake
551 or peptide stem cleavage. By contrast, single disruptions in the sugar recycling pathways generally did not
552 result in cell elongation, suggesting that the observed filamentation phenotype is linked to impaired
553 peptide recycling. Interestingly, while completely abolishing sugar recycling through inactivation of NagZ
554 did not cause any obvious morphological defects, blocking both the Glc*N*Ac and anhMur*N*Ac recycling
555 branches led to cell filamentation. This conundrum may be explained by the accumulation of metabolic
556 intermediates in the double mutant that may cause misregulation of PG biosynthesis by affecting gene
557 expression or enzyme activities. The precise link between PG recycling and cell division remains to be
558 clarified. However, we observed that blocking the initial steps of PG recycling leads to a severe reduction
559 in the levels of PG precursors such as UDP-Glc*N*Ac and UDP-Mur*N*Ac (**Figure 9E**). This effect may be even
560 more pronounced for the peptide-containing downstream products of the PG biosynthetic pathway, which
561 were not detectable with our methods, in particular in mutant backgrounds preventing the recycling of
562 the peptide stem. Importantly, the cell division defects caused by impaired PG recycling were alleviated
563 by hyperactivation of the FtsW-PBP3 complex (**Figure 10**). Together, these findings suggest that reduced
564 PG precursor levels impair the association of divisome-associated GTases and PBPs with their substrates,
565 leading to lower catalytic rates and a slow-down of cell constriction. This effect may be further aggravated
566 in the presence of ampicillin, because β-lactam-mediated inhibition of transpeptidase activity can
567 hyperactivate the GTase domain of bifunctional PBPs. As a consequence, they produce an abundance of

568 non-crosslinked glycan strands that are rapidly degraded after synthesis by LTs, leading to further
569 depletion of the lipid II pool (Banzhaf et al., 2012; Cho et al., 2014; Kohlrausch and Höltje, 1991). Moreover,
570 apart from decreasing PG synthase activity, defects in PG recycling may also cause an accumulation of
571 anhydro-muropeptides in the periplasm, which could potentially interfere with normal PG biosynthesis by
572 occupying binding sites or promoting non-productive side-reactions. Interestingly, in contrast to cell divi-
573 sion, longitudinal growth proceeds normally in the absence of PG recycling, possibly because it requires
574 less PG incorporation than cell constriction and the formation of the new cell poles. The morphological
575 defects caused by PG precursor limitation can be compensated by enhancing the activity of the FtsW-PBP3
576 complex and thereby increasing its catalytic rate under conditions of reduced binding site occupancy,
577 confirming that defective PG recycling affects cell division at the level of the septal PG biosynthetic
578 complex.

579 Defects in PG recycling not only caused cell filamentation but also strongly reduced the intrinsic resistance
580 of *C. crescentus* to ampicillin. This phenomenon was most pronounced for mutants with defects in the first
581 PG recycling steps that completely abolished peptide and/or sugar recycling (**Figure 4**). A milder effect was
582 observed for mutants blocked in the MurU pathway, whereas disrupting Glc*N*Ac recycling did not produce
583 any obvious ampicillin sensitivity phenotype. Our results suggest that the formation of UDP-Mur*N*Ac as
584 the first committed step in PG biosynthesis represents a metabolic bottleneck (**Figure 9E**), making
585 anhMur*N*Ac recycling through the MurU shunt essential for maintaining adequate PG precursor levels.
586 UDP-Glc*N*Ac, by contrast, which is used in the biosynthesis in various cell envelope polysaccharides, can
587 be more readily replenished because its biosynthesis is supported not only by *de novo* synthesis and
588 peptidoglycan (PG) recycling but also by the uptake of external Glc*N*Ac from the growth medium (Eisenbeis
589 et al., 2008) (**Figure 5D,E**). Notably, even high concentrations of external Glc*N*Ac were not sufficient to
590 restore ampicillin resistance in any of the PG recycling-deficient mutants tested (**Figure 9–figure supple-**
591 **ment 2**). Contrary to a previous report (Modi et al., 2025), this finding supports the notion that their β-
592 lactam sensitivity is not attributable to an inadequate supply of Glc*N*Ac for PG precursor biosynthesis.

593 A role of PG recycling in β-lactam resistance has been previously reported for gammaproteobacteria such
594 as *P. aeruginosa* and *C. freundii*. In these species, β-lactam exposure leads to an increase in the cytoplasmic
595 level of anhMur*N*Ac-pentapeptide, thereby stimulating its interaction with the transcriptional regulator
596 AmpR and inducing expression of the *ampC* β-lactamase gene (Dik et al., 2018). However, recent work has
597 indicated that different mechanisms may be at work in Alphaproteobacteria (Gilmore and Cava, 2022;
598 Modi et al., 2025). Our data show that, in *C. crescentus*, the accumulation and activity of the main β-
599 lactamase BlaA remain unchanged in the presence of ampicillin and upon inhibition of PG recycling. The

600 lower ampicillin resistance level of PG recycling-deficient mutants may therefore not be due to less effici-
601 ent inactivation of ampicillin but rather an increased susceptibility of PBPs to this antibiotic. This effect
602 could potentially be explained by competition of ampicillin and PG precursors for the substrate-binding
603 sites of target PBPs (**Figure 11**). In wild-type cells, the abundant supply of precursor ensures the saturation
604 of PBPs with their cognate substrate. As a consequence, most ampicillin molecules will be cleaved by BlaA
605 before they manage to covalently modify their target proteins, leaving the vast majority of PBPs in a
606 functional state. However, if defects in PG recycling limit the availability of PG precursors, the substrate
607 binding sites of PBPs remain unoccupied for extended periods of time. As a consequence, they become
608 more susceptible to interaction with residual ampicillin molecules, leading to an increase in the fraction of
609 inactive enzymes. The resulting defects in cell division and cell wall integrity may be further aggravated by
610 reduced activity of the remaining PBPs due to insufficient substrate availability and by the accumulation
611 of periplasmic anhydro-muropeptides, which could block the substrate-binding sites of PG metabolic
612 enzymes. Conversely, while interfering with cell division, the increased occupation of binding sites by
613 excess anhydro-muropeptides may also hinder the interaction of ampicillin with its target PBPs – especially
614 in the Δ*ampG* mutant – thereby reducing the susceptibility of cells to the antibiotic. In different PG
615 recycling-deficient mutants, these factors may be manifested to varying degrees, which could account for
616 differences in the severity between the cell filamentation and ampicillin sensitivity phenotypes in many of
617 the mutant strains.

618 Collectively, our results demonstrate that PG recycling is critical for proper growth, cell division and β-
619 lactam resistance in *C. crescentus*, thus playing a more significant role in bacterial fitness and survival than
620 previously appreciated. Moreover, they support the idea that bacterial β-lactam resistance is a complex
621 trait, determined not only by specific resistance proteins but also by the supply of PG building blocks and
622 the dynamics of PG biosynthesis. Given the widespread occurrence of PG recycling among bacteria, it will
623 be important to determine the impact of this process on cell viability and antibiotic resistance in other
624 species and to evaluate its inhibition as a potential new strategy to potentiate the efficacy of β-lactam
625 antibiotics in antibacterial therapies.

Methods

Experimental models

626 The bacterial strains used in this study are derivatives of *Caulobacter crescentus* NA1000 (CB15N)
627 (Poindexter, 1964), *Escherichia coli* TOP10 (Thermo Fisher Scientific, Germany) or *Escherichia coli*
628 Rosetta(DE3)pLysS (Merck, Germany). The sequences of all genes and proteins investigated are based on
629 the genome sequence of *C. crescentus* NA1000 (Nierman et al., 2001).

630 Cultivation of bacterial strains

631 *C. crescentus* NA1000 (CB15N) and its derivatives were grown at 28 °C in peptone-yeast-extract (PYE) medi-
632 um (Poindexter, 1964), double-concentrated PYE (2xPYE) medium or M2 salts-glucose (M2G) minimal
633 medium (Hottes et al., 2004) under aerobic conditions, shaking at 210 rpm. To prepare PYE plates, liquid
634 medium was solidified by the addition of 1.5% agar. To ensure the maintenance of integrative plasmids,
635 media were supplemented with kanamycin (5 µg/mL for liquid cultures, 25 µg/mL for plates). To counter-
636 select against cells carrying the *sacB* marker, solid PYE medium was supplemented with 3% D-sucrose.
637 *E. coli* TOP10 (Invitrogen, Germany) was used for cloning purposes, whereas *E. coli* Rosetta(DE3)pLysS
638 (Novagen, Germany) was used for protein overproduction. Cells were grown aerobically at 37 °C in LB
639 Broth or on LB Agar (Carl Roth, Germany), supplemented when appropriate with antibiotics at the follow-
640 ing concentrations (µg/mL; liquid/solid): kanamycin (30/50), ampicillin (200/200), chloramphenicol
641 (20/30).

642 Plasmid and strain construction

643 The bacterial strains, plasmids and oligonucleotides used in this study are listed in **Supplementary files 2-**
644 **4**. *E. coli* TOP10 (Invitrogen) was used as host for cloning purposes. *C. crescentus* was transformed by
645 electroporation (Ely, 1991). Gene replacement was achieved by double homologous recombination using
646 the counter-selectable *sacB* marker (Thanbichler and Shapiro, 2006). Proper chromosomal integration or
647 gene replacement was verified by colony PCR.

648 Antibiotic susceptibility assay

649 Overnight cultures were serially diluted (10^{-2} to 10^{-7}) in PYE medium and spotted on PYE plates containing
650 ampicillin (10-50 µg/mL) or aztreonam (95-105 µg/mL) at the indicated concentrations. When appropriate,
651 the media were additionally supplemented with 0.3% Glc*N*Ac. The plates were incubated for three days at
652 room temperature (25 °C) and imaged using a ChemiDocTM XRS+ Imager (Biorad, Germany) and Image

653 Lab™ software (version 5.0) (Biorad, Germany). To account for the high instability of ampicillin in aqueous
654 solution, ampicillin stocks were prepared freshly before every experiment.

655 The resistance against fosfomycin was assessed using Fosfomycin MIC Test Strips (Liofilchem, Italy). Over-
656 night cultures were diluted with PYE medium to an OD_{600} of 0.1. Subsequently, 100 µL of the suspensions
657 were added to 20 mL of sterile liquid PYE agar that had been cooled to slightly above the gelation temper-
658 ature (~45 °C). After mixing, the suspension was immediately poured into cultivation dishes. After solidifi-
659 cation of the medium, the plates were briefly dried and the test strips were applied on their top. Subse-
660 quently, they were incubated for three days at 28 °C and imaged using a ChemiDocTM XRS+ Imager and
661 Image Lab™ 5.0 software (Bio-Rad Laboratories, Germany).

662 **Widefield fluorescence microscopy**

663 Unless indicated otherwise, cells were grown in PYE medium, transferred to 1% agarose pads and imaged
664 with a Zeiss Axio Imager.Z1 microscope equipped with a Plan Apochromat 100×/1.45 Oil DIC and a
665 100×/1.40 Oil Ph3 M27 phase contrast objective. Images were recorded with a pco.edge 4.2 sCMOS
666 camera (PCO). An X-Cite 120PC metal halide light source (EXFO, Canada) and an ET-DAPI filter cube
667 (Chroma, USA) were used for the detection of fluorescence signals. Images were recorded with VisiView
668 4.0.0.14 (Visitron Systems, Germany) and processed with Fiji 1.53 (Schindelin et al., 2012). Cell length
669 measurements were performed with Oufti (Paintdakhi et al., 2016), using phase-contrast images as an
670 input.

671 **Microfluidics-based ampicillin sensitivity assay**

672 Microfluidic-based imaging was performed using a CellASIC ONIX B04A plate for bacterial cells (Merck,
673 Germany) that was connected to a CellASIC® ONIX2 microfluidic system (Merck, Germany) and imaged
674 with an Zeiss Axio Observer.Z1 (see above) in a heatable enclosure adjusted to 28 °C. Exponentially grow-
675 ing *C. crescentus* wild-type and Δ*amiR* cells were diluted to an OD_{600} of 0.2 and flushed into different cham-
676 bers of the microfluidic plate. They were then first incubated for 3 h with a constant flow of PYE medium
677 and then for 5 h with a constant flow of PYE medium containing 20 µg/mL ampicillin at a pressure of 5 kPa.
678 DIC images were taken at 5-min intervals to follow cell growth and division.

679 **β-lactamase activity assay**

680 ß-lactamase activity was assessed using the chromogenic cephalosporin derivative nitrocefin (Merck,
681 Germany) as a substrate (O'Callaghan et al., 1972). Cells were grown to exponential phase in 3 mL PYE
682 medium, harvested by centrifugation for 5 min at 7,000 ×*g* and room temperature, and resuspended in
683 1 mL PBS. After transfer of the suspensions into a 24-well polystyrene microplate (Carl Roth, Germany),

684 the reactions were started by the addition of 100 µL nitrocefin (1 mg/mL). The hydrolysis of nitrocefin was
685 then monitored by measuring the increase in absorbance at 482 nm every 2 min over a period of 180
686 minutes at 30 °C using an Epoch™ 2 microplate reader (BioTek, California, United States).

687 **Identification of ampicillin target proteins**

688 *C. crescentus* CS606 (Δ*blaA*) cells were grown to exponential phase in 100 mL PYE medium, harvested,
689 washed with PBS and lysed by three passages through a French press at 10,000 psi. Insoluble material,
690 including the membrane fraction, was collected by centrifugation for 15 min at 21,000 ×g (4 °C). After
691 resuspension of the pellet in 2 mL of PBS, 100-µL aliquots were incubated with 0, 1, 10 or 100 µg/mL
692 ampicillin, 5 µg/mL cefalexin or 100 µg/mL mecillinam for 2 h at room temperature. The membranes were
693 collected again by centrifugation (1 min, 13,000 ×g, room temperature), washed twice with PBS and resus-
694 pended in a final volume of 100 µL PBS containing 5 µg/mL Bocillin-FL (Thermo Fisher Scientific, Germany).
695 After 10 min of incubation, the membranes were collected by centrifugation (1 min, 13,000 ×g, room
696 temperature), washed with PBS, dissolved in 30 µL of 2x SDS sample buffer (0.125 M Tris Base, 20 % [v/v]
697 glycerol, 4 % [w/v] SDS, 200 mM DTT, 0.01 % [w/v] bromophenol blue, pH 6.8), heated for 10 min at 90 °C
698 and loaded onto an 8% SDS-polyacrylamide gel. After separation by electrophoresis, proteins labelled with
699 Bocillin-FL were detected with a ChemiDoc™ MP imager (Bio-Rad Laboratories, Germany) using a 526 nm
700 short-pass filter.

701 **β-galactosidase assay**

702 Cultures were grown to exponential phase in PYE medium. After determining the cell densities (OD_{600}), the
703 cells were harvested by centrifugation for 7 min at 12,000 ×*g* and 4 °C and resuspended in 1 mL of Z-buffer
704 (60 mM Na_2PO_4, 40 mM NaH_2PO_4, 10 mM KCl, 1 mM $MgSO_4$, 50 mM β-mercaptoethanol, pH 7.0). Following
705 the addition of 100 µL chloroform and 0.1 % SDS, the suspensions were briefly agitated and then incubated
706 for 7 min at room temperature to permeabilize the cells. 500-µL samples of the suspensions were mixed
707 with 500 µL of Z-buffer. The reactions were then started by the addition of 200 µL *o*-nitrophenyl-β-D-
708 galactopyranoside (4 mg/mL), incubated at room temperature until the mixtures turned yellow, and
709 stopped by the addition of 500 µL 1 M Na_2CO_3. Cell remnants were pelleted by centrifugation and the
710 extinction of the supernatant was measured photometrically at 550 nm and 420 nm. β-galactosidase
711 activities were then calculated as follows: Activity (in Miller units)=$1000*(OD_{420}–1.75*OD_{550})/(t*V*OD_{600})$,
712 where *t* is the time of incubation (min) and *V* the culture volume used for the reaction (mL).

713 **Protein purification**

714 To purify **AmiR and AmiR*** (H26A/H133A/D143A), *E. coli* Rosetta(DE3)pLysS was transformed with plas-
715 mids encoding His_6-SUMO-tagged derivatives (Marblestone et al., 2006) of the proteins (pPR029 or
716 pPR041) and grown in LB medium to an OD_{600} o 0.4. After reduction of the growth temperature to 18 °C,
717 the cultures were supplemented with isopropyl-β-D-thiogalactopyranoside (IPTG) to a final concentration
718 of 1 mM, and incubated further overnight. The cells were harvested by centrifugation (12 min, 5000 ×g,
719 4 °C), washed in buffer A (50 mM Tris-HCl, 500 mM NaCl, 10 mM imidazole, 10% glycerol, pH 7.0) and
720 stored at -80 °C until needed. After thawing, the cells were resuspended in buffer A containing 100 µg/mL
721 phenylmethylsulfonyl fluoride (PMSF) and 10 µg/mL DNaseI and lysed by three passages through a French
722 press at a pressure of 10,000 psi. The lysate was cleared by centrifugation (30 min, 25,000 ×g, 4 °C) and
723 loaded onto a His-Trap HP 5 mL Ni-NTA affinity column (Cytiva, Germany) equilibrated with buffer A. After
724 washing of the column with buffer A, protein was eluted at a flow rate of 2 mL/min with a linear gradient
725 of imidazole generated by mixing buffer A and buffer B (50 mM Tris-HCl, 500 mM NaCl, 250 mM imidazole,
726 10% glycerol, pH 7.0). The peak fractions were pooled, supplemented with SUMO protease (His_6-Ulp)
727 (Marblestone et al., 2006) at a molar ratio of 1:1,000 relative to the purified protein, and dialyzed overnight
728 at 4 °C against buffer C (50 mM Tris-HCl, 500 mM NaCl, 10% glycerol, 1 mM dithiothreitol, pH 7.0). The
729 solution was then loaded again onto a His-Trap HP 5 mL column to remove His_6-SUMO and His_6-Ulp. Flow-
730 through fractions containing the protein of interest were collected, concentrated using Amicon® Ultra cen-
731 trifugation filters (10kDa MWCO; Merck, Germany), and loaded onto a Superdex 75 GL10/300 size-
732 exclusion column (Cytiva, Germany) equilibrated with buffer D (50 mM HEPES-NaOH, 500 mM NaCl, pH
733 7.0) and eluted at a flow rate of 10 mL/min. Fractions containing the protein of interest at high concen-
734 tration and purity were combined, concentrated, snap-frozen in liquid nitrogen and stored at -80 °C until
735 further use.

736 To purify **NagZ and NagZ*** (D259A), His_6-SUMO-tagged derivatives of the proteins were overproduced in
737 *E. coli* Rosetta(DE3)pLysS carrying suitable plasmids (pPR102 or pPR107) as described above. The fusion
738 proteins were then purified on a His-Trap HP 5 mL column, cleaved with SUMO protease, and separated
739 from His_6-SUMO and His_6-Ulp by a second affinity purification step essentially as described for AmiR, with
740 the exceptions that buffers A and B contained 300 mM instead of 500 mM NaCl and buffer C contained
741 150 mM instead of 500 mM NaCl. Flow-through fractions from the His-Trap HP column that contained the
742 protein of interest at high concentration and purity were concentrated, snap-frozen in liquid nitrogen and
743 stored at -80 °C.

744 **Muropeptide analysis**

745 The *C. crescentus* wild type and the Δ*amiR* mutant were grown to stationary phase ($OD_{600} \approx 1.2$) in 400 mL
746 PYE medium and harvested by centrifugation at 16,000 ×*g* and 4 °C for 30 min. The pelleted cells were
747 resuspended in 6 mL of ice-cold double-ionized water ($_{dd}H_2O$) and added dropwise to 6 mL of a boiling
748 solution of 8% sodium dodecylsulfate (SDS), which was vigorously stirred. The suspension was boiled for
749 an additional 30 min, and double-deionized water was added regularly to maintain a constant volume.
750 Subsequently, the lysate was cooled to room temperature and stored at 4 °C until further use. Peptido-
751 glycan was isolated following previously described procedures (Glauner, 1988; Takacs et al., 2010) and
752 digested with the muramidase cellosyl (kindly provided by Hoechst, Frankfurt, Germany). The resulting
753 muropeptides were reduced with sodium borohydride and separated by HPLC as described previously
754 (Takacs et al., 2010). The identity of eluted fragments was assigned based on the retention times of known
755 muropeptides (Takacs et al., 2010).

756 **AmiR and NagZ activity assays**

757 To test the activity of AmiR towards anhydro-muropeptides, peptidoglycan from *E. coli* D456 (Edwards and
758 Donachie, 1993), which lacks three major DD-carboxypeptidases and thus has elevated levels of penta-
759 peptides, was treated with the soluble lytic transglycosylase Slt70 from *E. coli* (Banzhaf et al., 2020; Betzner
760 and Keck, 1989). The products were incubated with wild-type AmiR or a catalytically inactive AmiR deriva-
761 tive (AmiR*) in a total volume of 50 µl in buffer H (20 mM HEPES-NaOH, 50 mM NaCl, 1 mM $MgCl_2$, pH 7.5)
762 at 37 °C for 16 h in a thermal shaker set to 900 rpm. The reactions were stopped by incubation at 100 °C
763 for 10 min in a dry-bed heater. After clearance of the mixtures by centrifugation at 17,000 ×*g* for 10 min,
764 the supernatants were acidified to pH 4.0 – pH 4.5 with 20% phosphoric acid. Subsequently, the reaction
765 products were separated by HPLC as described previously (Izquierdo-Martinez et al., 2023). The activity of
766 AmiR towards muropeptides with reducing ends was tested in a similar manner. However, peptidoglycan
767 from *E. coli* D456 was treated with the muramidase cellosyl from *Streptomyces coelicolor* (Bräu et al.,
768 1991). After incubation with the enzyme, heat inactivation and centrifugation, the supernatants were
769 mixed with an equal volume of 0.5 M sodium borate (pH 9.0), followed by reduction of the muropeptides
770 with ~1 mg of sodium borohydride. The samples were then acidified to pH 4.0 – pH 4.5 with 20% phos-
771 phoric acid and analyzed by HPLC as described previously (Glauner, 1988).

772 The enzymatic activity of NagZ towards anhydro-muropeptides or reducing muropeptides was analyzed as
773 described for AmiR, but with the following modifications. Peptidoglycan from *E. coli* CS703-1 (Meberg et
774 al., 2001), which lacks all major DD-carboxypeptidases, was treated with the lytic transglycosylase MltA
775 from *E. coli* (Lommatzsch et al., 1997) to produce anhydro-muropeptides or with cellosyl to produce muro-

776 peptides with reducing ends. The lytic products were incubated with NagZ or a catalytically inactive NagZ
777 variant (NagZ*) (10 µM) and processed as described above.

778 To determine the activity of AmiR towards undigested peptidoglycan, sacculi isolated from *E. coli* D456
779 (Glauner, 1988; Takacs et al., 2010) were incubated with AmiR or AmiR* (10 µM) in buffer H at 37 °C for
780 16 h in a thermal shaker set to 900 rpm. The reactions were stopped by heating at 100 °C for 10 min in a
781 dry-bed heater. Subsequently, the sacculi were digested with cellosyl overnight. After heat inactivation of
782 cellosyl at 100 °C for 10 min and clearance of the mixtures by centrifugation, the reaction products were
783 reduced with borohydride. The samples were then acidified to pH 4.0 – pH 4.5 with 20% phosphoric acid
784 and analyzed by HPLC as described previously (Glauner, 1988).

785 In the above analyses, disaccharide-containing muropeptides and anhydro-muropeptides were identified
786 based on their known retention times and peak patterns (Glauner, 1988). The identities of the Glc*N*Ac–
787 anhMur*N*Ac disaccharide generated by AmiR and the anhMur*N*Ac-peptides generated by NagZ were
788 determined by HPLC separation of the reaction products and mass spectrometric analysis of the different
789 peak fractions (**Figure 2–figure supplement 4**).

790 To assess the activity of AmiR against anhydro-muropeptide species lacking the Glc*N*Ac moiety, a solution
791 of purified Glc*N*Ac–anhMur*N*Ac-tetrapeptide (5 µL) was incubated with purified NagZ (10 µM) in 90 µL
792 reaction buffer (50 mM HEPES, 200 mM NaCl, 10 % [v/v] glycerol, pH 7.2) with shaking for 16 h at 37°C.
793 Subsequently, the reactions were supplemented with AmiR or AmiR* (10 µM) and incubated for another
794 4 h. The mixtures were acidified by the addition of 10 µL of 10% [v/v] formic acid, and precipitated protein
795 was removed by centrifugation for 10 min at 30,130 ×g. The cleared solutions were then subjected to liquid
796 chromatography-mass spectrometry (LC-MS) analysis for semi-quantitative determination of the reaction
797 products, as described under 'Metabolomics analysis'. The compounds of interest were identified based
798 on their theoretical mass-to-charge (m/z) ratios.

799 **Metabolomics analysis**

800 Anhydro-muropeptides were quantified essentially as described previously (Jacobs et al., 1994; Simpson
801 et al., 2023). In brief, cultures were grown overnight in 10 mL PYE medium (OD_{600} = 1.2) and harvested by
802 centrifugation for 10 min at 21,000 ×*g* and 4 °C. The pelleted cells were washed three times with 0.9%
803 NaCl, resuspended to a final volume of 100 µL in 0.9% NaCl and heated for 7 min at 98 °C. The suspension
804 was cleared by centrifugtation for 15 min at 21,000 ×*g.* The supernatant was isolated, centrifuged again
805 to remove residual cell debris, and then subjected to liquid chromatography-mass spectrometry (LC-MS)
806 analysis for semi-quantitative determination of PG recycling or biosynthesis intermediates. The chromato-

807 graphic separation was performed on an Agilent Infinity II 1290 HPLC system using a ZicHILIC SeQuant
808 column (150 × 2.1 mm, 3.5 µm particle size, 100 Å pore size) connected to a ZicHILIC guard column (20 ×
809 2.1 mm, 5 µm particle size) (Merck KgAA) at 25° C and at a constant flow rate of 0.3 mL/min, with mobile
810 phase A being 0.1% formic acid in 99:1 water:acetonitrile (Honeywell, Morristown, NJ, USA) and phase B
811 being 0.1% formic acid in 99:1 acetonitrile:water (Honeywell, Morristown, NJ, USA). The injection volume
812 was 5 µL. The mobile phase profile comprised the following steps and linear gradients: 0 – 1 min constant
813 at 80% B; 1 – 10 min from 80 to 10% B; 10 – 12 min constant at 10% B; 12 – 12.1 min from 10 to 80% B; 12
814 to 14 min constant at 80% B. An Agilent 6546A QTOF mass spectrometer was used in high-resolution,
815 positive mode with a mass range of 70 – 1700 m/z and a scan rate of 1.5 spectra/second. An electrospray
816 ionization source was used at the following conditions: ESI spray voltage 4000 V, nozzle voltage 500 V,
817 sheath gas 250° C at 12 l/min, nebulizer pressure 60 psig and drying gas 100 °C at 11 l/min. Compounds
818 were identified based on their accurate mass and retention time, applying an extraction tolerance of 5
819 ppm. Chromatograms were integrated using MassHunter software (Agilent, CA, USA). Relative abundance
820 was determined based on the peak area.

821 To determine the cytoplasmic amounts of the PG precursors UDP-Glc*N*Ac and UDP-Mur*N*Ac, the strains to
822 be analyzed were cultivated overnight in PYE medium, followed by determination of their optical densities
823 (OD_{600}). Subsequently, 1-mL samples of the cultures were mixed with 1 mL of 70% LC-MS-Grade MeOH
824 (Merck, Germany) and subjected to centrifugation at 13,000 ×*g* and -9 °C for 10 min. To extract the endo-
825 metabolome, the pelleted cells were mixed with 100 µL per OD_{600} unit of extraction fluid (50% LC-MS-
826 Grade MeOH, 5 mM Tris, 0.5 mM EDTA) and the same amount of chloroform, followed by incubation at
827 4 °C for 2 h. After separation of the phases by centrifugation (max. speed, -9 °C, 10 min), the upper phase
828 was isolated, filtered using PTFE membrane filters (0.2 µm pore size) (Sartorius, Germany) and subjected
829 to LC-MS analysis. The chromatographic separation was performed on an Agilent Infinity II 1290 HPLC
830 system using a SeQuant ZIC-pHILIC column (150 × 2.1 mm, 5 µm particle size, peek coated, Merck) con-
831 nected to a guard column of similar specificity (20 × 2.1 mm, 5 µm particle size, Phenomoenex) at 40° C
832 and at a constant flow rate of 0.1 mL/min, with mobile phase A composed of 10 mM ammonium acetate
833 in water (pH 9) supplemented with medronic acid to a final concentration of 5 µM and mobile phase B
834 composed of 10 mM ammonium acetate in 90:10 acetonitrile:water (pH 9). The injection volume was 5
835 µL. The mobile phase profile comprised the following steps and linear gradients: 0 – 1 min constant at 75
836 % B; 1 – 6 min from 75 to 40% B; 6 to 9 min constant at 40% B; 9 – 9.1 min from 40 to 75% B; 9.1 to 20 min
837 constant at 75% B. An Agilent 6546A QTOF mass spectrometer was used in high-resolution, negative mode
838 with a mass range of 50 – 1700 m/z and a scan rate of 1.5 spectra/second. An electrospray ionization

839 source was used at the following conditions: ESI spray voltage 4000 V, nozzle voltage 500 V, sheath gas
840 300° C at 12 L/min, nebulizer pressure 20 psig and drying gas 150° C at 11 L/min. Compounds were
841 identified based on their accurate mass and retention time applying an extraction tolerance of 5 ppm.
842 Chromatograms were integrated using MassHunter software (Agilent, Santa Clara, CA, USA). Relative
843 abundance was determined based on the peak area.

844 **Whole-cell proteomics**

845 Cells were grown to exponential phase in 10 mL PYE medium, harvested by centrifugation (15,000 ×g, 10
846 min, 4 °C), washed three times with ice-cold PBS and resuspended in 300 µL of lysis buffer (2% sodium
847 lauroyl sarcosinate [SLS], 100 mM ammonium bicarbonate). The samples were then heated for 10 min at
848 90 °C, followed by sonication with a VialTweeter Sonicator (Hielscher Ultrasonics, Germany). Proteins were
849 reduced with 5 mM Tris(2-carboxyethyl)phosphine (Thermo Fischer Scientific, Germany) at 90 °C for 15
850 min and alkylated using 10 mM iodoacetamid (Sigma Aldrich, Germany) at 20 °C for 30 min in the dark.
851 Subsequently, they were precipitated by the addition of a sixfold excess of ice-cold acetone and incubation
852 for 2 h at -20 °C, followed by two washing steps with methanol. After drying, the proteins were reconsti-
853 tuted in 0.2% SLS and their amount was determined using a bicinchoninic acid (BCA) protein assay (Thermo
854 Scientific, Germany). Subsequently, 50 µg protein were subjected to tryptic digestion by incubation with 1
855 µg of trypsin (Serva) in 0.5% SLS at 30 °C overnight. After digestion, SLS was precipitated by adding a final
856 concentration of 1.5% trifluoroacetic acid (TFA, Thermo Fisher Scientific, Germany). The peptides were
857 desalted using CHROMAFIX C18 solid phase extraction cartridges (Macherey-Nagel, Germany), which were
858 prepared by the addition of acetonitrile and subsequent equilibration with 0.1% TFA. They were then
859 loaded on the equilibrated cartridges, washed with a mixture of 5% acetonitrile and 0.1% TFA, and finally
860 eluted with a mixture of 50% ACN and 0.1% TFA. After drying, the peptides were reconstituted in 0.1% TFA
861 and then analyzed using liquid-chromatography-mass spectrometry on an Exploris 480 instrument con-
862 nected to an UltiMate 3000 RSLCnano HPLC system and a Nanospray Flex ion source (all Thermo Scientific,
863 Germany). The following gradient was used for separation: 94% solvent A (0.15% formic acid) and 6%
864 solvent B (99.85% acetonitrile, 0.15% formic acid) to 25% solvent B over 40 min, followed by an increase
865 to 35% solvent B over 20 min at a flow rate of 300 nl/min. Peptides were ionized at a spray voltage of 2.3
866 kV, with the ion transfer tube temperature set at 275 °C. 445.12003 m/z was used as internal calibrant.

867 MS raw data were acquired on an Orbitrap Exploris 480 instrument (Thermo Scientific, Germany) in data-
868 independent acquisition (DIA) mode. The funnel RF level was set to 40. For DIA experiments, full MS resolu-
869 tion was set to 120.000 at m/z 200. The AGC target value for fragment spectra was set at 3000%. 45 win-
870 dows of 14 Da were used with an overlap of 1 Da between m/z 320-950. Resolution was set to 15,000 and

871 IT to 22 ms. A stepped HCD collision energy of 25, 27.5, 30 % was used. MS1 data were acquired in profile,
872 MS2 DIA data in centroid mode.

873 The analysis of DIA data was performed with DIA-NN version 1.8 (Demichev et al., 2020), based on a
874 protein database for *Caulobacter crescentus* NA1000 retrieved from UniProt (UniProt Consortium, 2025)
875 to generate a dataset-specific spectral library. The DIA-NN suite was used to perform noise interference
876 correction (mass correction, RT prediction and precursor/fragment co-elution correlation) and peptide
877 precursor signal extraction on the DIA-NN raw data. The following parameters were used: Full tryptic
878 digest was allowed with two missed cleavage sites, oxidized methionines and carbamidomethylated
879 cysteins. "Match between runs" and "Remove likely interferences" were enabled. The precursor FDR was
880 set to 1%. The neural network classifier was set to the single-pass mode, and protein inference was based
881 on genes. The quantification strategy was set to any LC (high accuracy). Cross-run normalization was set
882 to RT-dependent. Library generation was set to smart profiling. DIA-NN outputs were further evaluated
883 using the SafeQuant script (Ahrné et al., 2013; Glatter et al., 2012), modified to process DIA-NN outputs.
884 A detailed summary of the proteomics data obtained is provided in **Supplementary file 1**.

885 **Bioinformatic analysis**

886 Protein similarity searches were performed with BLAST (Altschul et al., 1990), using the BLAST server of
887 the National Institutes of Health (https://blast.ncbi.nlm.nih.gov/Blast.cgi). Protein structures were
888 predicted with Alphafold 3 (Abramson et al., 2024) and visualized using PyMOL v2.6.0a0 (Schrödinger LLC).
889 Proteomics data were visualized with VolcaNoseR (Goedhart and Luijsterburg, 2020).

890 **Quantification and statistical analysis**

891 Details on the number of replicates and the sample sizes are given in the figure legends. Datasets were
892 displayed using the SuperPlotsOfData web application (Goedhart, 2021), and an unpaired two-sided
893 Welch's *t*-test implemented in the application was used to assess the statistical significance of differences
894 between strains or conditions. Standard deviations were calculated in Microsoft Excel 2019.

895 **Availability of biological material**

896 The plasmids and strains used in this study are available from the corresponding author upon request.

References

897 Abramson, J, Adler, J, Dunger, J, Evans, R, Green, T, Pritzel, A, Ronneberger, O, Willmore, L, Ballard, AJ,
898 Bambrick, J*, et al.* (2024). Accurate structure prediction of biomolecular interactions with AlphaFold 3.
899 *Nature* **630**:493-500.

900 Ahrné, E, Molzahn, L, Glatter, T, Schmidt, A (2013). Critical assessment of proteome-wide label-free
901 absolute abundance estimation strategies. *Proteomics* **13**:2567-2578.

902 Altschul, SF, Gish, W, Miller, W, Myers, EW, Lipman, DJ (1990). Basic local alignment search tool. *J Mol Biol*
903 **215**:403-410.

904 Álvarez-Añorve, LI, Gaugué, I, Link, H, Marcos-Viquez, J, Diaz-Jiménez, DM, Zonszein, S, Bustos-Jaimes, I,
905 Schmitz-Afonso, I, Calcagno, ML, Plumbridge, J (2016). Allosteric activation of *Escherichia coli* glucos-
906 amine-6-phosphate deaminase (NagB) *in vivo* justified by intracellular amino sugar metabolite concen-
907 trations. *J Bacteriol* **198**:1610-1620.

908 Bacik, JP, Whitworth, GE, Stubbs, KA, Vocadlo, DJ, Mark, BL (2012). Active site plasticity within the glyco-
909 side hydrolase NagZ underlies a dynamic mechanism of substrate distortion. *Chem Biol* **19**:1471-1482.

910 Banzhaf, M, van den Berg van Saparoea, B, Terrak, M, Fraipont, C, Egan, A, Philippe, J, Zapun, A, Breukink,
911 E, Nguyen-Disteche, M, den Blaauwen, T*, et al.* (2012). Cooperativity of peptidoglycan synthases active
912 in bacterial cell elongation. *Mol Microbiol* **85**:179-194.

913 Banzhaf, M, Yau, HC, Verheul, J, Lodge, A, Kritikos, G, Mateus, A, Cordier, B, Hov, AK, Stein, F, Wartel, M*,*
914 *et al.* (2020). Outer membrane lipoprotein NlpI scaffolds peptidoglycan hydrolases within multi-enzyme
915 complexes in *Escherichia coli*. *EMBO J* **39**:e102246.

916 Barreteau, H, Kovac, A, Boniface, A, Sova, M, Gobec, S, Blanot, D (2008). Cytoplasmic steps of peptidogly-
917 can biosynthesis. *FEMS Microbiol Rev* **32**:168-207.

918 Beier, S, Bertilsson, S (2013). Bacterial chitin degradation–mechanisms and ecophysiological strategies.
919 *Front Microbiol* **4**:149.

920 Bendezu, FO, Hale, CA, Bernhardt, TG, de Boer, PA (2009). RodZ (YfgA) is required for proper assembly of
921 the MreB actin cytoskeleton and cell shape in *E. coli*. *EMBO J* **28**:193-204.

922 Bertsche, U, Kast, T, Wolf, B, Fraipont, C, Aarsman, ME, Kannenberg, K, von Rechenberg, M, Nguyen-
923 Disteche, M, den Blaauwen, T, Holtje, JV*, et al.* (2006). Interaction between two murein (peptidoglycan)
924 synthases, PBP3 and PBP1B, in *Escherichia coli*. *Mol Microbiol* **61**:675-690.

925 Betzner, AS, Keck, W (1989). Molecular cloning, overexpression and mapping of the *slt* gene encoding the
926 soluble lytic transglycosylase of *Escherichia coli*. *Mol Gen Genet* **219**:489-491.

927 Bi, EF, Lutkenhaus, J (1991). FtsZ ring structure associated with division in *Escherichia coli*. *Nature* **354**:161-
928 164.

929 Bisson-Filho, AW, Hsu, YP, Squyres, GR, Kuru, E, Wu, F, Jukes, C, Sun, Y, Dekker, C, Holden, S,
930 VanNieuwenhze, MS*, et al.* (2017). Treadmilling by FtsZ filaments drives peptidoglycan synthesis and
931 bacterial cell division. *Science* **355**:739-743.

932 Borisova, M, Gisin, J, Mayer, C (2014). Blocking peptidoglycan recycling in *Pseudomonas aeruginosa*
933 attenuates intrinsic resistance to fosfomycin. *Microb Drug Resist* **20**:231-237.

934 Borisova, M, Gisin, J, Mayer, C (2017). The *N*-acetylmuramic acid 6-phosphate phosphatase MupP
935 completes the *Pseudomonas* peptidoglycan recycling pathway leading to intrinsic fosfomycin resis-
936 tance. *mBio* **8**:e00092-00017.

937 Bräu, B, Hilgenfeld, R, Schlingmann, M, Marquardt, R, Birr, E, Wohlleben, W, Aufderheide, K, Puhler, A
938 (1991). Increased yield of a lysozyme after self-cloning of the gene in *Streptomyces coelicolor* "Müller".
939 *Appl Microbiol Biotechnol* **34**:481-487.

940 Bugg, TD, Braddick, D, Dowson, CG, Roper, DI (2011). Bacterial cell wall assembly: still an attractive
941 antibacterial target. *Trends Biotechnol* **29**:167-173.

942 Bush, K, Freudenberger, JS, Sykes, RB (1982). Interaction of azthreonam and related monobactams with β-
943 lactamases from Gram-negative bacteria. *Antimicrob Agents Chemother* **22**:414-420.

944 Chang, N, Kim, H, Kim, U, Cho, Y, Yoo, Y, Lee, H, Kim, JW, Kim, MS, Lee, J, Cho, YL*, et al.* (2025). Structural
945 and functional insights of AmpG in muropeptide transport and multiple β-lactam antibiotics resistance.
946 *Nat Commun* **16**:5744.

947 Cheng, Q, Li, H, Merdek, K, Park, JT (2000). Molecular characterization of the beta-*N*-acetylglucosamini-
948 dase of *Escherichia coli* and its role in cell wall recycling. *J Bacteriol* **182**:4836-4840.

949 Cheng, Q, Park, JT (2002). Substrate specificity of the AmpG permease required for recycling of cell wall
950 anhydro-muropeptides. *J Bacteriol* **184**:6434-6436.

951 Cho, H, Uehara, T, Bernhardt, TG (2014). Beta-lactam antibiotics induce a lethal malfunctioning of the
952 bacterial cell wall synthesis machinery. *Cell* **159**:1300-1311.

953 Cho, H, Wivagg, CN, Kapoor, M, Barry, Z, Rohs, PDA, Suh, H, Marto, JA, Garner, EC, Bernhardt, TG (2016).
954 Bacterial cell wall biogenesis is mediated by SEDS and PBP polymerase families functioning semi-
955 autonomously. *Nat Microbiol* **1**:16172.

956 Dai, Y, Pinedo, V, Tang, AY, Cava, F, Geisinger, E (2021). A new class of cell wall-recycling l,d-carboxy-
957 peptidase determines β-lactam susceptibility and morphogenesis in *Acinetobacter baumannii*. *mBio*
958 **12**:e0278621.

959 Demichev, V, Messner, CB, Vernardis, SI, Lilley, KS, Ralser, M (2020). DIA-NN: neural networks and
960 interference correction enable deep proteome coverage in high throughput. *Nat Methods* **17**:41-44.

961 Dietz, H, Pfeifle, D, Wiedemann, B (1997). The signal molecule for β-lactamase induction in *Enterobacter*
962 *cloacae* is the anhydromuramyl-pentapeptide. *Antimicrob Agents Chemother* **41**:2113-2120.

963 Dik, DA, Fisher, JF, Mobashery, S (2018). Cell-wall recycling of the Gram-negative bacteria and the nexus
964 to antibiotic resistance. *Chem Rev* **118**:5952-5984.

965 Dik, DA, Marous, DR, Fisher, JF, Mobashery, S (2017). Lytic transglycosylases: concinnity in concision of the
966 bacterial cell wall. *Crit Rev Biochem Mol Biol* **52**:503-542.

967 Docquier, JD, Pantanella, F, Giuliani, F, Thaller, MC, Amicosante, G, Galleni, M, Frère, JM, Bush, K, Rossolini,
968 GM (2002). CAU-1, a subclass B3 metallo-β-lactamase of low substrate affinity encoded by an ortholog
969 present in the *Caulobacter crescentus* chromosome. *Antimicrob Agents Chemother* **46**:1823-1830.

970 Edwards, D, Donachie, WD (1993). Construction of a triple deletion of penicillin-binding proteins 4, 5, and
971 6 in *Escherichia coli*. In Bacterial growth and lysis, M. de Pedro, J.-V. Höltje, and W. Löffelhardt, eds.
972 (New York and London: Plenum Press), pp. 369–374.

973 Egan, AJF, Errington, J, Vollmer, W (2020). Regulation of peptidoglycan synthesis and remodelling. *Nat Rev*
974 *Microbiol* **18**:446-460.

975 Eisenbeis, S, Lohmiller, S, Valdebenito, M, Leicht, S, Braun, V (2008). NagA-dependent uptake of *N*-acetyl-
976 glucosamine and *N*-acetyl-chitin oligosaccharides across the outer membrane of *Caulobacter cres-*
977 *centus*. *J Bacteriol* **190**:5230-5238.

978 Ely, B (1991). Genetics of *Caulobacter crescentus*. *Method Enzymol* **204**:372-384.

979 Evinger, M, Agabian, N (1977). Envelope-associated nucleoid from *Caulobacter crescentus* stalked and
980 swarmer cells. *J Bacteriol* **132**:294-301.

981 Fumeaux, C, Bernhardt, TG (2017). Identification of MupP as a new peptidoglycan recycling factor and
982 antibiotic resistance determinant in *Pseudomonas aeruginosa*. *mBio* **8**:e00102-00117.

983 Garner, EC, Bernard, R, Wang, W, Zhuang, X, Rudner, DZ, Mitchison, T (2011). Coupled, circumferential
984 motions of the cell wall synthesis machinery and MreB filaments in *B. subtilis*. *Science* **333**:222-225.

985 Généreux, C, Dehareng, D, Devreese, B, Van Beeumen, J, Frère, JM, Joris, B (2004). Mutational analysis of
986 the catalytic centre of the *Citrobacter freundii* AmpD *N*-acetylmuramyl-L-alanine amidase. *Biochem J*
987 **377**:111-120.

988 Gilmore, MC, Cava, F (2022). Peptidoglycan recycling mediated by an ABC transporter in the plant
989 pathogen *Agrobacterium tumefaciens*. *Nat Commun* **13**:7927.

990 Gilmore, MC, Cava, F (2025). Bacterial peptidoglycan recycling. *Trends Microbiol* **33**:340-353.

991 Gisin, J, Schneider, A, Nagele, B, Borisova, M, Mayer, C (2013). A cell wall recycling shortcut that bypasses
992 peptidoglycan *de novo* biosynthesis. *Nat Chem Biol* **9**:491-493.

993 Glatter, T, Ludwig, C, Ahrne, E, Aebersold, R, Heck, AJ, Schmidt, A (2012). Large-scale quantitative assess-
994 ment of different in-solution protein digestion protocols reveals superior cleavage efficiency of tandem
995 Lys-C/trypsin proteolysis over trypsin digestion. *J Proteome Res* **11**:5145-5156.

996 Glauner, B (1988). Separation and quantification of muropeptides with high-performance liquid
997 chromatography. *Anal Biochem* **172**:451-464.

998 Goedhart, J (2021). SuperPlotsOfData – a web app for the transparent display and quantitative comparison
999 of continuous data from different conditions. *Mol Biol Cell* **32**:470-474.

1000 Goedhart, J, Luijsterburg, MS (2020). VolcaNoseR is a web app for creating, exploring, labeling and sharing
1001 volcano plots. *Sci Rep* **10**:20560.

1002 Goodell, EW (1985) Recycling of murein by *Escherichia coli*. *J. Bacteriol.* **163**:305-310.

1003 Goodell, EW, Schwarz, U (1985). Release of cell wall peptides into culture medium by exponentially grow-
1004 ing *Escherichia coli*. *J Bacteriol* **162**:391-397.

1005 Hernández, SB, Dörr, T, Waldor, MK, Cava, F (2020). Modulation of peptidoglycan synthesis by recycled
1006 cell wall tetrapeptides. *Cell Rep* **31**:107578.

1007 Höltje, JV (1998). Growth of the stress-bearing and shape-maintaining murein sacculus of *Escherichia coli*.
1008 *Microbiol Mol Biol Rev* **62**:181-203.

1009 Höltje, JV, Kopp, U, Ursinus, A, Wiedemann, B (1994). The negative regulator of β-lactamase induction
1010 AmpD is a *N*-acetyl-anhydromuramyl-L-alanine amidase. *FEMS Microbiol Lett* **122**:159-164.

1011 Hottes, AK, Meewan, M, Yang, D, Arana, N, Romero, P, McAdams, HH, Stephens, C (2004). Transcriptional
1012 profiling of *Caulobacter crescentus* during growth on complex and minimal media. *J Bacteriol* **186**:1448-
1013 1461.

1014 Hottmann, I, Borisova, M, Schaffer, C, Mayer, C (2021). Peptidoglycan salvage enables the periodontal
1015 pathogen *Tannerella forsythia* to survive within the oral microbial community. *Microb Physiol* **31**:123-
1016 134.

1017 Izquierdo-Martinez, A, Billini, M, Miguel-Ruano, V, Hernandez-Tamayo, R, Richter, P, Biboy, J, Batuecas,
1018 MT, Glatter, T, Vollmer, W, Graumann, PL*, et al.* (2023). DipM controls multiple autolysins and mediates
1019 a regulatory feedback loop promoting cell constriction in *Caulobacter crescentus*. *Nat Commun*
1020 **14**:4095.

1021 Jacobs, C, Frère, JM, Normark, S (1997). Cytosolic intermediates for cell wall biosynthesis and degradation
1022 control inducible β-lactam resistance in Gram-negative bacteria. *Cell* **88**:823-832.

1023 Jacobs, C, Huang, LJ, Bartowsky, E, Normark, S, Park, JT (1994). Bacterial cell wall recycling provides
1024 cytosolic muropeptides as effectors for β-lactamase induction. *EMBO J* **13**:4684-4694.

1025 Jacobs, C, Joris, B, Jamin, M, Klarsou, K, Van Beeumen, J, Mengin-Lecreulx, D, van Heijenoort, J, Park, JT,
1026 Normark, S, Frère, J-M. (1995) AmpD, essential for both β-lactamase regulation and cell wall recycling,
1027 is a novel cytosolic *N*-acetylmuramyl-L-alanine amidase. *Mol. Microbiol.* **15**:553-559.

1028 Jaeger, T, Arsic, M, Mayer, C (2005). Scission of the lactyl ether bond of N-acetylmuramic acid by
1029 *Escherichia coli* "etherase". *J Biol Chem* **280**:30100-30106.

1030 Jones, LJ, Carballido-Lopez, R, Errington, J (2001). Control of cell shape in bacteria: helical, actin-like
1031 filaments in *Bacillus subtilis*. *Cell* **104**:913-922.

1032 Kocaoglu, O, Carlson, EE (2015). Profiling of beta-lactam selectivity for penicillin-binding proteins in
1033 *Escherichia coli strain* DC2. *Antimicrob Agents Chemother* **59**:2785-2790.

1034 Kohlrausch, U, Höltje, JV (1991). Analysis of murein and murein precursors during antibiotic-induced lysis
1035 of *Escherichia coli*. *J Bacteriol* **173**:3425-3431.

1036 Lariviere, PJ, Mahone, CR, Santiago-Collazo, G, Howell, M, Daitch, AK, Zeinert, R, Chien, P, Brown, PJB,
1037 Goley, ED (2019). An essential regulator of bacterial division links FtsZ to cell wall synthase activation.
1038 *Curr Biol* **29**:1460-1470.

1039 Liepinsh, E, Généreux, C, Dehareng, D, Joris, B, Otting, G (2003). NMR structure of *Citrobacter freundii*
1040 AmpD, comparison with bacteriophage T7 lysozyme and homology with PGRP domains. *J Mol Biol*
1041 **327**:833-842.

1042 Lima, LM, Silva, B, Barbosa, G, Barreiro, EJ (2020). β-lactam antibiotics: an overview from a medicinal
1043 chemistry perspective. *Eur J Med Chem* **208**:112829.

1044 Lindquist, S, Galleni, M, Lindberg, F, Normark, S (1989). Signalling proteins in enterobacterial AmpC beta-
1045 lactamase regulation. *Mol Microbiol* **3**:1091-1102.

1046 Lommatzsch, J, Templin, MF, Kraft, AR, Vollmer, W, Höltje, JV (1997). Outer membrane localization of
1047 murein hydrolases: MltA, a third lipoprotein lytic transglycosylase in *Escherichia coli*. *J Bacteriol*
1048 **179**:5465-5470.

1049 Marblestone, JG, Edavettal, SC, Lim, Y, Lim, P, Zuo, X, Butt, TR (2006). Comparison of SUMO fusion
1050 technology with traditional gene fusion systems: enhanced expression and solubility with SUMO.
1051 *Protein Sci* **15**:182-189.

1052 Meberg, BM, Sailer, FC, Nelson, DE, Young, KD (2001). Reconstruction of *Escherichia coli mrcA* (PBP 1a)
1053 mutants lacking multiple combinations of penicillin binding proteins. *J Bacteriol* **183**:6148-6149.

1054 Meeske, AJ, Riley, EP, Robins, WP, Uehara, T, Mekalanos, JJ, Kahne, D, Walker, S, Kruse, AC, Bernhardt, TG,
1055 Rudner, DZ (2016). SEDS proteins are a widespread family of bacterial cell wall polymerases. *Nature*
1056 **537**:634-638.

1057 Mengin-Lecreulx, D, van Heijenoort, J, Park, JT (1996). Identification of the *mpl* gene encoding UDP-N-
1058 acetylmuramate: L-alanyl-gamma-D-glutamyl-meso-diaminopimelate ligase in *Escherichia coli* and its
1059 role in recycling of cell wall peptidoglycan. *J Bacteriol* **178**:5347-5352.

1060 Modell, JW, Kambara, TK, Perchuk, BS, Laub, MT (2014). A DNA damage-induced, SOS-independent
1061 checkpoint regulates cell division in *Caulobacter crescentus*. *PLoS Biol* **12**:e1001977.

1062 Modi, M, Chauhan, D, Gilmore, MC, Cava, F, Priyadarshini, R (2025). Deficiency in peptidoglycan recycling
1063 promotes beta-lactam sensitivity in *Caulobacter crescentus*. *mBio* **16**:e0297524.

1064 Mora-Ochomogo, M, Lohans, CT (2021). β-Lactam antibiotic targets and resistance mechanisms: from
1065 covalent inhibitors to substrates. *RSC Med Chem* **12**:1623-1639.

1066 More, N, Martorana, AM, Biboy, J, Otten, C, Winkle, M, Serrano, CKG, Monton Silva, A, Atkinson, L, Yau, H,
1067 Breukink, E*, et al.* (2019). Peptidoglycan remodeling enables *Escherichia coli* to survive severe outer
1068 membrane assembly defect. *mBio* **10**:e02729-02718.

1069 Mukhija, S, Erni, B (1996). Purification by Ni2+ affinity chromatography, and functional reconstitution of
1070 the transporter for N-acetylglucosamine of *Escherichia coli*. *J Biol Chem* **271**:14819-14824.

1071 Navarro, PP, Vettiger, A, Hajdu, R, Ananda, VY, Lopez-Tavares, A, Schmid, EW, Walter, JC, Loose, M, Chao,
1072 LH, Bernhardt, TG (2025). The aPBP-type cell wall synthase PBP1b plays a specialized role in fortifying
1073 the *Escherichia coli* division site against osmotic rupture. *bioRxiv*, DOI:
1074 10.1101/2025.1104.1102.646830.

1075 Nierman, WC, Feldblyum, TV, Laub, MT, Paulsen, IT, Nelson, KE, Eisen, J, Heidelberg, JF, Alley, MRK, Ohta,
1076 N, Maddock, JR*, et al.* (2001). Complete genome sequence of *Caulobacter crescentus*. *Proc Natl Acad*
1077 *Sci U S A* **98**:4136-4141.

1078 O'Callaghan, CH, Morris, A, Kirby, SM, Shingler, AH (1972). Novel method for detection of beta-lactamases
1079 by using a chromogenic cephalosporin substrate. *Antimicrob Agents Chemother* **1**:283-288.

1080 Paintdakhi, A, Parry, B, Campos, M, Irnov, I, Elf, J, Surovtsev, I, Jacobs-Wagner, C (2016). Oufti: an
1081 integrated software package for high-accuracy, high-throughput quantitative microscopy analysis. *Mol*
1082 *Microbiol* **99**:767-777.

1083 Park, JT, Uehara, T (2008). How bacteria consume their own exoskeletons (turnover and recycling of cell
1084 wall peptidoglycan). *Microbiol Mol Biol Rev* **72**:211-227.

1085 Pazos, M, Vollmer, W (2021). Regulation and function of class A penicillin-binding proteins. *Curr Opin*
1086 *Microbiol* **60**:80-87.

1087 Perez-Riverol Y, Bandla C, Kundu DJ, Kamatchinathan S, Bai J, Hewapathirana S, John NS, Prakash A, Walzer
1088 M, Wang S, Vizcaíno JA. (2025) The PRIDE database at 20 years: 2025 update. *Nucleic Acids Res* **53**:
1089 D543-D553.

1090 Plumbridge, J (1996). How to achieve constitutive expression of a gene within an inducible operon: the
1091 example of the *nagC* gene of *Escherichia coli*. *J Bacteriol* **178**:2629-2636.

1092 Plumbridge, J (2009). An alternative route for recycling of N-acetylglucosamine from peptidoglycan
1093 involves the N-acetylglucosamine phosphotransferase system in *Escherichia coli*. *J Bacteriol* **191**:5641-
1094 4647.

1095 Plumbridge, J, Vimr, E (1999). Convergent pathways for utilization of the amino sugars *N*-acetylglucos-
1096 amine, *N*-acetylmannosamine, and *N*-acetylneuraminic acid by *Escherichia coli*. *J Bacteriol* **181**:47-54.

1097 Plumbridge, JA (1991). Repression and induction of the *nag* regulon of *Escherichia coli* K-12: the roles of
1098 *nagC* and *nagA* in maintenance of the uninduced state. *Mol Microbiol* **5**:2053-2062.

1099 Poindexter, JS (1964). Biological properties and classification of the *Caulobacter* group. *Bacteriological*
1100 *Reviews* **28**:231-295.

1101 Ratna, S, Pradhan, L, Vasconcelos, MP, Acharya, A, Carnahan, B, Wang, A, Ghosh, A, Bolt, A, Ellis, J, Hyland,
1102 SN*, et al.* (2025). The *Legionella pneumophila* peptidoglycan recycling kinase, AmgK, is essential for
1103 survival and replication inside host alveolar macrophages. *bioRxiv*, DOI:
1104 10.1101/2025.1103.1121.644609.

1105 Rohs, PDA, Buss, J, Sim, SI, Squyres, GR, Srisuknimit, V, Smith, M, Cho, H, Sjodt, M, Kruse, AC, Garner, EC,
1106 *et al.* (2018). A central role for PBP2 in the activation of peptidoglycan polymerization by the bacterial
1107 cell elongation machinery. *PLoS Genet* **14**:e1007726.

1108 Santos, PM, Di Bartolo, I, Blatny, JM, Zennaro, E, Valla, S (2001). New broad-host-range promoter probe
1109 vectors based on the plasmid RK2 replicon. *FEMS Microbiol Lett* **195**:91-96.

1110 Sauvage, E, Kerff, F, Terrak, M, Ayala, JA, Charlier, P (2008). The penicillin-binding proteins: structure and
1111 role in peptidoglycan biosynthesis. *FEMS Microbiol Rev* **32**:234-258.

1112 Schindelin, J, Arganda-Carreras, I, Frise, E, Kaynig, V, Longair, M, Pietzsch, T, Preibisch, S, Rueden, C,
1113 Saalfeld, S, Schmid, B*, et al.* (2012). Fiji: an open-source platform for biological-image analysis. *Nat*
1114 *Methods* **9**:676-682.

1115 Sham, LT, Butler, EK, Lebar, MD, Kahne, D, Bernhardt, TG, Ruiz, N (2014). MurJ is the flippase of lipid-linked
1116 precursors for peptidoglycan biogenesis. *Science* **345**:220-222.

1117 Simpson, BW, Gilmore, MC, McLean, AB, Cava, F, Trent, MS (2023). *Escherichia coli* utilizes multiple
1118 peptidoglycan recycling permeases with distinct strategies of recycling. *Proc Natl Acad Sci U S A*
1119 **120**:e2308940120.

1120 Simpson, BW, Nieckarz, M, Pinedo, V, McLean, AB, Cava, F, Trent, MS (2021). *Acinetobacter baumannii* can
1121 survive with an outer membrane lacking lipooligosaccharide due to structural support from
1122 elongasome peptidoglycan synthesis. *mBio* **12**:e0309921.

1123 Strobel, W, Möll, A, Kiekebusch, D, Klein, KE, Thanbichler, M (2014). Function and localization dynamics of
1124 bifunctional penicillin-binding proteins in *Caulobacter crescentus*. *J Bacteriol* **196**:1627-1639.

1125 Taguchi, A, Welsh, MA, Marmont, LS, Lee, W, Sjodt, M, Kruse, AC, Kahne, D, Bernhardt, TG, Walker, S
1126 (2019). FtsW is a peptidoglycan polymerase that is functional only in complex with its cognate penicillin-
1127 binding protein. *Nat Microbiol* **4**:587-594.

1128 Takacs, CN, Poggio, S, Charbon, G, Pucheault, M, Vollmer, W, Jacobs-Wagner, C (2010). MreB drives *de*
1129 *novo* rod morphogenesis in *Caulobacter crescentus* via remodeling of the cell wall. *J Bacteriol* **192**:1671-
1130 1684.

1131 Templin, MF, Ursinus, A, Höltje, JV (1999). A defect in cell wall recycling triggers autolysis during the
1132 stationary growth phase of *Escherichia coli*. *EMBO J* **18**:4108-4117.

1133 Thanbichler, M, Shapiro, L (2006). MipZ, a spatial regulator coordinating chromosome segregation with
1134 cell division in *Caulobacter*. *Cell* **126**:147-162.

1135 Trindade, BC, Chen, GY (2020). NOD1 and NOD2 in inflammatory and infectious diseases. *Immunol Rev*
1136 **297**:139-161.

1137 Typas, A, Banzhaf, M, Gross, CA, Vollmer, W (2012). From the regulation of peptidoglycan synthesis to
1138 bacterial growth and morphology. *Nat Rev Microbiol* **10**:123-136.

1139 Uehara, T, Park, JT (2007). An anhydro-*N*-acetylmuramyl-L-alanine amidase with broad specificity tethered
1140 to the outer membrane of *Escherichia coli*. *J Bacteriol* **189**:5634-5641.

1141 Uehara, T, Suefuji, K, Jaeger, T, Mayer, C, Park, JT (2006). MurQ etherase is required by *Escherichia coli* in
1142 order to metabolize anhydro-*N*-acetylmuramic acid obtained either from the environment or from its
1143 own cell wall. *J Bacteriol* **188**:1660-1662.

1144 Uehara, T, Suefuji, K, Valbuena, N, Meehan, B, Donegan, M, Park, JT (2005). Recycling of the anhydro-N-
1145 acetylmuramic acid derived from cell wall murein involves a two-step conversion to *N*-acetylglucos-
1146 amine-phosphate. *J Bacteriol* **187**:3643-3649.

1147 UniProt Consortium (2025). UniProt: the Universal Protein Knowledgebase in 2025. *Nucleic Acids Res*
1148 **53**:D609-D617.

1149 Vadlamani, G, Thomas, MD, Patel, TR, Donald, LJ, Reeve, TM, Stetefeld, J, Standing, KG, Vocadlo, DJ, Mark,
1150 BL (2015). The β-lactamase gene regulator AmpR is a tetramer that recognizes and binds the D-Ala-D-
1151 Ala motif of its repressor UDP-*N*-acetylmuramic acid (MurNAc)-pentapeptide. *J Biol Chem* **290**:2630-
1152 2643.

1153 van Heijenoort, J (2011). Peptidoglycan hydrolases of *Escherichia coli*. *Microbiol Mol Biol Rev* **75**:636-663.

1154 van Teeffelen, S, Wang, S, Furchtgott, L, Huang, KC, Wingreen, NS, Shaevitz, JW, Gitai, Z (2011). The bacter-
1155 ial actin MreB rotates, and rotation depends on cell-wall assembly. *Proc Natl Acad Sci U S A* **108**:15822-
1156 15827.

1157 Vollmer, W, Bertsche, U (2008). Murein (peptidoglycan) structure, architecture and biosynthesis in
1158 Escherichia coli. *Biochim Biophys Acta* **1778**:1714-1734.

1159 Vollmer, W, Blanot, D, de Pedro, MA (2008a). Peptidoglycan structure and architecture. *FEMS Microbiol*
1160 *Rev* **32**:149-167.

1161 Vollmer, W, Joris, B, Charlier, P, Foster, S (2008b). Bacterial peptidoglycan (murein) hydrolases. *FEMS*
1162 *Microbiol Rev* **32**:259-286.

1163 Weaver, AI, Alvarez, L, Rosch, KM, Ahmed, A, Wang, GS, van Nieuwenhze, MS, Cava, F, Dörr, T. (2022) Lytic
1164 transglycosylases mitigate periplasmic crowding by degrading soluble cell wall turnover products. *Elife*
1165 **11**:e73178.

1166 West, L, Yang, D, Stephens, C (2002). Use of the *Caulobacter crescentus* genome sequence to develop a
1167 method for systematic genetic mapping. *J Bacteriol* **184**:2155-2166.

1168 Yakhnina, AA, Gitai, Z (2013). Diverse functions for six glycosyltransferases in *Caulobacter crescentus* cell
1169 wall assembly. *J Bacteriol* **195**:4527-4535.

1170 Yang, X, Lyu, Z, Miguel, A, McQuillen, R, Huang, KC, Xiao, J (2017). GTPase activity-coupled treadmilling of
1171 the bacterial tubulin FtsZ organizes septal cell wall synthesis. *Science* **355**:744-747.

1172 Zhao, G, Meier, TI, Kahl, SD, Gee, KR, Blaszczak, LC (1999). BOCILLIN FL, a sensitive and commercially
1173 available reagent for detection of penicillin-binding proteins. *Antimicrob Agents Chemother* **43**:1124-
1174 1128.

1175 Zielinska, A, Billini, M, Möll, A, Kremer, K, Briegel, A, Izquierdo Martinez, A, Jensen, GJ, Thanbichler, M
1176 (2017). LytM factors affect the recruitment of autolysins to the cell division site in *Caulobacter*
1177 *crescentus*. *Mol Microbiol* **106**:419-438.

Acknowledgements

We thank Julia Rausch for excellent technical assistance and Daniela Vollmer for the purification of peptidoglycan.

Additional information

Funding

Funder	Grant reference number	Author
Marburg University	Core funding	Martin Thanbichler
Max Planck Society	Max Planck Fellowship	Martin Thanbichler
United Kingdom Biotechnology and Biological Sciences Research Council	grant BB/W013630/1	Waldemar Vollmer
The funders had no role in the design of the study, the collection and interpretation of the data, or the decision to submit the work for publication.		

Data availability

The proteomics data generated in this study have been deposited to the ProteomeXchange Consortium via the PRIDE partner repository (Perez-Riverol et al., 2025) under the dataset identifier PXD069004. All other data supporting the findings of this study are included in the main text, the supplementary material and the source data file.

Competing interests

The authors declare no competing interests.

Author contributions

P.R. and M.T. conceived the study. P.R. generated plasmids and strains, performed the *in vivo* experiments, purified the proteins and prepared the samples for metabolomics analysis. A.M. generated plasmids and strains. J.B. conducted the enzyme assays and muropeptide analysis. N.P. performed the metabolomics analysis. J.N. prepared GlcNAc–anhMur*N*Ac-tetrapeptide. P.R., J.B., N.P., W.V. and M.T. analyzed the data. V.M. and M.T. secured funding and supervised the study. P.R. and M.T. wrote the manuscript, with input from all other authors.

Table

1191 **Table 1. List of PG recycling enzymes found in *E. coli* and *P. aeruginosa* and the corresponding homologs of *C.*
1192 *crescentus* identified by reciprocal BLAST analysis.**

Protein	Homolog(s)	Sequence identity (%)	E value	Function
E. coli [1)]	***C. crescentus***			
AmpG	CCNA_00136	40.4	3E-40	Muropeptide permease
NagE	CCNA_00572 CCNA_00458	45.0 45.0	2E-131 3E-131	*N*-acetylglucosamine-specific IIBC component (PTS system)
LdcA	-	-	-	LD-Carboxypeptidase
AmpD	CCNA_02650	33.5	5E-20	1,6-anhydro-*N*-acetylmuramyl-L-alanine amidase
NagZ	CCNA_02085	34.7	6E-44	β-*N*-acetyl-D-glucosaminidase
NagK	CCNA_03849	41.1	2E-66	*N*-actely-D-glucosamine kinase
AnmK	CCNA_01945	34.6	2E-49	anhydro-*N*-acetylmuramic acid kinase
MurQ	-	-	-	*N*-acetylmuramic acid-6-phosphate etherase
NagA	CCNA_00568 CCNA_00452	36.3 39.5	6E-76 1E-84	*N*-acetylglucosamine-6-phosphate deacetylase
GlmM	CCNA_00116	51.5	4E-153	Phosphoglucosamine mutase
GlmU	CCNA_02389	40.4	2E-97	UDP-*N*-acetylglucosamine pyrophosphorylase
P. aeruginosa [2)]	***C. crescentus***			
MupP	CCNA_02390	32.6	3E-27	Phosphoglycolate phosphatase
AmgK	CCNA_03649	30.1	1E-32	*N*-acetylmuramate/*N*-acetylglucosamine kinase
MurU	CCNA_03650	36.6	4E-26	*N*-acetylmuramate-α-1-phosphate uridylyltransferase

[1)] strain *E. coli* K-12 substr. MG1655 (Genbank accession code: U00096.3)
[2)] strain *P. aeruginosa* PAO1 (Genbank accession code: AE004091.2)

Figure legends

1193 **Figure 1. The *C. crescentus* genome encodes a complete PG recycling pathway.** *De novo* PG biosynthesis
1194 starts with the conversion of fructose-6-phosphate, supplied by central carbon metabolism, to glucosam-
1195 ine-6-phosphate. This key metabolite is then transformed by multiple enzymatic steps into the membrane-
1196 attached PG precursor lipid II, which is flipped to the periplasmic face and incorporated into the existing
1197 PG sacculus by glycosyltransferases (GTases) and transpeptidases (TPases). To enable PG remodeling,
1198 growth and cell separation, the PG meshwork is cleaved by a diverse set of enzymes. The anhydro-
1199 muropeptides and Glc*N*Ac molecules generated in this process are imported into the cytoplasm by the
1200 permease AmpG or two homologs of the phosphotransferase system (PTS) transporter NagE, respectively.
1201 In the cytoplasm, the peptide is released by AmiR and the sugars are separated by NagZ. Afterwards, two
1202 independent pathways feed the two sugars back into the *de novo* PG biosynthetic pathway. The enzymes
1203 are named as established for *E. coli* and *P. aeruginosa*, with the exception of the *C. crescentus* homolog of
1204 AmpD, which was renamed to AmiR due to its different domain organization. The enzymes analyzed in this
1205 study are indicated in bold type. Symbols are defined in the legend on the right.

1206 **Figure 2. The AmiR and NagZ homologs are functional and have a broad substrate specificity. (A)** Over-
1207 view of the PG digestion assay used to assess the hydrolytic activities of AmiR and NagZ. **(B)** HPLC chro-
1208 matograms showing the products generated upon incubation of anhydro-muropeptides from LT-treated
1209 PG sacculi without added proteins (Buffer), with AmiR or with a catalytically inactive AmiR variant (AmiR*).
1210 The identities of anhMur*N*Ac-peptides were determined based on their known retention times (Glauner,
1211 1988). The AmiR reaction product Glc*N*Ac-1,6-anhMur*N*Ac was identified by mass spectrometry (**Figure 2–**
1212 **figure supplement 4A**). **(C)** HPLC chromatograms showing the products generated upon incubation of
1213 anhydro-muropeptides from LT-treated PG sacculi without added proteins (Buffer), with NagZ or with a
1214 catalytically inactive NagZ variant (NagZ*). Disaccharide-containing anhydro-muropeptides were identi-
1215 fied based on their known retention times (Glauner, 1988). The identities of anhMur*N*Ac-peptides were
1216 validated by mass spectrometry analysis of the reaction products obtained after NagZ treatment of
1217 anhydro-muropeptide mixtures (**Figure 2–figure supplement 4B**). Note that the PG sacculi used in the
1218 AmiR and NagZ activity assays were isolated from different *E. coli* strains that exhibit distinct muropeptide
1219 profiles (see Methods).

1220 **Figure 2–figure supplement 1. Substrate specificity of AmiR. (A)** Structural models of AmiR and the cata-
1221 lytically inactive AmiR* variant, generated with AlphaFold 3 (Abramson et al., 2024). The magnified region
1222 shows the predicted catalytic site of AmiR and the amino acid substitutions introduced to generate AmiR*.

1223 **(B)** HPLC chromatograms showing the products generated upon incubation of anhydro-muropeptides
1224 from LT-treated PG sacculi for 16 h without added proteins (Buffer) or with the indicated concentrations
1225 of AmiR. **(C)** HPLC chromatograms showing the products generated upon incubation of muropeptides from
1226 muramidase-treated PG sacculi for 16 h without added proteins (Buffer) or with the indicated concentra-
1227 tions of AmiR. Reaction products were identified based on their known retention times (Glauner, 1988).

1228 **Figure 2–figure supplement 2. Lack of AmiR activity towards intact PG sacculi. (A)** Overview of the PG
1229 digestion assay used to assess the hydrolytic activity of AmiR on intact PG sacculi. **(B)** HPLC chromatograms
1230 showing the products generated upon incubation of intact PG sacculi without added proteins (Buffer), with
1231 AmiR or with the catalytically inactive AmiR variant AmiR* and subsequent cellosyl-mediated cleavage of
1232 the pre-treated sacculi into muropeptides. Muropeptides were identified based on their known retention
1233 times (Glauner, 1988).

1234 **Figure 2–figure supplement 3. Activity of NagZ with muropeptides. (A)** Structural models of NagZ and the
1235 catalytically inactive NagZ* variant, generated with AlphaFold 3 (Abramson et al., 2024). The magnified
1236 region shows the predicted catalytic site of NagZ and the amino acid substitution introduced to generate
1237 NagZ*. **(B)** HPLC chromatograms showing the products generated upon incubation of muropeptides from
1238 muramidase-treated PG sacculi without added proteins (Buffer), with NagZ or with a catalytically inactive
1239 NagZ variant (NagZ*). Disaccharide-containing muropeptides were identified based on their known reten-
1240 tion times (Glauner, 1988). The identities of Mur*N*Ac-peptides were validated by mass spectrometry
1241 analysis of the reaction products obtained after NagZ treatment of anhydro-muropeptide mixtures (**Figure**
1242 **2–figure supplement 4B**).

1243 **Figure 2–figure supplement 4. Mass spectrometric identification of AmiR and NagZ reaction products.**
1244 **(A)** Identification of the Glc*N*Ac–anhMur*N*Ac disaccharide generated by treatment of anhydro-muropep-
1245 tides with AmiR. Sacculi isolated from *E. coli* D456 (Edwards and Donachie, 1993) were treated with the LT
1246 Slt70 *E. coli*. The graph shows the chromatogram obtained after separation of the sugar-containing reac-
1247 tion products by HPLC. The observed m/z ratios of the main product in peak 1 and the calculated molecular
1248 mass of the Glc*N*Ac-1,6-anhMur*N*Ac disaccharide are given in the table on the right. **(B)** Identification of
1249 the anhMur*N*Ac-peptide species generated by treatment of anhydro-muropeptides with NagZ. Sacculi iso-
1250 lated from *E. coli* CS703-1 (Meberg et al., 2001) were treated with the LT MltA from *E. coli*. The graph
1251 shows the chromatogram obtained after separation of the reaction products by HPLC. The table on the
1252 right gives the observed m/z ratios of the main product detected contained in the indicated peaks as well
1253 as the calculated molecular masses of the anhMur*N*Ac-peptides assigned to these peaks.

Figure 2-figure supplement 5: Activity of AmiR against anhMur*N*Ac-tetrapeptide. (A) Overview of the assay used to assess the activity of AmiR against purified anhMur*N*Ac-tetrapeptide. **(B)** Relative levels of free anhMur*N*Ac and tetrapeptide (L-Ala–D-Glu–*m*DAP–D-Ala) detected after incubation of anhMur*N*Ac-tetrapeptide in the absence of added protein or in the presence of the amidase AmiR or its catalytically inactive variant AmiR*. The reaction products were identified by liquid chromatography-mass spectrometry (LC-MS) analysis. For each product, the mass spectrometric peak areas were normalized to the mean peak area of the AmiR-containing reactions. nd, not detectable.

1254 **Figure 3. Metabolomic analysis reveals aberrant levels of PG recycling intermediates in recycling-defi-**
1255 **cient strains. (A)** Overview of the analysis pipeline used to identify cytoplasmic PG recycling products. **(B)**
1256 Relative levels of the indicated anhMur*N*Ac-peptide species in the cytoplasm of *C. crescentus* wild-type,
1257 Δ*amiR* (PR033) and Δ*amiR* Δ*ampG* (PR221) cells, measured by metabolomics analysis. For each anhydro-
1258 muropeptide, the mass spectrometric peak areas were normalized against the mean obtained for the
1259 Δ*amiR* mutant. The statistical significance of differences between the wild type and the mutant strains
1260 was determined using a two-sided Welch's t-test. ns indicates p-values > 0.1. **(C)** Relative levels of the
1261 Glc*N*Ac–anhMur*N*Ac disaccharide in *C. crescentus* wild-type, Δ*ampG* (PR207), Δ*amiR* (PR033) and Δ*nagZ*
1262 (PR188) cells, assessed as for panel B. The mass spectrometric peak areas were normalized against the
1263 mean obtained for the Δ*nagZ* mutant. Statistical significance was determined as described for panel B.

1264 **Figure 4. AmpG, AmiR and NagZ are required for proper cell shape and β-lactam resistance in *C. cres-***
1265 ***centus*. (A)** Phase contrast images of *C. crescentus* wild-type, Δ*ampG* (PR207), Δ*amiR* (PR033) and Δ*nagZ*
1266 (PR188) cells harvested in the exponential and stationary growth phase. Scale bar: 5 µm. **(B)** Superplots
1267 showing the distribution of cell lengths in populations of *C. crescentus* wild-type, Δ*ampG* (PR207), Δ*amiR*
1268 (PR033) and Δ*nagZ* (PR188) cells in the exponential (exp) and stationary (stat) growth phase. Small dots
1269 represent the data of three independent replicates (shown in light blue, teal and dark grey; *n*=100 cells
1270 per replicate). Large dots represent the mean values of the three datasets, with their average indicated by
1271 a red horizontal line. The statistical significance (*p*-value) of differences between conditions was assessed
1272 using a two-sided Welch's *t*-test. ns indicates *p*-values > 0.1. **(C)** Serial dilution spot assay investigating the
1273 growth of wild-type, Δ*ampG* (PR207), Δ*amiR* (PR033), Δ*nagZ* (PR188) and Δ*blaA* (CS606) cells on agar
1274 plates with different concentrations of ampicillin. See **Source data 1** for all replicates (n=3 independent
1275 experiments).

1276 **Figure 4-figure supplement 1. Reversion of the phenotypes of PG recycling-deficient strains through**
1277 **complementation with the corresponding wild-type genes. (A)** Phase contrast images of *C. crescentus*

1278 wild-type, Δ*ampG* (PR207), Δ*ampG* P_{xyl}::P_{xyl}-*ampG* (PR285), Δ*amiR* (PR033), Δ*amiR* P_{xyl}::P_{xyl}-*amiR* (PR037),
1279 Δ*nagZ* (PR188) and Δ*nagZ* P_{xyl}::P_{xyl}-*nagZ* (PR284) cells harvested in the exponential growth phase. The com-
1280 plementation strains (compl.) were not induced. Scale bar: 5 µm. **(B)** Superplots showing the distribution
1281 of cell lengths in populations of the strains described in panel A. Data (*n*=100 cells per replicate) are
1282 presented as described for **Figure 4B**. The statistical significance (*p*-value) of differences between condi-
1283 tions was assessed using a two-sided Welch's *t*-test. ns indicates *p*-values > 0.1. The data for wild-type,
1284 Δ*amiR* and Δ*nagZ* cells are taken from **Figure 4B** and shown as a reference. **(C)** Serial dilution spot assay
1285 investigating the growth of wild-type, P_{xyl}::P_{xyl}-*ampG* (PR285), Δ*amiR* P_{xyl}::P_{xyl}-*amiR* (PR037), Δ*nagZ* P_{xyl}::P_{xyl}-
1286 *nagZ* (PR284) and Δ*blaA* (CS606) cells on agar plates with different concentrations of ampicillin. See **Source**
1287 **data 1** for all replicates (n=3 independent experiments).

1288 **Figure 4–figure supplement 2. Morphological characterization of catalytically inactive AmiR and NagZ**
1289 **variants. (A)** Phase contrast images of *C. crescentus* wild-type, Δ*amiR* (PR033), *amiR::amiR** (PR173),
1290 Δ*nagZ* (PR188) and *nagZ::nagZ** (PR196) cells harvested in the exponential and stationary growth phase.
1291 Scale bar: 5 µm. **(B)** Superplots showing the distribution of cell lengths in populations of wild-type, Δ*amiR*
1292 (PR033), *amiR::amiR** (PR173), Δ*nagZ* (PR188) and *nagZ::nagZ** (PR196) cells in the exponential (exp) and
1293 stationary (stat) growth phase. Data (*n*=100 cells per replicate) are presented as described for **Figure 4B**.
1294 The statistical significance (*p*-value) of differences between conditions was assessed using a two-sided
1295 Welch's *t*-test. ns indicates *p*-values > 0.1. The data for wild-type, Δ*amiR* and Δ*nagZ* cells are taken from
1296 **Figure 3** and shown as a reference.

1297 **Figure 4–figure supplement 3. Growth of PG recycling-deficient mutants in minimal medium. (A)** Phase
1298 contrast images of *C. crescentus* wild-type, Δ*ampG* (PR207), Δ*amiR* (PR033) and Δ*nagZ* (PR188) cells grown
1299 in minimal (M2G) medium and harvested in the stationary growth phase. **(B)** Superplots showing the
1300 distribution of cell lengths in populations of wild-type, Δ*ampG* (PR207), Δ*amiR* (PR033) and Δ*nagZ* (PR188)
1301 cells grown in rich medium (PYE) and minimal medium (M2G). Data (*n*=100 cells per replicate) are
1302 presented as described for **Figure 4B**. The statistical significance (*p*-value) of differences between condi-
1303 tions was assessed using a two-sided Welch's *t*-test. ns indicates *p*-values > 0.1. The distributions of cell
1304 lengths in rich medium are taken from **Figure 3** and shown as a reference. **(C)** Serial dilution spot assay
1305 investigating the growth of wild-type, Δ*ampG* (PR207), Δ*amiR* (PR033), Δ*nagZ* (PR188) and Δ*blaA* (CS606)
1306 cells on minimal medium agar plates with different concentrations of ampicillin. See **Source data 1** for all
1307 replicates (n=3 independent experiments).

1308 **Figure 4–figure supplement 4. Redundant role of the LT SdpA in the production of anhydro-muropep-**
1309 **tides. (A)** Serial dilution spot assay investigating the growth of *C. crescentus* Δ*sdpA* (AM399) cells on agar
1310 plates containing different concentrations of ampicillin. The cells were spotted on the same plates as those
1311 depicted in **Figure 4C**. See **Source data 1** for all replicates (n=3 independent experiments). **(B)** Phase con-
1312 trast images of *C. crescentus* wild-type and Δ*sdpA* (AM399) cells harvested in the exponential or stationary
1313 growth phase. **(C)** Superplots showing the distribution of cell lengths in populations of wild-type and Δ*sdpA*
1314 (AM399) cells harvested in the exponential (exp) and stationary (stat) growth phase. Data (*n*=100 cells per
1315 replicate) are presented as described for **Figure 4B**. The statistical significance (*p*-value) of differences
1316 between conditions was assessed using a two-sided Welch's *t*-test. ns indicates *p*-values > 0.1. **(D)** Levels
1317 of the indicated anhMur*N*Ac-peptide species in the cytoplasm of *C. crescentus* wild-type, Δ*amiR* (PR033)
1318 and Δ*amiR* Δ*sdpA* (PR260) cells, measured by metabolomics analysis through quantification of the
1319 corresponding mass spectrometric peak areas. For each anhydro-muropeptide, the mass spectrometric
1320 peak areas were normalized against the mean obtained for the Δ*amiR* mutant. The statistical significance
1321 of differences between the wild type and the mutant strains was determined using a two-sided Welch's *t*-
1322 test. ns indicates *p*-values > 0.1.

1323 **Figure 5. The Glc*N*Ac recycling pathway is dispensable for proper cell division and β-lactam resistance.**
1324 **(A)** Phase contrast images of *C. crescentus* Δ*nagK* (PR255), Δ*nagA1* (PR256) and Δ*nagA2* (PR257) cells
1325 harvested in the exponential and stationary growth phase. Scale bar: 5 µm. **(B)** Superplots showing the
1326 distribution of cell lengths in populations of *C. crescentus* wild-type, Δ*nagK* (PR255), Δ*nagA1* (PR256) and
1327 Δ*nagA2* (PR257) cells in the exponential (exp) and stationary (stat) growth phase. Data (*n*=100 cells per
1328 replicate) are presented as described for **Figure 4B**. The statistical significance (*p*-value) of differences bet-
1329 ween conditions was assessed using a two-sided Welch's *t*-test. ns indicates *p*-values > 0.1. **(C)** Serial
1330 dilution spot assays investigating the growth of *C. crescentus* Δ*nagK* (PR255), Δ*nagA1* (PR256) and Δ*nagA2*
1331 (PR257) cells on agar plates containing different concentrations of ampicillin. The cells were spotted on
1332 the same plates as those depicted in **Figure 4C**. See **Source data 1** for all replicates (n=3 independent
1333 experiments). **(D)** Volcano plot illustrating differential protein abundance in *C. crescentus* wild-type cells
1334 grown in M2G minimal medium with Glc*N*Ac compared to plain M2G medium. Grey dots represent
1335 proteins identified by mass spectrometry. The x-axis indicates the log2 of the average difference in the
1336 peptide counts for the two different conditions (*n*=3 independent replicates). The y-axis shows the -log10
1337 of the corresponding *p*-value. Proteins encoded in the two *nag* gene clusters are highlighted in color and
1338 annotated. The colors correspond to those used in panel E. **(E)** Schematic representation of the two *nag*
1339 gene clusters. The predicted functions of the gene products are specified in the legend on the right.

1340 **Figure 6. *C. crescentus* recycles anhMur*N*Ac through a functional MurU pathway. (A)** Phase contrast
1341 images of *C. crescentus* Δ*anmK* (PR252) and Δ*amgK* (PR262) cells, harvested in the exponential and station-
1342 ary growth phase. Scale bar: 5 µm. **(B)** Superplots showing the distribution of cell lengths in populations
1343 of *C. crescentus* wild-type, Δ*anmK* (PR252), and Δ*amgK* (PR262) cells in the exponential (exp) and station-
1344 ary (stat) growth phase. Data (*n*=100 cells per replicate) are presented as described for **Figure 4B**. The
1345 statistical significance (*p*-value) of differences between conditions was assessed using a two-sided Welch's
1346 *t*-test. ns indicates *p*-values > 0.1. **(C)** Serial dilution spot assay investigating the growth of *C. crescentus*
1347 Δ*anmK* (PR252) and Δ*amgK* (PR262) on plates containing different concentrations of ampicillin. The cells
1348 were spotted on the same plates as those depicted in **Figure 4C**. See **Source data 1** for all replicates (n=3
1349 independent experiments). **(D)** Levels of Mur*N*Ac in the cytoplasm of *C. crescentus* wild-type and Δ*amgK*
1350 (PR262) cells, measured by metabolomics analysis through quantification of the corresponding mass
1351 spectrometric peak areas. The mass spectrometric peak areas were normalized against the mean obtained
1352 for the Δ*amgK* mutant. The statistical significance of differences between the two strains was determined
1353 using a two-sided Welch's t-test. **(E)** Analysis of the growth of *C. crescentus* wild-type, Δ*nagK* (PR255) and
1354 Δ*amgK* (PR262) cells on agar containing a fosfomycin gradient. The fosfomycin concentrations on the MIC
1355 test strip are indicate in the legend on the right.

1356 **Figure 7. Recycling of the disaccharide moiety plays only a minor role in cell division and β-lactam resis-**
1357 **tance. (A)** Phase contrast images of *C. crescentus* Δ*amgK* Δ*nagK* (PR261) cells, harvested in the exponential
1358 and stationary growth phase. Scale bar: 5 µm. **(B)** Superplots showing the distribution of cell lengths in
1359 populations of *C. crescentus* wild-type and Δ*amgK* Δ*nagK* (PR261) cells in the exponential (exp) and station-
1360 ary (stat) growth phase. Data (*n*=100 cells per replicate) are presented as described for **Figure 4B**. The
1361 statistical significance (*p*-value) of differences between conditions was assessed using a two-sided Welch's
1362 *t*-test. ns indicates *p*-values > 0.1. **(C)** Levels of Mur*N*Ac in the cytoplasm of *C. crescentus* wild-type, Δ*nagK*
1363 (PR255), Δ*amgK* (PR262) and Δ*nagK* Δ*amgK* (PR261) cells, as determined by metabolomics analysis. Data
1364 were normalized to the mean Mur*N*Ac levels of Δ*amgK* cells. The statistical significance of differences
1365 between strains was determined using a two-sided Welch's *t*-test. ns indicates *p*-values < 0.1. **(D)** Serial
1366 dilution spot assays investigating the growth of *C. crescentus* Δ*amgK* Δ*nagK* (PR261) cells on agar plates
1367 containing different concentrations of ampicillin. The cells were spotted on the same plates as those
1368 depicted in **Figure 4C**. See **Source data 1** for all replicates (n=3 independent experiments).

1369 **Figure 8. BlaA function is not regulated at the levels of transcription, protein accumulation or enzymatic**
1370 **activity. (A)** Organization of the putative five-gene operon containing the *blaA* gene. The annotation or
1371 ORF number of the open reading frames and the predicted functions of their gene products are indicated.

1372 **(B)** Activity of the promoter likely driving the expression of the *blaA*-containing operon in different strain
1373 backgrounds. The *C. crescentus* wild-type, Δ*ampG* (PR207), Δ*amiR* (PR033) and Δ*nagZ* (PR188) strains were
1374 transformed with a plasmid carrying a 400 bp fragment of the CCNA_02225 upstream region fused to a β-
1375 galactosidase reporter gene and assayed for reporter activity. Strains transformed with the empty plasmid
1376 served as negative controls (NC). The underlying data are shown as grey dots. The statistical significance
1377 (*p*-value) of differences between strains was calculated using a two-sided Welch's t-test. ns indicates p-
1378 values > 0.1. **(C)** β-lactamase activity of *C. crescentus* wild-type, Δ*ampG* (PR207), Δ*amiR* (PR033) and Δ*nagZ*
1379 (PR188) cells, as determined by monitoring the hydrolysis of the chromogenic β-lactam nitrocefin in
1380 permeabilized cells over time. **(D)** Volcano plots showing differential protein abundance in *C. crescentus*
1381 Δ*ampG* (PR207), Δ*amiR* (PR033) and Δ*nagZ* (PR188) cells compared to wild-type cells. Grey dots represent
1382 proteins identified by mass spectrometry. The x-axis indicates the log2 of the average difference in the
1383 peptide counts for the two different conditions (*n*=4 independent replicates). The y-axis shows the -log10
1384 of the corresponding *p*-value. The BlaA protein is highlighted in magenta. **(E)** Serial dilution spot assays
1385 investigating the growth of *C. crescentus* wild-type, Δ*ampG* (PR207), Δ*amiR* (PR033), Δ*nagZ* (PR188) and
1386 Δ*blaA* cells (CS606) on agar plates containing different concentrations of aztreonam. See **Source data 1** for
1387 all replicates (n=3 independent experiments).

1388 **Figure 8–figure supplement 1. The two genes forming an operon with *amiR* are dispensible for PG recy-**
1389 **cling or β-lactam resistance. (A)** Genomic context of *amiR*. The gene names and the predicted functions
1390 of the respective gene products are indicated. **(B)** Levels of the indicated anhMur*N*Ac-peptide species in
1391 the cytoplasm of *C. crescentus* wild-type, Δ*amiR* (PR033) and Δ*amiR* Δ*traX* (PR258) cells, measured by
1392 metabolomics analysis through quantification of the corresponding mass spectrometric peak areas. **(C)**
1393 Volcano plot showing differences in protein abundance in *C. crescentus* Δ*regX* (PR154) cells in comparison
1394 to wild-type cells. Grey dots represent proteins identified by mass spectrometry. The x-axis indicates the
1395 log2 of the average difference in the peptide counts for the two different conditions (n=3 independent
1396 replicates). The y-axis shows the -log10 of the corresponding *p*-value. Proteins with a fold change smaller
1397 than 0.5 or larger than 2 are highlighted in color and numbered. Details on these proteins are given in
1398 **Figure 8–table supplement 1**. **(D)** Phase contrast images of Δ*traX* (PR153) and Δ*regX* (PR154) cells,
1399 harvested in the exponential or stationary growth phase. Scale bar: 5 µm. **(E)** Superplots showing the distri-
1400 bution of cell lengths in populations of *C. crescentus* wild-type, Δ*traX* (PR153) and Δ*regX* (PR154) cells in
1401 the exponential (exp) and stationary (stat) growth phase. Data (*n*=100 cells per replicate) are presented as
1402 described for **Figure 4B**. The statistical significance (*p*-value) of differences between conditions was
1403 assessed using a two-sided Welch's *t*-test. ns indicates *p*-values > 0.1. **(F)** Serial dilution spot assays investi-

1404 gating the growth of *C. crescentus* wild-type, Δ*traX* (PR153), Δ*regX* (PR154) and Δ*blaA* (CS606) cells on agar
1405 plates in the absence or presence of ampicillin. See **Source data 1** for all replicates (n=3 independent
1406 experiments).

1407 **Figure 8–figure supplement 2. Changes in protein accumulation upon deletion of CCNA_02225. (A)** Vol-
1408 cano plot showing differential protein abundance in *C. crescentus* ΔCC*NA_02225* (PR218) vs. wild-type
1409 cells. Grey dots represent proteins identified by mass spectrometry. The x-axis indicates the log2 of the
1410 average difference in the peptide counts for the two different conditions (*n*=3 independent replicates).
1411 The y-axis shows the -log10 of the corresponding *p*-value. The 20 proteins with the highest fold change
1412 according to Manhattan distance are highlighted in color and numbered. The functional categorization of
1413 these genes is indicated in the lower left corner of the plot. Proteins encoded in the five-gene operon are
1414 labeled in orange. **(B)** List of the most highly deregulated proteins in the ΔCC*NA_02225* (PR218) mutant.
1415 The table gives the gene name or ORF number, the fold change, the *p*-value and the predicted function for
1416 the proteins numbered in panel A.

1417 **Figure 9. PG recycling defects increase the sensitivity of the septal PG synthetic machinery to ampicillin**
1418 **and reduce PG precursor biosynthesis. (A)** Phase contrast images of *C. crescentus* wild-type and Δ*amiR*
1419 (PR033) cells, incubated for 3 h in the presence of different concentrations of ampicillin. Scale bar: 5 µm.
1420 **(B)** Quantification of the fraction of lysed cells in cultures of *C. crescentus* wild-type and Δ*amiR* (PR033)
1421 cells, incubated for 3 h in the presence of different concentrations of ampicillin. The bars represent the
1422 mean (±SD) of three independent replicates (*n*=100 cells per condition). The underlying data are shown as
1423 grey dots. The statistical significance (*p*-value) of differences between strains was calculated using a two-
1424 sided Welch's t-test. ns indicates *p*-values > 0.1. **(C)** Time-lapse microscopy analysis showing *C. crescentus*
1425 wild-type and Δ*amiR* (PR033) cells in a microfluidic flow cell before and after ampicillin treatment. After
1426 3 h of growth in antibiotic-free medium, the cells were shifted to medium containing 20 µg/mL ampicillin.
1427 Images were taken at 5 min intervals for a total duration of 8 h. Shown are representative frames of the
1428 time-lapse series. The full sequences are shown in **Figure 9-Video 1** and **Figure 9-Video 2**. **(D)** Image of an
1429 SDS-gel showing the labeling of PBPs with the fluorescent β-lactam bocillin-FL in the absence or presence
1430 of other β-lactams. Crude membrane fractions of *C. crescentus* Δ*blaA* (CS606) cells were pre-incubated
1431 with the indicated concentrations of ampicillin, 5 µg/mL cefalexin (Cfx) or 100 µg/mL mecillinam (Mec),
1432 treated with bocillin-FL and then subjected to SDS gel electrophoresis to separate the labeled PBPs prior
1433 to fluorescence imaging. **(E)** Levels of UDP-Glc*N*Ac and UDP-Mur*N*Ac in the cytoplasm of *C. crescentus* wild-
1434 type, Δ*ampG* (PR207), Δ*amiR* (PR033) and Δ*nagZ* (PR188) cells, measured by metabolomics analysis
1435 through quantification of the corresponding mass spectrometric peak areas. For each PG precursor, the

1436 mass spectrometric peak areas were normalized against the mean obtained for the wild-type strain. The
1437 statistical significance of differences between the wild type and the mutant strains was determined using
1438 a two-sided Welch's t-test. ns indicates *p*-values > 0.1; nd: not detectable.

1439 **Figure 9–video 1. Effect of ampicillin on the growth of *C. crescentus* wild-type cells.** *C. crescentus* wild-
1440 type cells were cultivated in a microfluidic flow cell for 3 h in antibiotic-free medium and then shifted to
1441 medium containing 20 µg/mL ampicillin. Phase contrast images were taken at 5-min intervals. Scale bar: 5
1442 µm.

1443 **Figure 9–video 2. Effect of ampicillin on the growth of *C. crescentus* Δ*amiR* cells.** *C. crescentus* Δ*amiR*
1444 (PR033) cells were cultivated in a microfluidic flow cell for 3 h in antibiotic-free medium and then shifted
1445 to medium containing 20 µg/mL ampicillin. Phase contrast images were taken at 5-min intervals. Scale bar:
1446 5 µm.

1447 **Figure 9–figure supplement 1. Muropeptide composition of PG sacculi from wild-type and Δ*amiR* cells.**
1448 Shown are HPLC chromatograms resolving the muropeptides obtained by muramidase treatment of PG
1449 sacculi isolated from stationary wild-type or Δ*amiR* (PR033) cells. The muropeptides contained in the
1450 different peaks are listed in **Figure 9–table supplement 1**. A summary of the data obtained is given in
1451 **Figure 9–table supplement 2**.

1452 **Figure 9–figure supplement 2. Ampicillin sensitivity of PG recycling-defective mutants in the presence**
1453 **of Glc*N*Ac. (A)** Serial dilution spot assay investigating the growth of *C. crescentus* wild-type, Δ*ampG*
1454 (PR207), Δ*amiR* (PR033), Δ*nagZ* (PR188) and Δ*blaA* (CS606) cells on agar plates containing different con-
1455 centrations of ampicillin in the presence of 0.3% Glc*N*Ac. **(B)** Serial dilution spot assay investigating the
1456 growth of *C. crescentus* wild-type, Δ*amiR* (PR033) and Δ*blaA* (CS606) cells on agar plates containing differ-
1457 ent concentrations of ampicillin in the presence of 100 µg/mL Mur*N*Ac. See **Source data 1** for all replicates
1458 (n=3 independent experiments).

1459 **Figure 10. The cell filamentation phenotype of Δ*amiR* cells is rescued by hyper-activation of the septal**
1460 **FtsW-PBP3 PG biosynthetic complex. (A)** Phase contrast images of *C. crescentus* wild-type, Δ*amiR* (PR033),
1461 *ftsW::ftsW** (ML2103) and Δ*amiR ftsW::ftsW** (PR246) cells, harvested in the exponential and stationary
1462 growth phase. **(B)** Superplots showing the distribution of cell lengths in populations of the strains
1463 described in panel A in the exponential (exp) and stationary (stat) growth phase. Data (*n*=100 cells per
1464 replicate) are presented as described for **Figure 4B**. The statistical significance (*p*-value) of differences
1465 between conditions was assessed using a two-sided Welch's *t*-test. ns indicates *p*-values > 0.1. **(C)** Serial
1466 dilution spot assay investigating the growth of *C. crescentus ftsW::ftsW** (ML2103), Δ*amiR* (PR033) and

1467 Δ*amiR ftsW::ftsW** (PR246) cells on agar plates containing no or 10 µg/mL ampicillin. See **Source data 1**
1468 for all replicates (n=3 independent experiments).

1469 **Figure 11. Model for the critical role of PG recycling in *C. crescentus* growth and β-lactam resistance. (A)**
1470 PBPs mediates the incorporation of new cell wall material into the growing PG sacculus. The PG precursors
1471 required for this process are synthesized in the cytoplasm, using building blocks that are provided by both
1472 *de novo* synthesis and PG recycling. **(B)** If β-lactams enter the periplasm, they compete with PG precursors
1473 for binding to their PBP targets. Most antibiotic molecules are rapidly hydrolyzed by the β-lactamase BlaA.
1474 However, a minor fraction manages to interact with PBPs before they are captured and degraded. The
1475 resulting inactivation of a small proportion of PBPs can be tolerated by cells, as long as they still contain
1476 sufficient active PBPs to maintain cell growth and division. **(C)** Upon disruption of PG recycling, the level of
1477 PG monomers strongly decreases, leaving the substrate binding sites of PBPs unoccupied for longer peri-
1478 ods of time and thus increasing their accessibility to β-lactam molecules. As a result, a larger fraction of
1479 PBPs is inactivated, leading to decreased cell wall integrity and ultimately cell lysis. This effect may be
1480 aggravated by the reduced activity of the remaining, active PBPs due to an insufficient supply of PG pre-
1481 cursors and by the accumulation of anhydro-muropentapeptides in the periplasm, which could interfere
1482 with the activities of PG biosynthetic enzymes, thereby further decreasing the incorporation of new mater-
1483 ial into the existing sacculus.

Figures

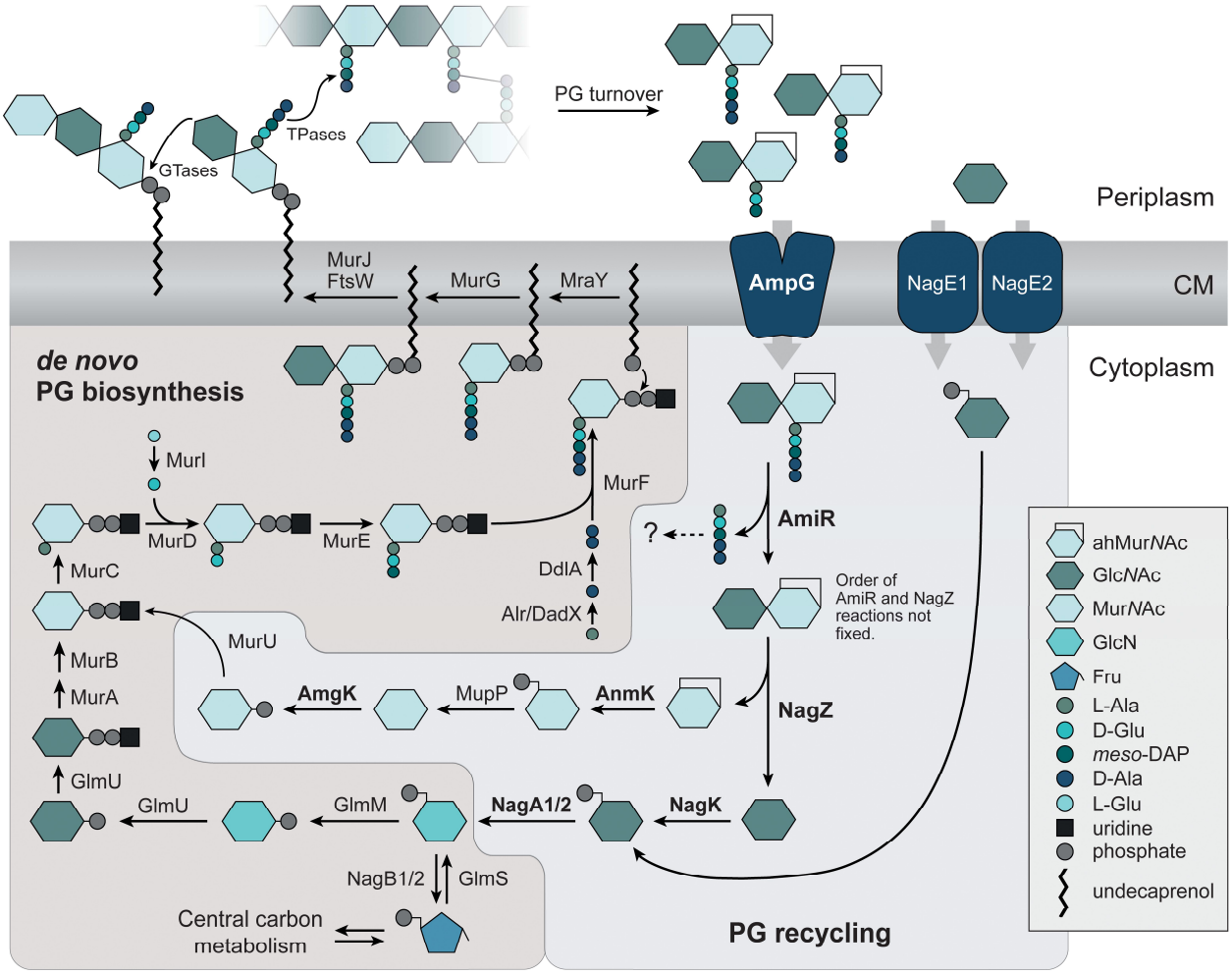

Figure 1. The *C. crescentus* genome encodes a complete PG recycling pathway. *De novo* PG biosynthesis starts with the conversion of fructose-6-phosphate, supplied by central carbon metabolism, to glucosamine-6-phosphate. This key metabolite is then transformed by multiple enzymatic steps into the membrane-attached PG precursor lipid II, which is flipped to the periplasmic face and incorporated into the existing PG sacculus by glycosyltransferases (GTases) and transpeptidases (TPases). To enable PG remodeling, growth and cell separation, the PG meshwork is cleaved by a diverse set of enzymes. The anhydro-muropeptides and Glc*N*Ac molecules generated in this process are imported into the cytoplasm by the permease AmpG or two homologs of the phosphotransferase system (PTS) transporter NagE, respectively. In the cytoplasm, the peptide is released by AmiR and the sugars are separated by NagZ. Afterwards, two independent pathways feed the two sugars back into the *de novo* PG biosynthetic pathway. The enzymes are named as established for *E. coli* and *P. aeruginosa*, with the exception of the *C. crescentus* homolog of AmpD, which was renamed to AmiR due to its different domain organization. The enzymes analyzed in this study are indicated in bold type. Symbols are defined in the legend on the right.

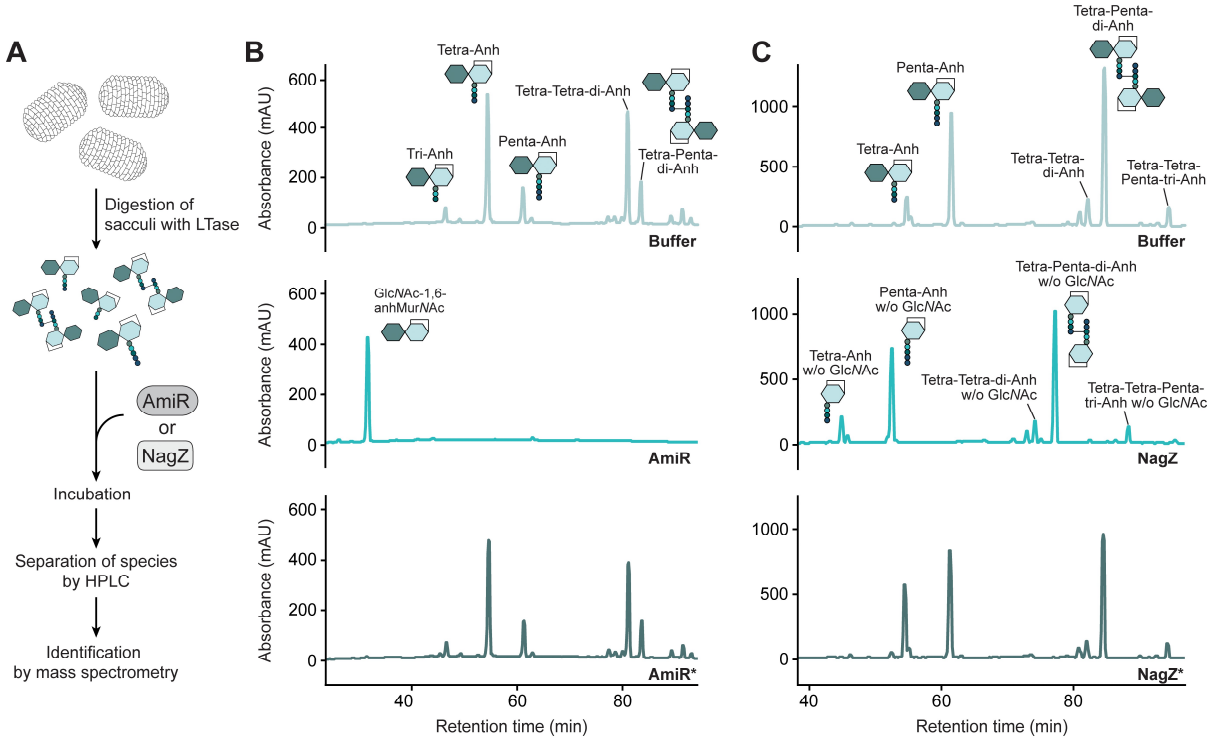

Figure 2. The AmiR and NagZ homologs are functional and have a broad substrate specificity. (A) Overview of the PG digestion assay used to assess the hydrolytic activities of AmiR and NagZ. **(B)** HPLC chromatograms showing the products generated upon incubation of anhydro-muropeptides from LT-treated PG sacculi without added proteins (Buffer), with AmiR or with a catalytically inactive AmiR variant (AmiR*). The identities of anhMur*N*Ac-peptides were determined based on their known retention times (Glauner, 1988). The AmiR reaction product Glc*N*Ac-1,6-anhMur*N*Ac was identified by mass spectrometry (**Figure 2–figure supplement 4A**). **(C)** HPLC chromatograms showing the products generated upon incubation of anhydro-muropeptides from LT-treated PG sacculi without added proteins (Buffer), with NagZ or with a catalytically inactive NagZ variant (NagZ*). Disaccharide-containing anhydro-muropeptides were identified based on their known retention times (Glauner, 1988). The identities of anhMur*N*Ac-peptides were validated by mass spectrometry analysis of the reaction products obtained after NagZ treatment of anhydro-muropeptide mixtures (**Figure 2–figure supplement 4B**). Note that the PG sacculi used in the AmiR and NagZ activity assays were isolated from different *E. coli* strains that exhibit distinct muropeptide profiles (see Methods).

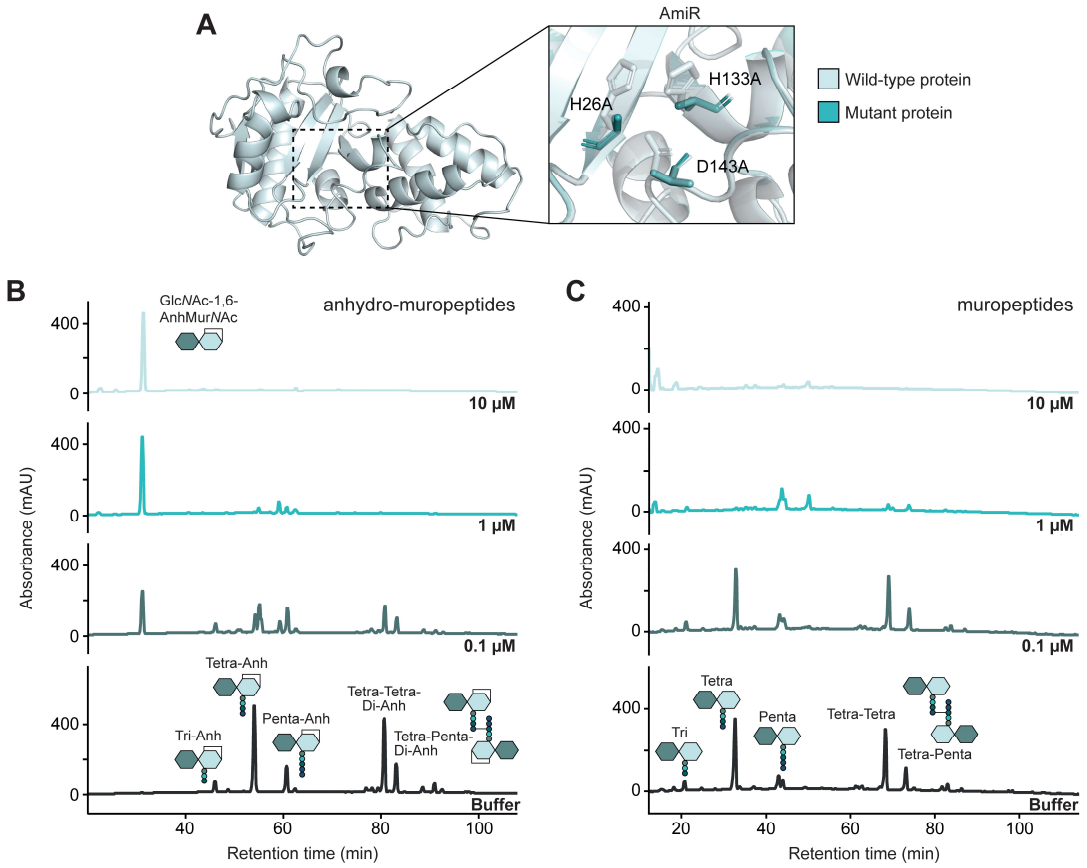

Figure 2–figure supplement 1. Substrate specificity of AmiR. (A) Structural models of AmiR and the catalytically inactive AmiR* variant, generated with AlphaFold 3 (Abramson et al., 2024). The magnified region shows the predicted catalytic site of AmiR and the amino acid substitutions introduced to generate AmiR*. **(B)** HPLC chromatograms showing the products generated upon incubation of anhydro-muropeptides from LT-treated PG sacculi for 16 h without added proteins (Buffer) or with the indicated concentrations of AmiR. **(C)** HPLC chromatograms showing the products generated upon incubation of muropeptides from muramidase-treated PG sacculi for 16 h without added proteins (Buffer) or with the indicated concentrations of AmiR. Reaction products were identified based on their known retention times (Glauner, 1988).

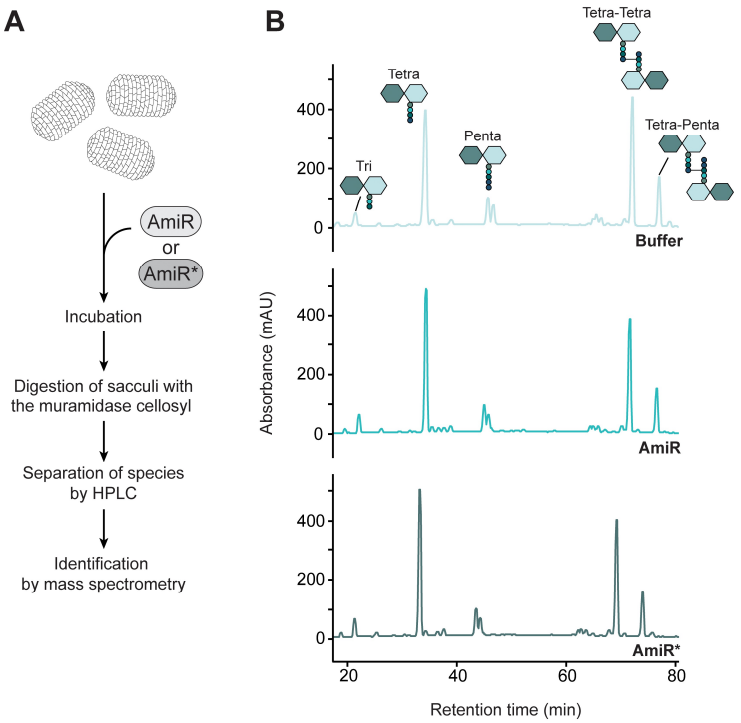

1513 **Figure 2–figure supplement 2. Lack of AmiR activity towards intact PG sacculi. (A)** Overview of the PG digestion assay used to
1514 assess the hydrolytic activity of AmiR on intact PG sacculi. **(B)** HPLC chromatograms showing the products generated upon incu-
1515 bation of intact PG sacculi without added proteins (Buffer), with AmiR or with the catalytically inactive AmiR variant AmiR* and
1516 subsequent cellosyl-mediated cleavage of the pre-treated sacculi into muropeptides. Muropeptides were identified based on their
1517 known retention times (Glauner, 1988).

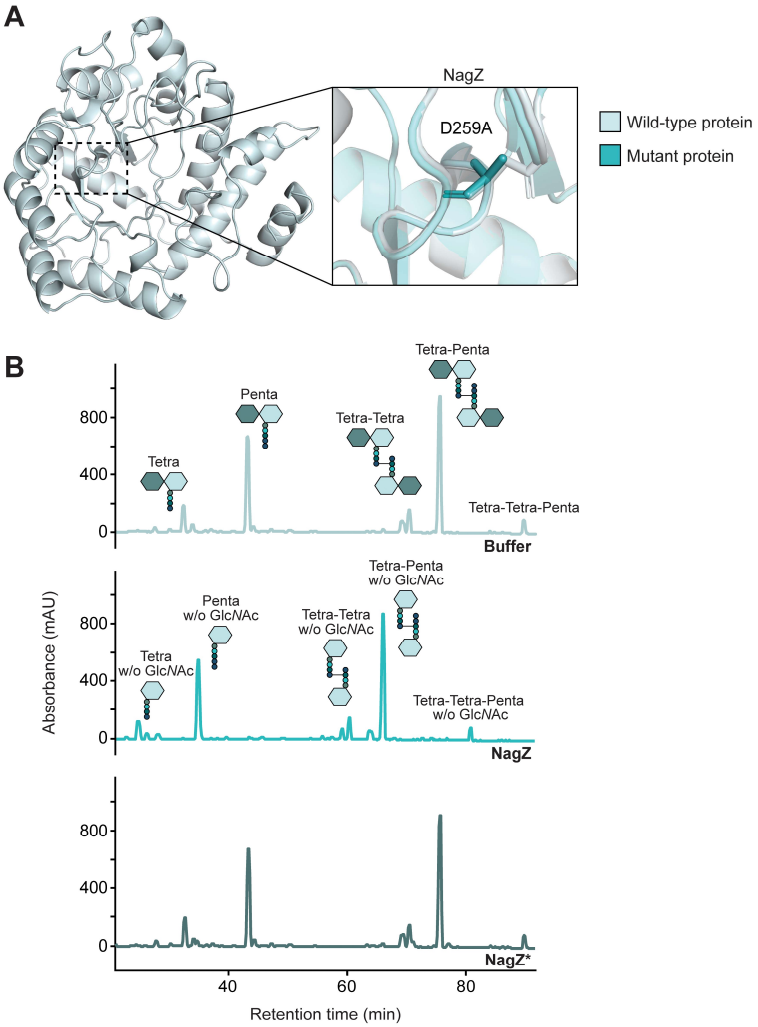

Figure 2–figure supplement 3. Activity of NagZ with muropeptides. (A) Structural models of NagZ and the catalytically inactive NagZ* variant, generated with AlphaFold 3 (Abramson et al., 2024). The magnified region shows the predicted catalytic site of NagZ and the amino acid substitution introduced to generate NagZ*. **(B)** HPLC chromatograms showing the products generated upon incubation of muropeptides from muramidase-treated PG sacculi without added proteins (Buffer), with NagZ or with a catalytically inactive NagZ variant (NagZ*). Disaccharide-containing muropeptides were identified based on their known retention times (Glauner, 1988). The identities of Mur*N*Ac-peptides were validated by mass spectrometry analysis of the reaction products obtained after NagZ treatment of anhydro-muropeptide mixtures (**Figure 2–figure supplement 4B**).

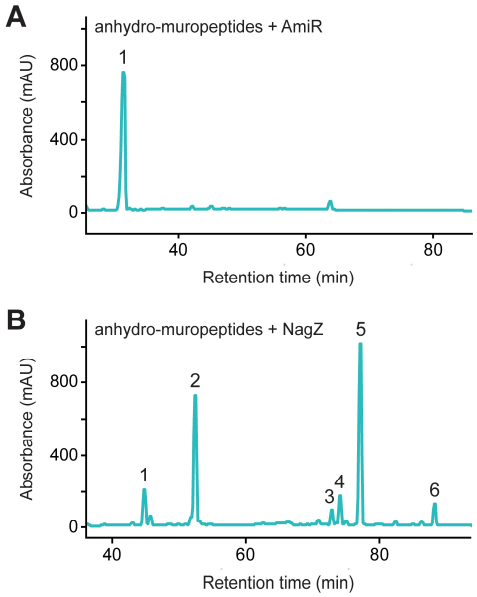

Peak ID	Observed m/z (charge)	Neutral mass (calculated)	Possible ID from MS/MS
1	478.97 (1+)	478.18	Glc*N*Ac-1,6-ahMur*N*Ac

Peak ID	Observed m/z (charge)	Neutral mass (calculated)	Possible ID from MS/MS
1	719.15 (1+)	718.15	Tetra-Anh minus Glc*N*Ac
2	790.18 (1+)	789.18	Penta-Anh minus Glc*N*Ac
3	738.75 (2+)	1475.5	TetraPenta(Gly5)-diAnh minus Glc*N*Ac (x2)
4	710.30 (2+)	1418.6	TetraTetra-diAnh minus Glc*N*Ac (x2)
5	745.92 (2+)	1489.84	TetraPenta-diAnh minus Glc*N*Ac (x2)
6	1095.97 (2+)	2189.94	TetraTetraPenta-triAnh minus Glc*N*Ac (x3)

Figure 2–figure supplement 4. Mass spectrometric identification of AmiR and NagZ reaction products. (A) Identification of the Glc*N*Ac–anhMur*N*Ac disaccharide generated by treatment of anhydro-muropeptides with AmiR. Sacculi isolated from *E. coli* D456 (Edwards and Donachie, 1993) were treated with the LT Slt70 *E. coli*. The graph shows the chromatogram obtained after separation of the sugar-containing reaction products by HPLC. The observed m/z ratios of the main product in peak 1 and the calculated molecular mass of the Glc*N*Ac-1,6-anhMur*N*Ac disaccharide are given in the table on the right. **(B)** Identification of the anhMur*N*Ac-peptide species generated by treatment of anhydro-muropeptides with NagZ. Sacculi isolated from *E. coli* CS703-1 (Meberg et al., 2001) were treated with the LT MltA from *E. coli*. The graph shows the chromatogram obtained after separation of the reaction products by HPLC. The table on the right gives the observed m/z ratios of the main product detected contained in the indicated peaks as well as the calculated molecular masses of the anhMur*N*Ac-peptides assigned to these peaks.

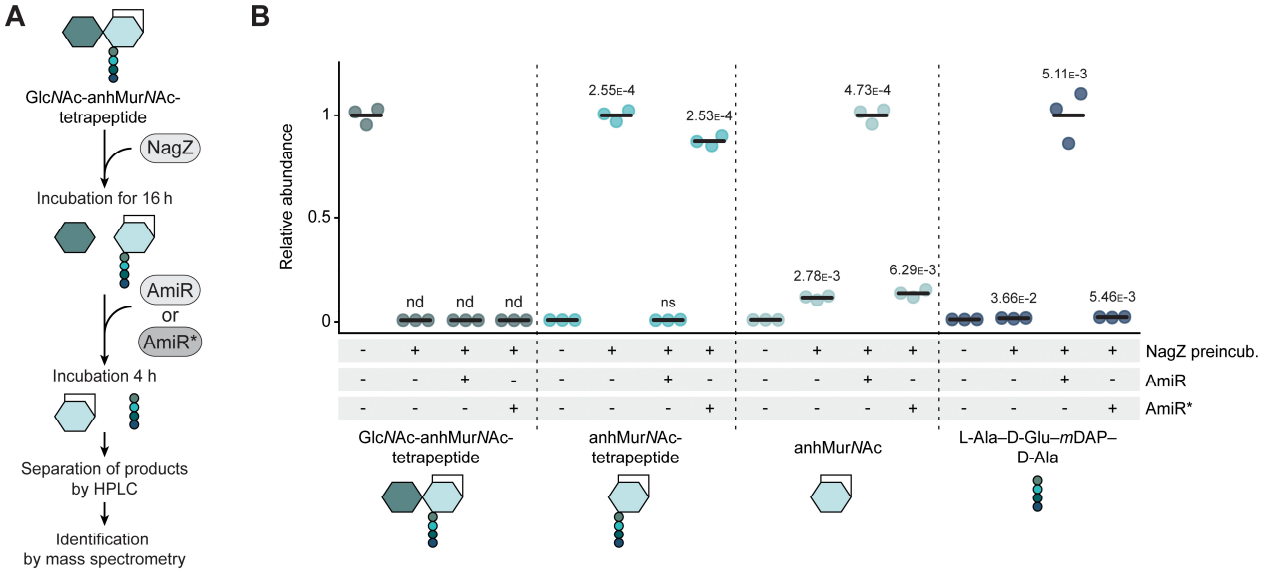

Figure 2–figure supplement 5: Activity of AmiR against anhMur*N*Ac-tetrapeptide. (A) Overview of the assay used to assess the activity of AmiR against anhMur*N*Ac-tetrapeptide. **(B)** Relative levels of Glc*N*Ac–anhMur*N*Ac-tetrapeptide, anhMur*N*Ac-tetrapeptide, anhMur*N*Ac and tetrapeptide (L-Ala–D-Glu–*m*DAP–D-Ala) obtained after preincubation of purified Glc*N*Ac–anhMur*N*Ac-tetrapeptide with (+) or without (-) NagZ, followed by incubation of the resulting products with or without AmiR or its catalytically inactive variant AmiR*. The final reaction products were identified by liquid chromatography-mass spectrometry (LC-MS). For each of them, the mass spectrometric peak area was normalized to the mean peak area measured for the reaction containing the highest product level. The statistical significance of differences between the protein-free and protein-containing reactions was determined using a two-sided Welch's t-test. ns indicates *p*-values > 0.1. nd, not detectable.

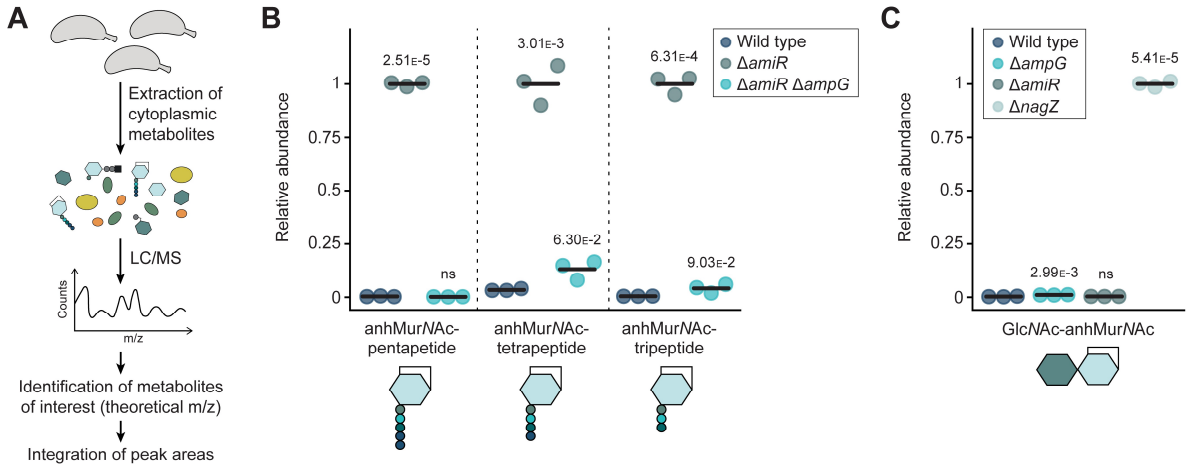

Figure 3. Metabolomic analysis reveals aberrant levels of PG recycling intermediates in recycling-deficient strains. (A) Overview of the analysis pipeline used to identify cytoplasmic PG recycling products. **(B)** Relative levels of the indicated anhMur*N*Ac-peptide species in the cytoplasm of *C. crescentus* wild-type, Δ*amiR* (PR033) and Δ*amiR* Δ*ampG* (PR221) cells, measured by metabolomics analysis. For each anhydro-muropeptide, the mass spectrometric peak areas were normalized against the mean obtained for the Δ*amiR* mutant. The statistical significance of differences between the wild type and the mutant strains was determined using a two-sided Welch's t-test. ns indicates p-values > 0.1. **(C)** Relative levels of the Glc*N*Ac–anhMur*N*Ac disaccharide in *C. crescentus* wild-type, Δ*ampG* (PR207), Δ*amiR* (PR033) and Δ*nagZ* (PR188) cells, assessed as for panel B. The mass spectrometric peak areas were normalized against the mean obtained for the Δ*nagZ* mutant. Statistical significance was determined as described for panel B.

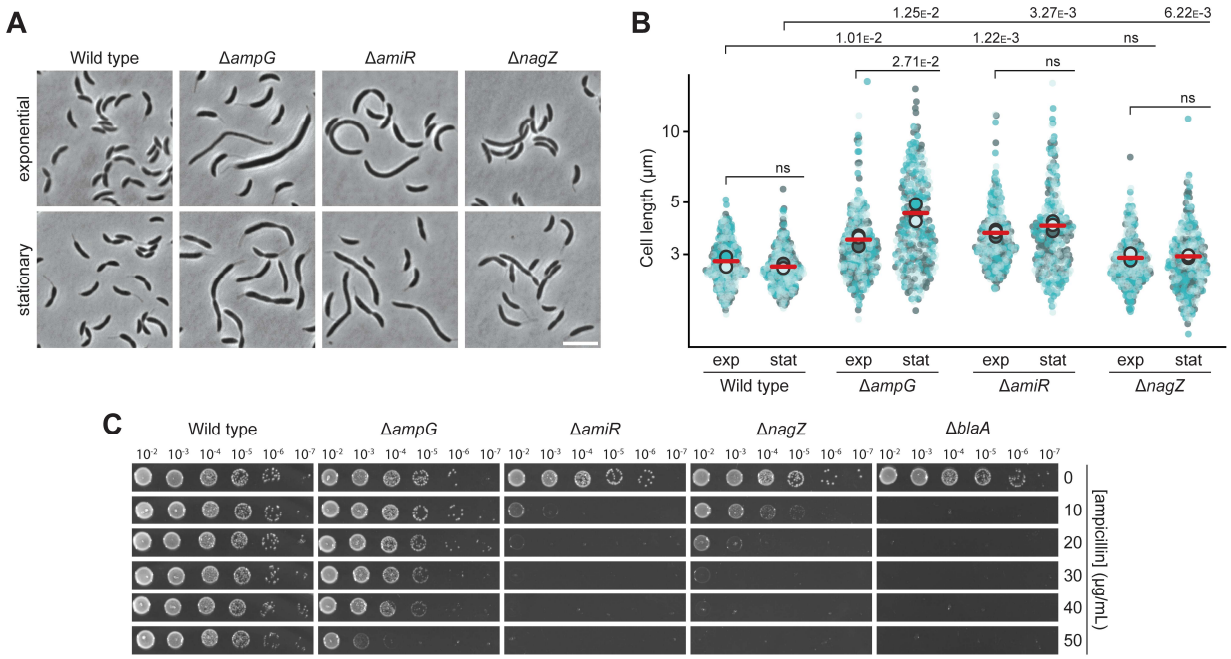

Figure 4. AmpG, AmiR and NagZ are required for proper cell shape and β-lactam resistance in *C. crescentus*. (A) Phase contrast images of *C. crescentus* wild-type, Δ*ampG* (PR207), Δ*amiR* (PR033) and Δ*nagZ* (PR188) cells harvested in the exponential and stationary growth phase. Scale bar: 5 µm. **(B)** Superplots showing the distribution of cell lengths in populations of *C. crescentus* wild-type, Δ*ampG* (PR207), Δ*amiR* (PR033) and Δ*nagZ* (PR188) cells in the exponential (exp) and stationary (stat) growth phase. Small dots represent the data of three independent replicates (shown in light blue, teal and dark grey; *n*=100 cells per replicate). Large dots represent the mean values of the three datasets, with their average indicated by a red horizontal line. The statistical significance (*p*-value) of differences between conditions was assessed using a two-sided Welch's *t*-test. ns indicates *p*-values > 0.1. **(C)** Serial dilution spot assay investigating the growth of wild-type, Δ*ampG* (PR207), Δ*amiR* (PR033), Δ*nagZ* (PR188) and Δ*blaA* (CS606) cells on agar plates with different concentrations of ampicillin. See **Source data 1** for all replicates (n=3 independent experiments).

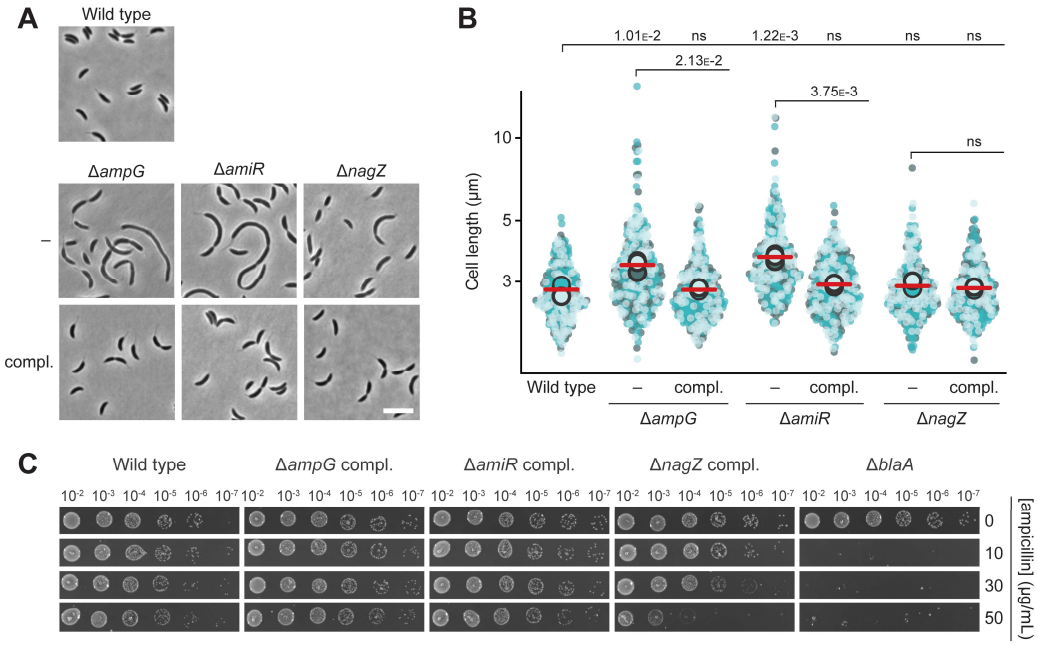

Figure 4-figure supplement 1. Reversion of the phenotypes of PG recycling-deficient strains through complementation with the corresponding wild-type genes. (A) Phase contrast images of *C. crescentus* wild-type, Δ*ampG* (PR207), Δ*ampG* P_{xyl}::P_{xyl}-*ampG* (PR285), Δ*amiR* (PR033), Δ*amiR* P_{xyl}::P_{xyl}-*amiR* (PR037), Δ*nagZ* (PR188) and Δ*nagZ* P_{xyl}::P_{xyl}-*nagZ* (PR284) cells harvested in the exponential growth phase. The complementation strains (compl.) were not induced. Scale bar: 5 µm. **(B)** Superplots showing the distribution of cell lengths in populations of the strains described in panel A. Data (*n*=100 cells per replicate) are presented as described for **Figure 4B**. The statistical significance (*p*-value) of differences between conditions was assessed using a two-sided Welch's *t*-test. ns indicates *p*-values > 0.1. The data for wild-type, Δ*amiR* and Δ*nagZ* cells are taken from **Figure 4B** and shown as a reference. **(C)** Serial dilution spot assay investigating the growth of wild-type, P_{xyl}::P_{xyl}-*ampG* (PR285), Δ*amiR* P_{xyl}::P_{xyl}-*amiR* (PR037), Δ*nagZ* P_{xyl}::P_{xyl}-*nagZ* (PR284) and Δ*blaA* (CS606) cells on agar plates with different concentrations of ampicillin. See **Source data 1** for all replicates (n=3 indepen¬dent experiments).

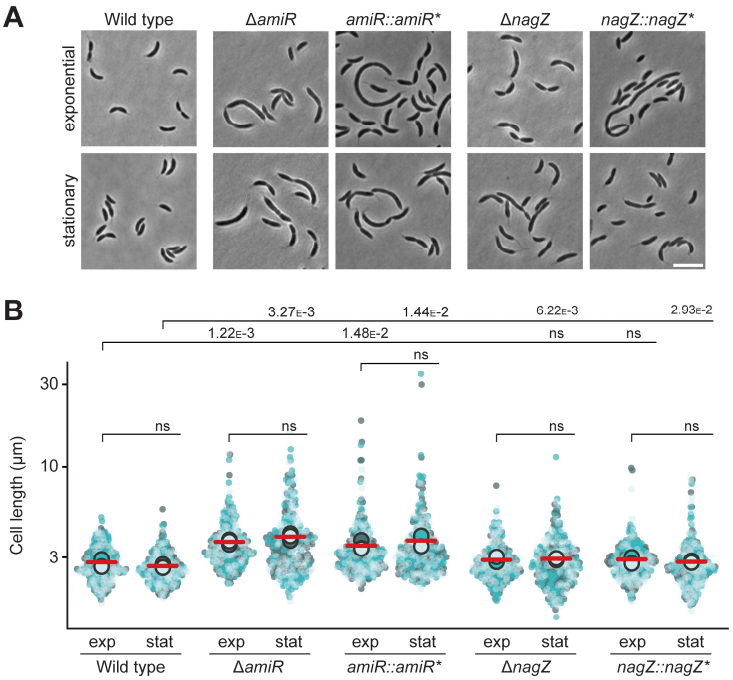

1563 **Figure 4–figure supplement 2. Morphological characterization of catalytically inactive AmiR and NagZ variants. (A)** Phase
1564 contrast images of *C. crescentus* wild-type, Δ*amiR* (PR033), *amiR::amiR** (PR173), Δ*nagZ* (PR188) and *nagZ::nagZ** (PR196) cells
1565 harvested in the exponential and stationary growth phase. Scale bar: 5 µm. **(B)** Superplots showing the distribution of cell lengths
1566 in populations of wild-type, Δ*amiR* (PR033), *amiR::amiR** (PR173), Δ*nagZ* (PR188) and *nagZ::nagZ** (PR196) cells in the exponential
1567 (exp) and stationary (stat) growth phase. Data (*n*=100 cells per replicate) are presented as described for **Figure 4B**. The statistical
1568 significance (*p*-value) of differences between conditions was assessed using a two-sided Welch's *t*-test. ns indicates *p*-values > 0.1.
1569 The data for wild-type, Δ*amiR* and Δ*nagZ* cells are taken from **Figure 3** and shown as a reference.

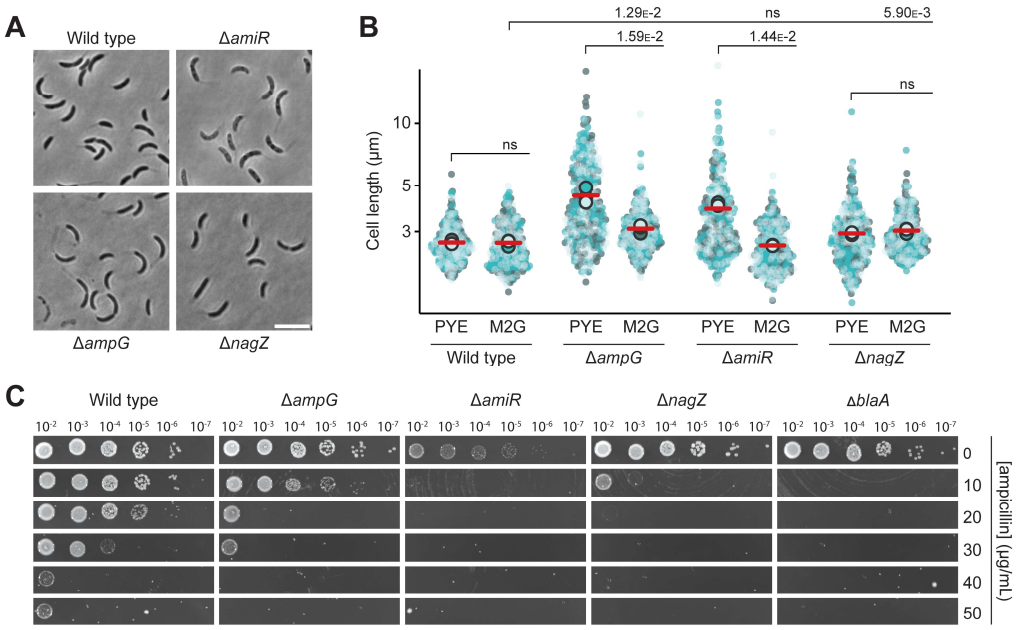

Figure 4–figure supplement 3. Growth of PG recycling-deficient mutants in minimal medium. (A) Phase contrast images of *C. crescentus* wild-type, Δ*ampG* (PR207), Δ*amiR* (PR033) and Δ*nagZ* (PR188) cells grown in minimal (M2G) medium and harvested in the stationary growth phase. **(B)** Superplots showing the distribution of cell lengths in populations of wild-type, Δ*ampG* (PR207), Δ*amiR* (PR033) and Δ*nagZ* (PR188) cells grown in rich medium (PYE) and minimal medium (M2G). Data (*n*=100 cells per replicate) are presented as described for **Figure 4B**. The statistical significance (*p*-value) of differences between conditions was assessed using a two-sided Welch's *t*-test. ns indicates *p*-values > 0.1. The distributions of cell lengths in rich medium are taken from **Figure 3** and shown as a reference. **(C)** Serial dilution spot assay investigating the growth of wild-type, Δ*ampG* (PR207), Δ*amiR* (PR033), Δ*nagZ* (PR188) and Δ*blaA* (CS606) cells on minimal medium agar plates with different concentrations of ampicillin. See **Source data 1** for all replicates (n=3 independent experiments).

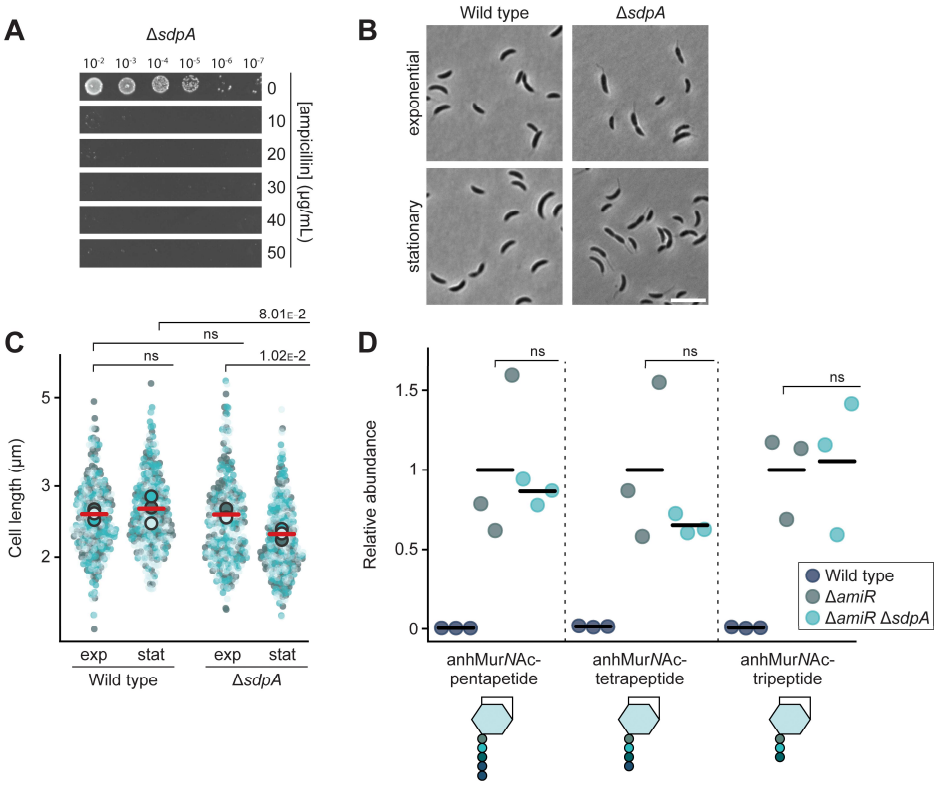

Figure 4–figure supplement 4. Redundant role of the LT SdpA in the production of anhydro-muropeptides. (A) Serial dilution spot assay investigating the growth of *C. crescentus* Δ*sdpA* (AM399) cells on agar plates containing different concentrations of ampicillin. The cells were spotted on the same plates as those depicted in **Figure 4C**. See **Source data 1** for all replicates (n=3 independent experiments). **(B)** Phase contrast images of *C. crescentus* wild-type and Δ*sdpA* (AM399) cells harvested in the exponential or stationary growth phase. **(C)** Superplots showing the distribution of cell lengths in populations of wild-type and Δ*sdpA* (AM399) cells harvested in the exponential (exp) and stationary (stat) growth phase. Data (*n*=100 cells per replicate) are presented as described for **Figure 4B**. The statistical significance (*p*-value) of differences between conditions was assessed using a two-sided Welch's *t*-test. ns indicates *p*-values > 0.1. **(D)** Levels of the indicated anhMur*N*Ac-peptide species in the cytoplasm of *C. crescentus* wild-type, Δ*amiR* (PR033) and Δ*amiR* Δ*sdpA* (PR260) cells, measured by metabolomics analysis through quantification of the corresponding mass spectrometric peak areas. For each anhydro-muropeptide, the mass spectrometric peak areas were normalized against the mean obtained for the Δ*amiR* mutant. The statistical significance of differences between the wild type and the mutant strains was determined using a two-sided Welch's *t*-test. ns indicates *p*-values > 0.1.

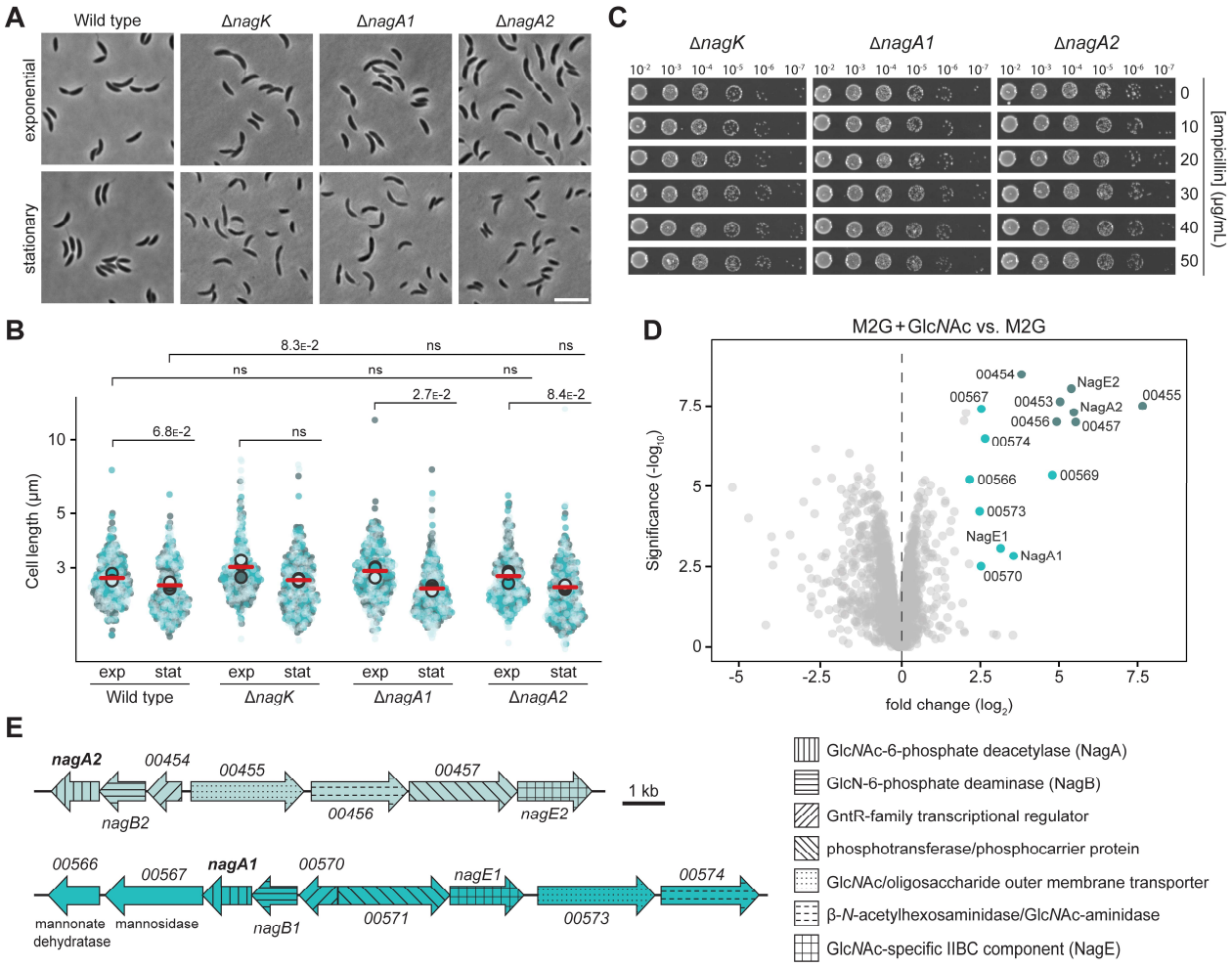

Figure 5. The Glc*N*Ac recycling pathway is dispensable for proper cell division and β-lactam resistance. (A) Phase contrast images of *C. crescentus* Δ*nagK* (PR255), Δ*nagA1* (PR256) and Δ*nagA2* (PR257) cells harvested in the exponential and stationary growth phase. Scale bar: 5 µm. **(B)** Superplots showing the distribution of cell lengths in populations of *C. crescentus* wild-type, Δ*nagK* (PR255), Δ*nagA1* (PR256) and Δ*nagA2* (PR257) cells in the exponential (exp) and stationary (stat) growth phase. Data (*n*=100 cells per replicate) are presented as described for **Figure 4B**. The statistical significance (*p*-value) of differences between conditions was assessed using a two-sided Welch's *t*-test. ns indicates *p*-values > 0.1. **(C)** Serial dilution spot assays investigating the growth of *C. crescentus* Δ*nagK* (PR255), Δ*nagA1* (PR256) and Δ*nagA2* (PR257) cells on agar plates containing different concentrations of ampicillin. The cells were spotted on the same plates as those depicted in **Figure 4C**. See **Source data 1** for all replicates (n=3 independent experiments). **(D)** Volcano plot illustrating differential protein abundance in *C. crescentus* wild-type cells grown in M2G minimal medium with Glc*N*Ac compared to plain M2G medium. Grey dots represent proteins identified by mass spectrometry. The x-axis indicates the log2 of the average difference in the peptide counts for the two different conditions (*n*=3 independent replicates). The y-axis shows the -log10 of the corresponding *p*-value. Proteins encoded in the two *nag* gene clusters are highlighted in color and annotated. The colors correspond to those used in panel E. **(E)** Schematic representation of the two *nag* gene clusters. The predicted functions of the gene products are specified in the legend on the right.

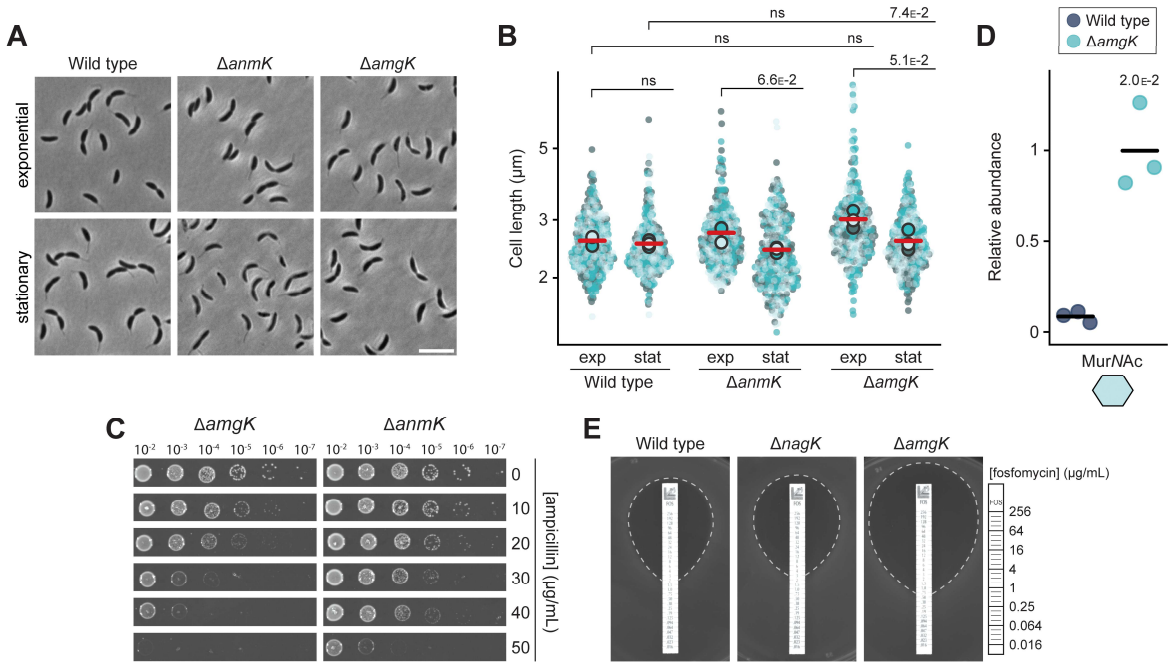

Figure 6. *C. crescentus* recycles anhMur*N*Ac through a functional MurU pathway. (A) Phase contrast images of *C. crescentus* Δ*anmK* (PR252) and Δ*amgK* (PR262) cells, harvested in the exponential and stationary growth phase. Scale bar: 5 µm. **(B)** Superplots showing the distribution of cell lengths in populations of *C. crescentus* wild-type, Δ*anmK* (PR252), and Δ*amgK* (PR262) cells in the exponential (exp) and stationary (stat) growth phase. Data (*n*=100 cells per replicate) are presented as described for **Figure 4B**. The statistical significance (*p*-value) of differences between conditions was assessed using a two-sided Welch's *t*-test. ns indicates *p*-values > 0.1. **(C)** Serial dilution spot assay investigating the growth of *C. crescentus* Δ*anmK* (PR252) and Δ*amgK* (PR262) on plates containing different concentrations of ampicillin. The cells were spotted on the same plates as those depicted in **Figure 4C**. See **Source data 1** for all replicates (n=3 independent experiments). **(D)** Levels of Mur*N*Ac in the cytoplasm of *C. crescentus* wild-type and Δ*amgK* (PR262) cells, measured by metabolomics analysis through quantification of the corresponding mass spectrometric peak areas. The mass spectrometric peak areas were normalized against the mean obtained for the Δ*amgK* mutant. The statistical significance of differences between the two strains was determined using a two-sided Welch's t-test. **(E)** Analysis of the growth of *C. crescentus* wild-type, Δ*nagK* (PR255) and Δ*amgK* (PR262) cells on agar containing a fosfomycin gradient. The fosfomycin concentrations on the MIC test strip are indicate in the legend on the right.

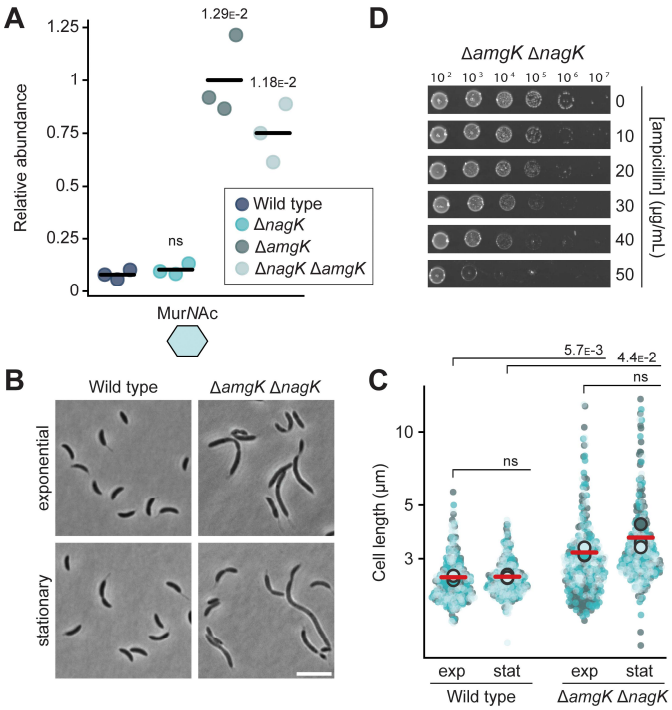

Figure 7. Recycling of the disaccharide moiety plays only a minor role in cell division and β-lactam resistance. (A) Phase contrast images of *C. crescentus* Δ*amgK* Δ*nagK* (PR261) cells, harvested in the exponential and stationary growth phase. Scale bar: 5 µm. **(B)** Superplots showing the distribution of cell lengths in populations of *C. crescentus* wild-type and Δ*amgK* Δ*nagK* (PR261) cells in the exponential (exp) and stationary (stat) growth phase. Data (*n*=100 cells per replicate) are presented as described for **Figure 4B**. The statistical significance (*p*-value) of differences between conditions was assessed using a two-sided Welch's *t*-test. ns indicates *p*-values > 0.1. **(C)** Levels of Mur*N*Ac in the cytoplasm of *C. crescentus* wild-type, Δ*nagK* (PR255), Δ*amgK* (PR262) and Δ*nagK* Δ*amgK* (PR261) cells, as determined by metabolomics analysis. Data were normalized to the mean Mur*N*Ac levels of Δ*amgK* cells. The statistical significance of differences between strains was determined using a two-sided Welch's *t*-test. ns indicates *p*-values < 0.1. **(D)** Serial dilution spot assays investigating the growth of *C. crescentus* Δ*amgK* Δ*nagK* (PR261) cells on agar plates containing different concentrations of ampicillin. The cells were spotted on the same plates as those depicted in **Figure 4C**. See **Source data 1** for all replicates (n=3 independent experiments).

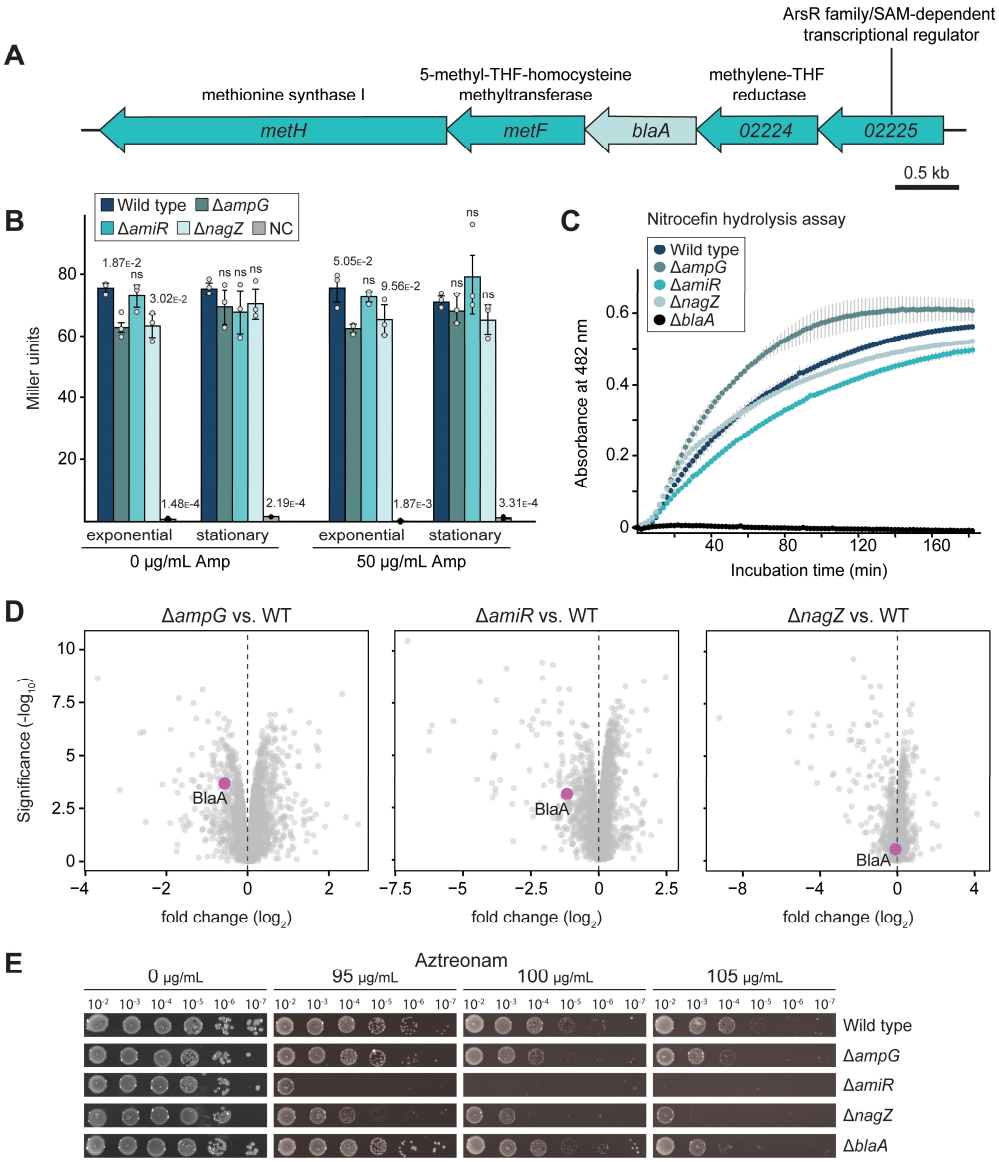

Figure 8. BlaA function is not regulated at the levels of transcription, protein accumulation or enzymatic activity. (A) Organization of the putative five-gene operon containing the *blaA* gene. The annotation or ORF number of the open reading frames and the predicted functions of their gene products are indicated. **(B)** Activity of the promoter likely driving the expression of the *blaA*-containing operon in different strain backgrounds. The *C. crescentus* wild-type, Δ*ampG* (PR207), Δ*amiR* (PR033) and Δ*nagZ* (PR188) strains were transformed with a plasmid carrying a 400 bp fragment of the CCNA_02225 upstream region fused to a β-galactosidase reporter gene and assayed for reporter activity. Strains transformed with the empty plasmid served as negative controls (NC). The underlying data are shown as grey dots. The statistical significance (*p*-value) of differences between strains was calculated using a two-sided Welch's t-test. ns indicates *p*-values > 0.1. **(C)** β-lactamase activity of *C. crescentus* wild-type, Δ*ampG* (PR207), Δ*amiR* (PR033) and Δ*nagZ* (PR188) cells, as determined by monitoring the hydrolysis of the chromogenic β-lactam nitrocefin in permeabilized cells over time. **(D)** Volcano plots showing differential protein abundance in *C. crescentus* Δ*ampG* (PR207), Δ*amiR* (PR033) and Δ*nagZ* (PR188) cells compared to wild-type cells. Grey dots represent proteins identified by mass spectrometry. The x-axis indicates the log2 of the average difference in the peptide counts for the two different conditions (*n*=4 independent replicates). The y-axis shows the -log10 of the corresponding *p*-value. The BlaA protein is highlighted in magenta. **(E)** Serial dilution spot assays investigating the growth of *C. crescentus* wild-type, Δ*ampG* (PR207), Δ*amiR* (PR033), Δ*nagZ* (PR188) and Δ*blaA* cells (CS606) on agar plates containing different concentrations of aztreonam. See **Source data 1** for all replicates (n=3 independent experiments).

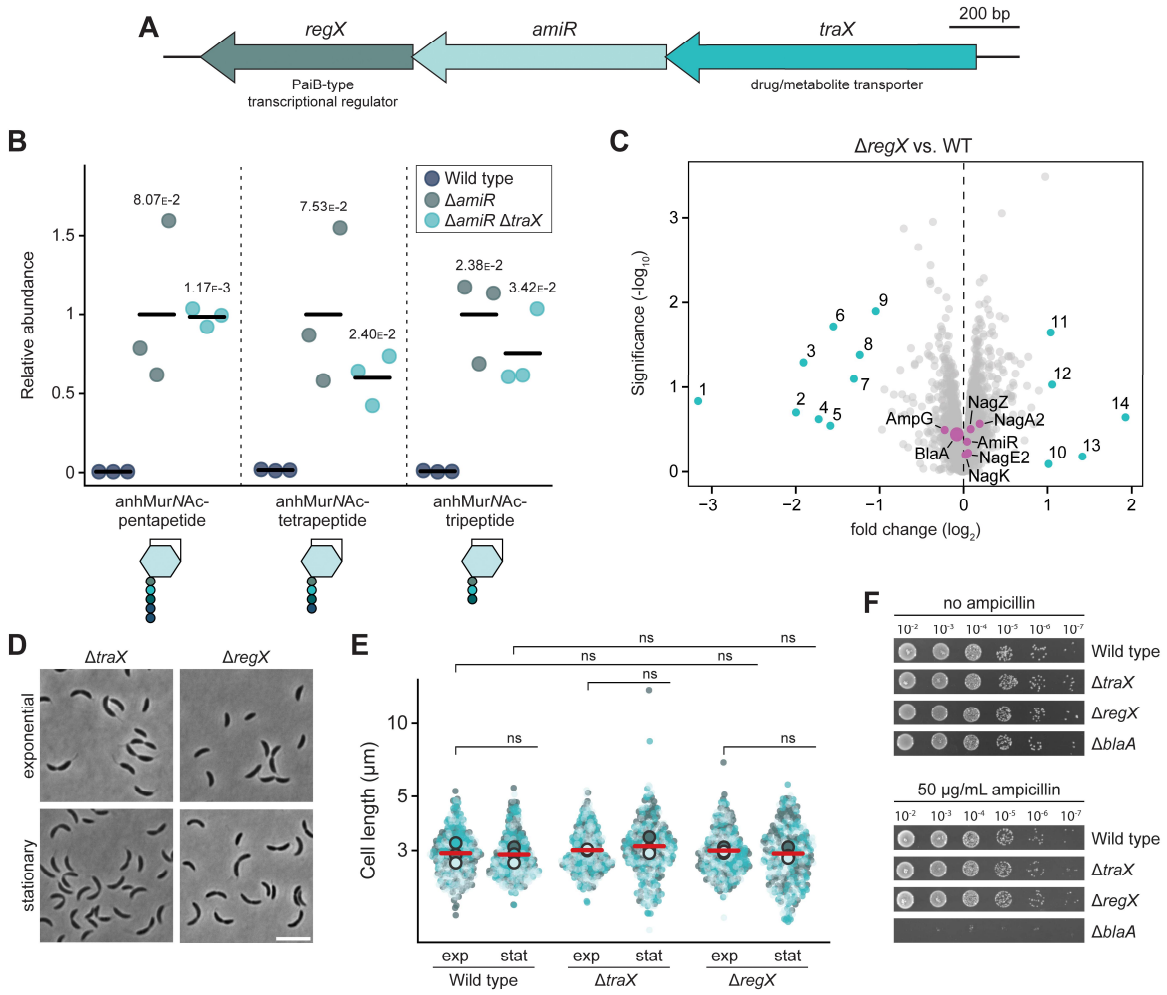

Figure 8–figure supplement 1. The two genes forming an operon with *amiR* are dispensible for PG recycling or β-lactam resistance. (A) Genomic context of *amiR*. The gene names and the predicted functions of the respective gene products are indicated. **(B)** Levels of the indicated anhMur*N*Ac-peptide species in the cytoplasm of *C. crescentus* wild-type, Δ*amiR* (PR033) and Δ*amiR* Δ*traX* (PR258) cells, measured by metabolomics analysis through quantification of the corresponding mass spectrometric peak areas. **(C)** Volcano plot showing differences in protein abundance in *C. crescentus* Δ*regX* (PR154) cells in comparison to wild-type cells. Grey dots represent proteins identified by mass spectrometry. The x-axis indicates the log2 of the average difference in the peptide counts for the two different conditions (n=3 independent replicates). The y-axis shows the -log10 of the corresponding *p*-value. Proteins with a fold change smaller than 0.5 or larger than 2 are highlighted in color and numbered. Details on these proteins are given in **Figure 8–table supplement 1**. **(D)** Phase contrast images of Δ*traX* (PR153) and Δ*regX* (PR154) cells, harvested in the exponential or stationary growth phase. Scale bar: 5 µm. **(E)** Superplots showing the distribution of cell lengths in populations of *C. crescentus* wild-type, Δ*traX* (PR153) and Δ*regX* (PR154) cells in the exponential (exp) and stationary (stat) growth phase. Data (*n*=100 cells per replicate) are presented as described for **Figure 4B**. The statistical significance (*p*-value) of differences between conditions was assessed using a two-sided Welch's *t*-test. ns indicates *p*-values > 0.1. **(F)** Serial dilution spot assays investigating the growth of *C. crescentus* wild-type, Δ*traX* (PR153), Δ*regX* (PR154) and Δ*blaA* (CS606) cells on agar plates in the absence or presence of ampicillin. See **Source data 1** for all replicates (n=3 independent experiments).

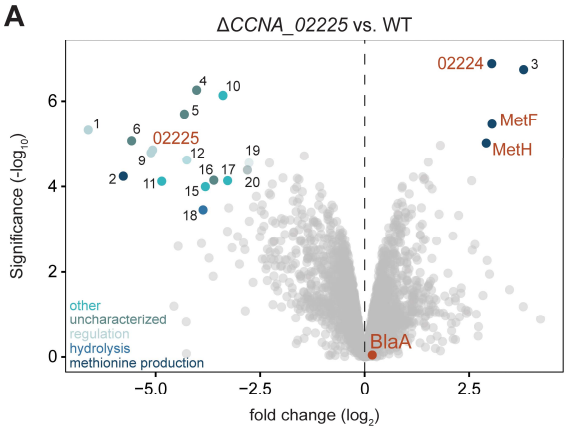

B

	Name	Fold change (log2)	Significance ($-\log_{10}$)	Protein
1	*fixK*	-6.6139	5.3295	Hypoxia transcriptional regulator FixK
2	*hemN*	-5.7751	4.2390	Coproporphyrinogen-III oxidase
3	*metE*	3.8010	6.7442	5-methyltetrahydropteroyltriglutamate-homocysteine methyltransferase
4	CCNA_01464	-4.0213	6.2515	Uncharacterized protein
5	CCNA_03363	-4.3145	5.7053	Conserved hypothetical membrane protein
6	CCNA_02604	-5.5765	5.0750	Host cell attachment protein
7	CCNA_02225	-5.0726	4.8569	ArsR family/SAM-dependent transcriptional regulator
8	CCNA_02224	3.0385	6.8826	Methylenetetrahydrofolate reductase
9	*ftrB*	-5.1131	4.7917	CRP-family transcription regulator FtrB
10	CCNA_01592	-3.3914	6.1318	SN-glycerol-3-phosphate transport ATP-binding protein
11	CCNA_01144	-4.8556	4.1205	Cytochrome c oxidase polypeptide II
12	CCNA_01704	-4.2552	4.6199	Cytochrome c
13	CCNA_02222	3.0447	5.4711	5-methyltetrahydrofolate-homocysteine methyltransferase homocysteine-binding subunit
14	CCNA_02221	2.9066	5.0214	Methionine synthase
15	*fixH*	-3.8114	3.9951	Cation pump-linked membrane protein fixH
16	CCNA_00391	-3.6098	4.1459	Secreted protein
17	CCNA_01745	-3.2790	4.1348	thioredoxin-dependent peroxiredoxin
18	CCNA_02313	-3.8669	3.4553	Alpha/beta hydrolase family protein
19	CCNA_00220	-2.7669	4.5496	Thiol-disulfide isomerase and thioredoxin
20	CCNA_01716	-2.8058	4.3821	MotA/TolQ/ExbB proton channel family protein

Figure 8–figure supplement 2. Changes in protein accumulation upon deletion of CCNA_02225. (A) Volcano plot showing differential protein abundance in *C. crescentus* ΔCC*NA_02225* (PR218) vs. wild-type cells. Grey dots represent proteins identified by mass spectrometry. The x-axis indicates the log2 of the average difference in the peptide counts for the two different conditions (*n*=3 independent replicates). The y-axis shows the -log10 of the corresponding *p*-value. The 20 proteins with the highest fold change according to Manhattan distance are highlighted in color and numbered. The functional categorization of these genes is indicated in the lower left corner of the plot. Proteins encoded in the five-gene operon are labeled in orange. **(B)** List of the most highly deregulated proteins in the ΔCC*NA_02225* (PR218) mutant. The table gives the gene name or ORF number, the fold change, the *p*-value and the predicted function for the proteins numbered in panel A.

1668 **Figure 8–table supplement 1. Proteins found to be differentially accumulated in Δ*regX* cells compared to wild-type cells.** The
1669 table lists the ORF numbers and predicted functions of the numbered proteins in **Figure 8–figure supplement 1C**.

Protein number	ORF number	Predicted function
1	*CCNA_00845*	Antitoxin protein RelB-1
2	*CCNA_02277*	TonB-dependent outer membrane channel HutA
3	*CCNA_00081*	uncharacterized protein
4	*CCNA_03558*	ATP synthase epsilon chain AtpC
5	*CCNA_02275*	ABC transporter, periplasmic component
6	*CCNA_00437*	Methyl-accepting chemotaxis protein
7	*CCNA_03263*	TonB-dependent receptor
8	*CCNA_01707*	Gluconate 2-dehydrogenase subunit 3-family protein
9	*CCNA_03446*	Feruloyl-CoA synthetase
10	*CCNA_01186*	uncharacterized protein
11	*CCNA_00987*	Stress response protein CsbD
12	*CCNA_00928*	GntR family transcriptional regulator
13	*CCNA_00374*	ATP synthase protein I
14	*CCNA_01205*	ABC transporter ATP-binding protein

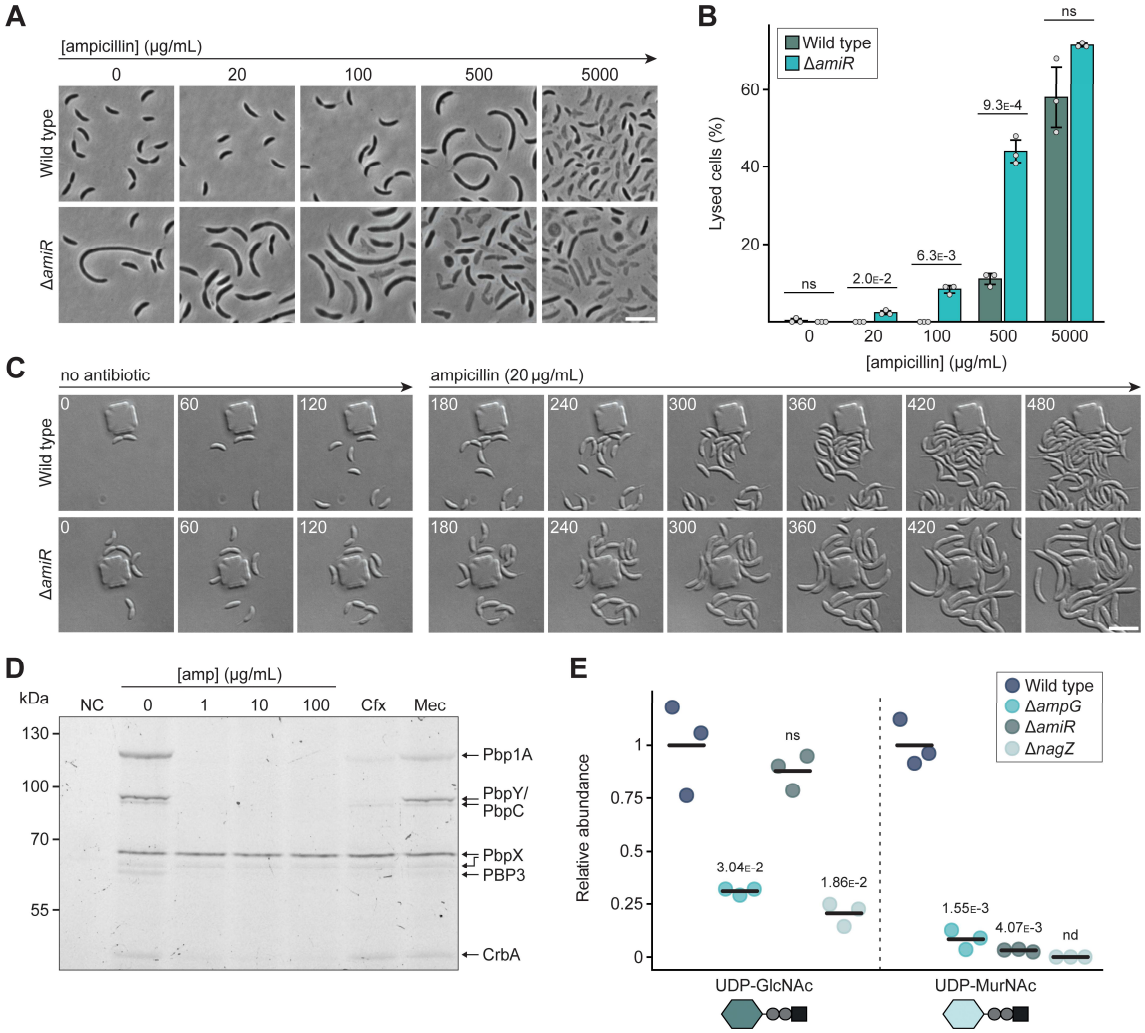

Figure 9. PG recycling defects increase the sensitivity of the septal PG synthetic machinery to ampicillin and reduce PG precursor biosynthesis. (A) Phase contrast images of *C. crescentus* wild-type and Δ*amiR* (PR033) cells, incubated for 3 h in the presence of different concentrations of ampicillin. Scale bar: 5 µm. **(B)** Quantification of the fraction of lysed cells in cultures of *C. crescentus* wild-type and Δ*amiR* (PR033) cells, incubated for 3 h in the presence of different concentrations of ampicillin. The bars represent the mean (±SD) of three independent replicates (*n*=100 cells per condition). The underlying data are shown as grey dots. The statistical significance (*p*-value) of differences between strains was calculated using a two-sided Welch's t-test. ns indicates *p*-values > 0.1. **(C)** Time-lapse microscopy analysis showing *C. crescentus* wild-type and Δ*amiR* (PR033) cells in a microfluidic flow cell before and after ampicillin treatment. After 3 h of growth in antibiotic-free medium, the cells were shifted to medium containing 20 µg/mL ampicillin. Images were taken at 5 min intervals for a total duration of 8 h. Shown are representative frames of the time-lapse series. The full sequences are shown in **Figure 9-Video 1** and **Figure 9-Video 2**. **(D)** Image of an SDS-gel showing the labeling of PBPs with the fluorescent β-lactam bocillin-FL in the absence or presence of other β-lactams. Crude membrane fractions of *C. crescentus* Δ*blaA* (CS606) cells were pre-incubated with the indicated concentrations of ampicillin, 5 µg/mL cefalexin (Cfx) or 100 µg/mL mecillinam (Mec), treated with bocillin-FL and then subjected to SDS gel electrophoresis to separate the labeled PBPs prior to fluorescence imaging. **(E)** Levels of UDP-Glc*N*Ac and UDP-Mur*N*Ac in the cytoplasm of *C. crescentus* wild-type, Δ*ampG* (PR207), Δ*amiR* (PR033) and Δ*nagZ* (PR188) cells, measured by metabolomics analysis through quantification of the corresponding mass spectrometric peak areas. For each PG precursor, the mass spectrometric peak areas were normalized against the mean obtained for the wild-type strain. The statistical significance of differences between the wild type and the mutant strains was determined using a two-sided Welch's t-test. ns indicates *p*-values > 0.1; nd: not detectable.

1688 **Figure 9–video 1. Effect of ampicillin on the growth of *C. crescentus* wild-type cells.** *C. crescentus* wild-type cells were cultivated
1689 in a microfluidic flow cell for 3 h in antibiotic-free medium and then shifted to medium containing 20 µg/mL ampicillin. Phase
1690 contrast images were taken at 5-min intervals. Scale bar: 5 µm.

1691 **Figure 9–video 2. Effect of ampicillin on the growth of *C. crescentus* Δ*amiR* cells.** *C. crescentus* Δ*amiR* (PR033) cells were culti-
1692 vated in a microfluidic flow cell for 3 h in antibiotic-free medium and then shifted to medium containing 20 µg/mL ampicillin.
1693 Phase contrast images were taken at 5-min intervals. Scale bar: 5 µm.

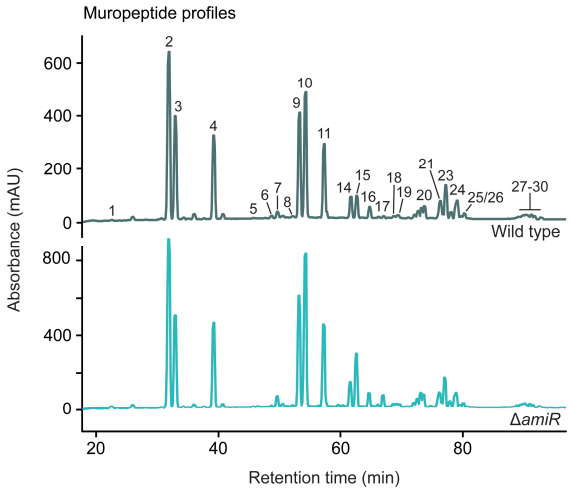

1694 **Figure 9–figure supplement 1. Muropeptide composition of PG sacculi from wild-type and Δ*amiR* cells.** Shown are HPLC
1695 chromatograms resolving the muropeptides obtained by muramidase treatment of PG sacculi isolated from stationary wild-type
1696 or Δ*amiR* (PR033) cells. The muropeptides contained in the different peaks are listed in **Figure 9–table supplement 1**. A summary
1697 of the data obtained is given in **Figure 9–table supplement 2**.

1698 **Figure 9–table supplement 1. Muropeptide composition of peptidoglycan isolated from stationary *C. crescentus* wild-type and**
1699 **Δ*amiR* cells.** The table gives the relative abundance of the indicated muropeptide species, calculated from the areas of the
1700 corresponding peaks in the HPLC chromatograms from **Figure 9–figure supplement 1**. Two independent replicates were analyzed
1701 per strain.

Peak no.	Muropeptide	Peak area (%)			
		Wild type		Δ*amiR*	
1	Tri	0.0	0.0	0.3	0.0
2	Tetra	20.2	20.1	19.2	19.3
3	Penta(Gly5)	11.7	11.6	9.7	10.9
	unknown-possibly Di	0.6	0.7	0.4	0.7
4	Penta	9.2	9.2	8.6	9.7
5	TriTri(Dap)	0.0	0.0	0.0	0.0
6	TetraTri (Dap))	0.2	0.2	1.0	0.2
7	Tri-Anh (+small amount of TetraTri (D,L))	0.7	0.7	0.3	0.7
8	TetraTetra(Dap)	0.0	0.2	0.2	0.2
9	TetraPenta(Gly5)	10.8	11.0	10.5	11.2
10	TetraTetra	13.5	13.4	16.2	13.3
11	TetraPenta	7.6	8.2	8.1	8.9
12	TetraTetraTri or TetraTetraTri(Dap)	0.0	0.0	0.0	0.0
13	TetraAnh	0.5	0.0	0.2	0.0
14	TetraTetraPenta(Gly5)	2.2	2.2	2.3	2.6
15	TetraTetraTetra	2.2	2.2	4.7	2.4
16	TetraTetraPenta	1.1	1.2	1.2	1.3
17	TetraTetraTetraTetra	0.2	0.2	1.0	0.3
18	TetraTetraTetraPenta	0.3	0.3	0.3	0.3
19	Penta-Anh	0.5	0.5	0.4	0.5
20	TetraTetra-Anh	2.4	2.2	2.4	2.3
21	TetraPenta-Anh	2.4	2.4	2.1	2.3
22	TetraTetraTriAnh or TetraTetraTri(Dap)Anh	0.4	0.4	0.4	0.4
23	TetraTetraTetra-Anh	3.4	3.3	2.7	3.0
24	TetraTetraPenta-Anh	2.9	2.8	2.1	2.6
25	TetraTetraTetraPenta-Anh I	0.3	0.3	0.3	0.3
26	TetraTetraTetraPenta-Anh II	0.6	0.6	0.4	0.6
27	TetraTetraTetra-diAnh	1.0	1.0	0.6	0.9
28	TetraTetraTetraPenta-diAnh	0.5	0.5	0.4	0.5
29	TetraTetra-diAnh	0.4	0.4	0.3	0.3
30	TetraTetraPenta-diAnh	0.3	0.3	0.0	0.2

1702 **Figure 9–table supplement 2. Overview of the muropeptide species identified in peptidoglycan from stationary *C. crescentus* wild-type and Δ*amiR* cells.** The table summarizes the relative abundance of different muropeptide species, calculated from the values listed in **Figure 9–table supplement 1**. Two independent replicates were analyzed per strain.

Muropeptide species	Peak area (%)			
	Wild type		Δ*amiR*	
All known	95.8	95.9	96.1	96.0
Monomers (total)	44.5	43.9	40.2	43.0
Dimers (total)	38.9	39.6	42.4	40.2
Trimers (total)	14.0	13.9	14.5	14.1
Tetramers (total)	1.9	2.0	2.5	2.0
Tripeptides (total)	0.9	1.0	1.3	1.0
Tetrapeptides (total)	62.6	62.2	65.7	61.8
Pentapeptides (total)	35.8	36.2	32.6	36.5
Chain ends (anhydros)	8.3	7.6	6.1	7.4
Average chain length	12.0	13.1	16.2	13.4
3-3 crosslinks	0.3	0.4	0.8	0.3
Degree of cross-linkage	30.2	30.5	32.7	31.0
% peptides in cross-links	55.5	56.1	59.8	57.0

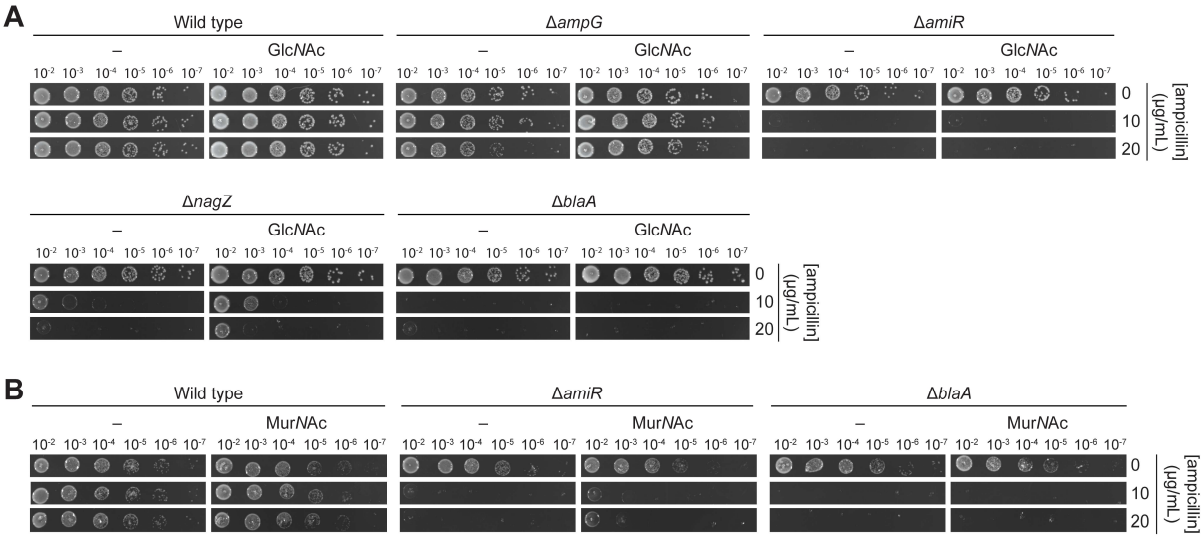

Figure 9–figure supplement 2. Ampicillin sensitivity of PG recycling-defective mutants in the presence of Glc*N*Ac. (A) Serial dilution spot assay investigating the growth of *C. crescentus* wild-type, Δ*ampG* (PR207), Δ*amiR* (PR033), Δ*nagZ* (PR188) and Δ*blaA* (CS606) cells on agar plates containing different concentrations of ampicillin in the presence of 0.3% Glc*N*Ac. (B) Serial dilution spot assay investigating the growth of *C. crescentus* wild-type, Δ*amiR* (PR033) and Δ*blaA* (CS606) cells on agar plates containing different concentrations of ampicillin in the presence of 100 µg/mL Mur*N*Ac. See **Source data 1** for all replicates (n=3 independent experiments).

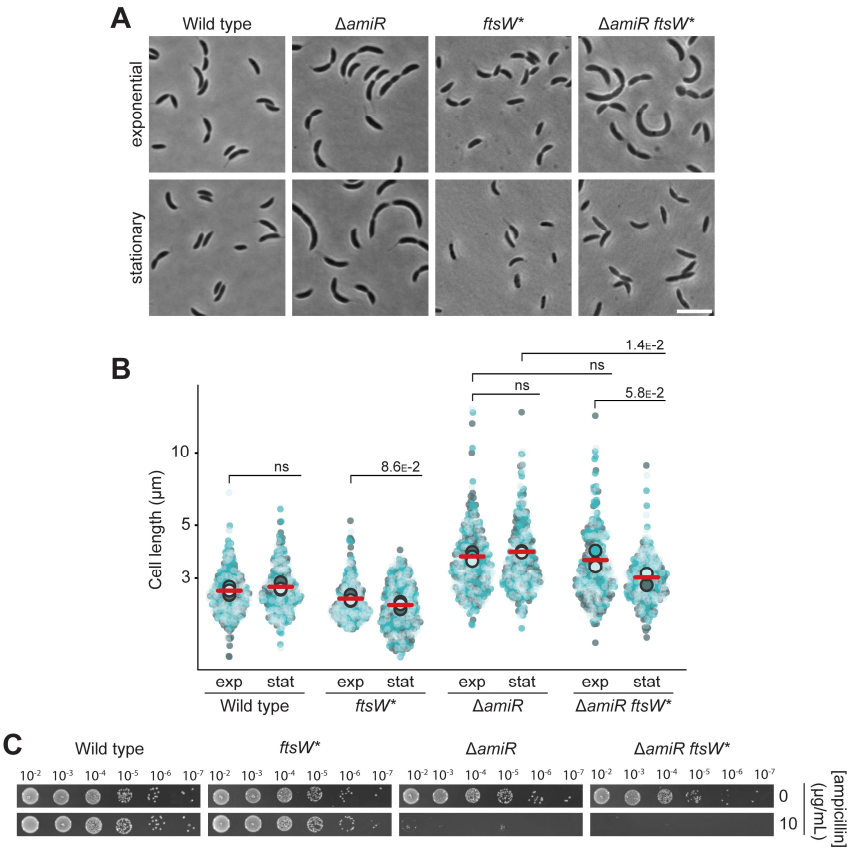

Figure 10. The cell filamentation phenotype of Δ*amiR* cells is rescued by hyper-activation of the septal FtsW-PBP3 PG biosynthetic complex. (A) Phase contrast images of *C. crescentus* wild-type, Δ*amiR* (PR033), *ftsW::ftsW** (ML2103) and Δ*amiR ftsW::ftsW** (PR246) cells, harvested in the exponential and stationary growth phase. **(B)** Superplots showing the distribution of cell lengths in populations of the strains described in panel A in the exponential (exp) and stationary (stat) growth phase. Data (*n*=100 cells per replicate) are presented as described for **Figure 4B**. The statistical significance (*p*-value) of differences between conditions was assessed using a two-sided Welch's *t*-test. ns indicates *p*-values > 0.1. **(C)** Serial dilution spot assay investigating the growth of *C. crescentus ftsW::ftsW** (ML2103), Δ*amiR* (PR033) and Δ*amiR ftsW::ftsW** (PR246) cells on agar plates containing no or 10 µg/mL ampicillin. See **Source data 1** for all replicates (n=3 independent experiments).

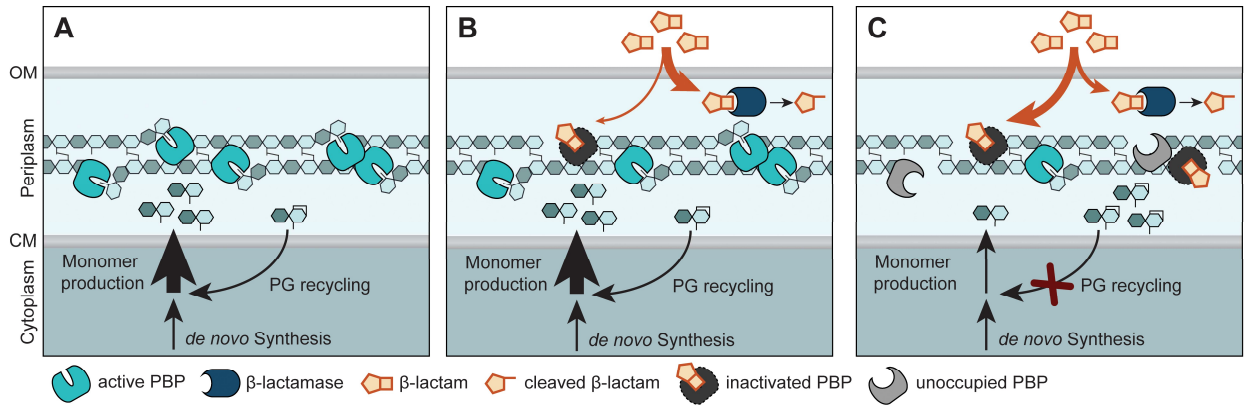

Figure 11. Model for the critical role of PG recycling in *C. crescentus* growth and β-lactam resistance. (A) PBPs mediates the incorporation of new cell wall material into the growing PG sacculus. The PG precursors required for this process are synthesized in the cytoplasm, using building blocks that are provided by both de novo synthesis and PG recycling. **(B)** If β-lactams enter the periplasm, they compete with PG precursors for binding to their PBP targets. Most antibiotic molecules are rapidly hydrolyzed by the β-lactamase BlaA. However, a minor fraction manages to interact with PBPs before they are captured and degraded. The resulting inactivation of a small proportion of PBPs can be tolerated by cells, as long as they still contain sufficient active PBPs to maintain cell growth and division. **(C)** Upon disruption of PG recycling, the level of PG monomers strongly decreases, leaving the substrate binding sites of PBPs unoccupied for longer periods of time and thus increasing their accessibility to β-lactam molecules. As a result, a larger fraction of PBPs is inactivated, leading to decreased cell wall integrity and ultimately cell lysis. This effect may be aggravated by the reduced activity of the remaining, active PBPs due to an insufficient supply of PG precursors and by the accumulation of anhydro-muropentapeptides in the periplasm, which could interfere with the activities of PG biosynthetic enzymes, thereby further decreasing the incorporation of new material into the existing sacculus.